The role of mitochondrial dynamics in muscle stem cell quiescence and cell cycle re-entry

Steven Wade

Thesis submitted to the University of Ottawa
in partial fulfillment of the requirements for the degree of
Master of Science in Biochemistry

Department of Biochemistry, Microbiology and Immunology
Faculty of Medicine
University of Ottawa

© Steven Wade, Ottawa, Canada, 2025

Abstract

Balanced stem cell fate decisions are essential for the maintenance and regeneration of tissues across the lifespan. The mitochondrial fusion protein OPA1 and mitochondrial shape changes are essential contributors to balanced fate decisions, however the full mechanistic scope of their signalling abilities are not fully known. Here, using OPA1-deficient and OPA1-overexpressing muscle stem cells (MuSCs), we show that mitochondrial shape changes alter the metabolome of MuSCs. These OPA1-regulated metabolites possess distinct abilities to alter MuSC progression and fate. Furthermore, OPA1 expression and mitochondrial shape alters the ratio of α-ketoglutarate (αKG) to succinate, and this ratio dictates the decisions to self-renew or commit. Manipulation of this ratio *in vitro* is sufficient to alter the fate of MuSCs by modifying mitochondrial shape and altering the expression of key stemness and myogenic genes. In addition, we find that committed and self-renewed MuSCs have opposing gene expression profiles indicative of differential [αKG]:[succinate] ratios. Lastly, in OPA1-deficient mice, *in vivo* restoration of this ratio prevents MuSC depletion and preserves the stem cell pool after injury and decreases precocious commitment and differentiation. Our studies present a novel role for mitochondrial shape as a signalling mechanism to guide MuSC progression and fate.

Key words: MuSCs, Mitochondria, Mitochondrial dynamics, Optic Atrophy Protein 1, Metabolites, Fate decisions, Metabolome

Acknowledgements

I must first express my sincere gratitude for my supervisor, Dr. Mireille Khacho, for the many scientific discussions, one-on-one impromptu meetings and her guidance across these last few years. This has been the most rewarding and challenging years of my life, and I am very grateful to have had your support and guidance during these times. You have helped me not only helped foster my journey as a scientist, but you have also provided me with tools that extend far beyond the bench. I hope that all those who enter her lab in the future may also leave with the abundance of knowledge and wisdom that I too leave with.

I am also very thankful to my committee members Dr. Alexandre Blais, Dr. Julie St-Pierre and Dr. Yannick Benoit for their mentorship, their guidance and for the stimulating discussions. Your support during these times, especially nearing the end, was invaluable.

I must also acknowledge the Khacho lab members, past and present, for helping me in this journey. I am deeply grateful to Nicole for spending the hours training me and welcoming me into the lab when I first started. To Rholls Tompsine, Kayla Ferguson, Olivia Sommers, Edward Gardner, I thank you all for the many laughs. To Nikita Larionov, none of this research could have been done without your help in managing animal colonies and animal work. To Matthew Triolo, I am grateful for your mentorship, the laughs and the many (so many) coffee runs. I am glad to have found not only a great work colleague, but also a friend.

None of this would have been possible without the everlasting support from my parents. I thank you for your support in helping me through these years. You have been a guiding light for me, and I am eternally grateful.

To my best friend, Trisha, words cannot describe what your friendship means to me. I hope as your read this work, you know that this was indeed, as we say, “ranked play”.

Lastly, I must thank my partner, Jeremie. Our almost 8 years together has been the greatest time of my life. You are my rock and my biggest supporter, and I can’t wait for this next journey in our life. I love you.

Table of Contents

List of Abbreviations

αKG	Alpha-ketoglutarate/2-oxoglutarate
2HG	2-hydroxyglutarate
ACN	Acetonitrile
Akt	Protein kinase B
AP-1	Activator Protein 1
BSA	Bovine serum albumin
CalcR	Calcitonin Receptor
cMET	Hepatocyte growth factor receptor
Cpt2	Carnitine palmitoyl transferase 2
CTX	Cardiotoxin
Dlk1	Delta-like homolog 1
DNA	Deoxyribonucleic acid
DRP1	Dynamin-related protein 1
ECM	Extracellular Matrix
EDTA	Ethylenediaminetetraacetic acid
eIF2α	Eukaryotic translation initiation factor 2A
eIF5A	Eukaryotic translation initiation factor 5A
ER	Endoplasmic reticulum
ETC	Electron transport chain
FACS	Fluorescence-activated cell sorting
FAO	Fatty acid oxidation
FBS	Fetal bovine serum
Fis1	Mitochondrial fission protein 1
G_0	Quiescence
GFP	Green fluorescent protein
GLUD1	Glutamate dehydrogenase 1
GSH	Glutathione
GTP	Guanosine triphosphate
H&E	Hematoxylin and Eosin

H4K16ac	Histone 4 lysine 16 acetylation
HGF	Hepatocyte growth factor
HGFA	Hepatocyte growth factor activator
IDH	Isocitrate dehydrogenase
IMM	Inner mitochondrial membrane
Ki67	Antigen Kiel 67
LC/MS	Liquid chromatography-Mass spectrometry
MAPK	Mitogen-activated protein kinase
MeOH	Methanol
MFN1	Mitofusin 1
MFN2	Mitofusin 2
MiD49	Mitochondrial dynamics protein 49
MiD51	Mitochondrial dynamics protein 51
MRF	Myogenic regulatory factor
mRNA	Messenger RNA
mtDNA	Mitochondrial DNA
mTORC1	Mechanistic target of rapamycin complex 1
MuSC	MuSC
Myf5	Myogenic factor 5
MyoD	Myoblast determination protein 1
MyoG	Myogenin
NAD+	Nicotinamide adenine dinucleotide
NCS	Newborn calf serum
NICD	Notch intracellular domain
OGDH	2-oxoglutarate dehydrogenase
OMM	Outer mitochondrial membrane
OPA1	Optic atrophy protein 1
OXHPHOS	Oxidative phosphorylation
Pax7	Paired box protein Pax-7
PBS	Phosphate-buffered saline
PFA	Paraformaldehyde

PI3K	Phosphoinositide 3-kinase
PSAT1	Phosphoserine aminotransferase 1
PTPN11	Protein tyrosine phosphatase non-receptor type 11
RB	Retinoblastoma protein
RNA	Ribonucleic acid
ROS	Reactive oxygen species
RT-qPCR	Real time quantitative polymerase chain reaction
SDH	Succinate dehydrogenase
SIRT1	Sirtuin 1
SIRT2	Sirtuin 2
Spry1	Sprouty RTK Signaling Antagonist 1
TA	Tibialis anterior
TCA	Tricarboxylic acid cycle
Tom20	Mitochondrial import receptor subunit Tom20 homolog
TTP	Tristetraprolin
UCP2	Uncoupling protein 2
VCAM	Vascular cell adhesion protein 1

List of tables

List of figures

Chapter 1: Introduction

1.1 Overview of MuSCs

Muscle stem cells (MuSCs), also known as satellite cells, are the resident stem cell population and primary source of regeneration in skeletal muscle[1]. The regenerative capacity of MuSCs ensures for the efficient maintenance of skeletal muscle across the lifespan[2-4]. MuSCs are anatomically located between the sarcolemma and the basal lamina of muscle cells[5,6]. The micro-environment surrounding MuSCs, also called the niche, is an essential contributor in the maintenance and regenerative capacity of MuSCs[6]. The MuSC niche provides regulatory signals that maintain MuSCs during homeostasis and promote regeneration in periods of insult. The niche is composed of various cell-types, a multitude of extracellular matrix (ECM) proteins, cell-cell contacts and interactions[6-13]. Thus, MuSCs reside in an environment upon which they may rapidly respond to the regenerative demands of muscle and execute efficient and timely regeneration. In homeostatic conditions, MuSCs reside in a state of reversible cell cycle arrest known as quiescence (G_0). Following a stimulus such as an injury, MuSCs will exit their quiescent state, activate, and re-enter the cell cycle to begin proliferating[14-17]. An important characteristic of MuSCs is their ability to undergo fate decisions whereby they may commit and differentiate towards the myogenic lineage to repair damaged muscle, or undergo self-renewal to re-populate the stem cell pool for future response[1].

1.2 Myogenesis

The process of myogenesis describes the trajectory from MuSCs towards the formation of new skeletal muscle fibers[18]. MuSCs transition from their state of stemness towards differentiation into myotubes, which fuse with other myotubes and existing muscle fibers[19]. This process is highly regulated at multiple levels and perturbations or malfunctions in any step of this process may lead to catastrophic regenerative failure.

1.2.1 Quiescence

As previously mentioned, MuSCs, under physiological conditions, reside in a state of reversible cell cycle arrest known as quiescence[15,20,21]. Maintenance of quiescence is

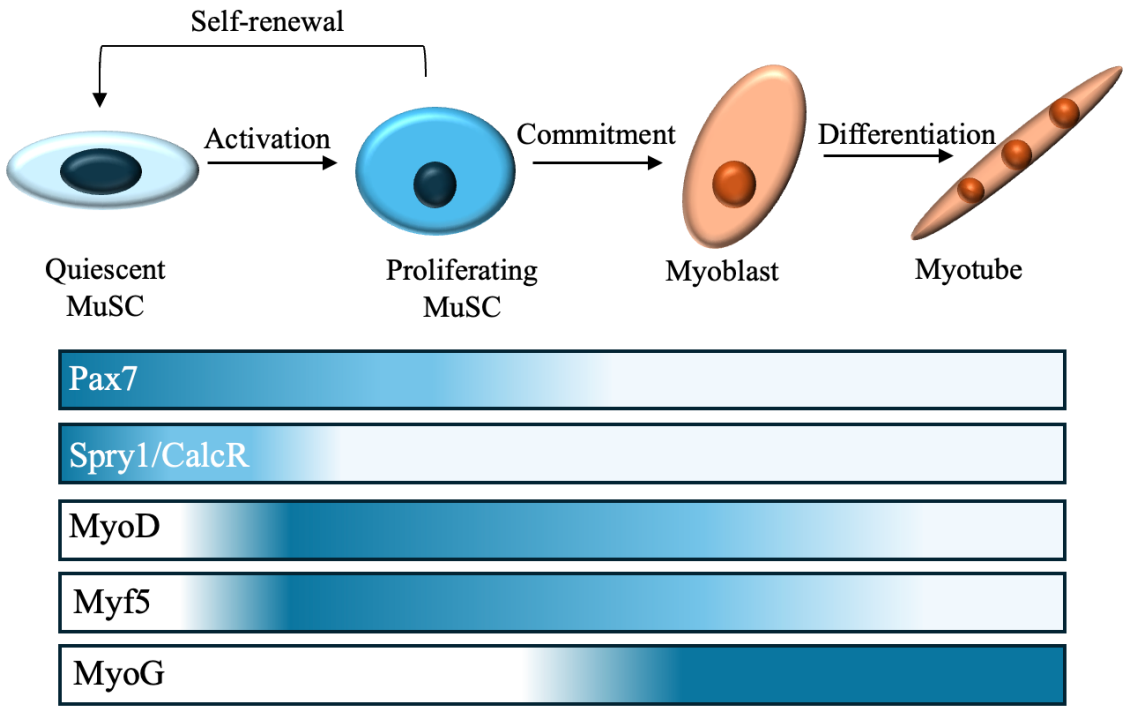

Figure 1. Overview of myogenesis and myogenic regulatory factors. In their quiescent state, MuSCs express high levels of the transcription factor Pax7. Quiescent MuSCs also uniquely express Spry1 and CalcR, which are rapidly downregulated upon activation. Following activation, expression of MyoD is rapidly increased concomitantly with Myf5. As MuSCs self-renew, Pax7 expression is reinstated. During commitment, Pax7 levels are further decreased and expression of MyoG increases until terminal differentiation. Figure adapted from Dumont et al (2015) *Comprehensive Physiology*.

essential for maintaining the stemness of MuSCs and preserving their regenerative capacity. Quiescent MuSCs can be identified by multiple cell surface markers and transcription factors. Notably, the paired box protein Pax7, is expressed in quiescent MuSCs, however its expression is not limited to quiescence.[22]. Pax7 is a transcription factor indispensable for MuSC function and the myogenic progression[22-24]. The protein Sprouty1, a reversible inhibitor of tyrosine kinase signalling, has also been demonstrated to be robustly expressed in quiescent MuSCs, and rapidly downregulated upon their activation[25]. Additionally, other markers of quiescent MuSCs include the cell surface markers CD34, Calcitonin receptor (CalcR), Integrin α-7 and VCAM, although VCAM expression is not exclusive to quiescent MuSCs.[26-33]. The extracellular matrix and adjacent

muscle fibers both play critical roles in regulating MuSC quiescence, particularly through Notch signalling[34,35]. Quiescent MuSCs express the Notch receptors Notch1-3, with its ligand Delta-like 1 (Dlk1) located on the muscle fiber[30,36,37]. Binding of the Notch receptor to its ligand leads to the Notch intracellular domain (NICD) translocating to the nucleus where it then regulates the expression of genes needed for the maintenance of quiescence[34]. Additionally, secretion of the Wnt ligand, Wnt4, favours the retention of quiescence through regulation of the cytoskeleton[8]. Furthermore, an important characteristic of quiescent MuSCs is their ability to repress mitogenic activity that would lead to their exit from quiescence. This inhibition is accomplished through cyclin-dependent kinase (CDK) inhibitors such as $p57^{Kip2}$ and $p21^{Kip1}$ [14,38,39]. Furthermore, quiescent MuSCs rely on the activity of the retinoblastoma protein (RB) to limit the activity of E2F transcription factors, thereby controlling cell cycle entry[40]. MuSC quiescence is also controlled post-transcriptionally. In quiescence, transcripts of the myogenic regulatory factors (MRFs) *MyoD* and *Myf5* are expressed, however only upon activation are their transcripts translated[41-43]. MyoD translation is inhibited by the RNA-binding proteins Staufen1 and TTP[41,42]. Intron retention has been identified as a regulatory mechanism of MuSC quiescence. In quiescent MuSCs, more than 1000 genes are incompletely spliced, while only 50 intron retention events occur in activated MuSCs[44]. This modulation of intron splicing ensures that undesired protein translation is prevented in quiescence but allows for a rapid response upon activation[44]. Quiescent MuSCs display reduced translation, which is accomplished through phosphorylation of eIF2α at Ser51[45].

A characteristic of quiescence in MuSCs is that it exists as a gradient, whereby cells can transition from a deep quiescent state, towards an alerted state, termed G_{alert}[46]. The depth of MuSC quiescence dictates their activation and cell cycle entry kinetics and allows MuSCs to respond more rapidly than from a deep quiescent state[46]. MuSCs can transition between these two states of quiescence in response to an injury-related stimulus[46,47]. This transition is mediated through mTORC1 activity and signalling through the hepatocyte growth factor (HGF) receptor, cMet. Upon an injury, the systemic protease HGFA is activated, cleaving pro-HGF into active HGF[47]. Active HGF circulates within the system and binds to the cMET receptor on MuSCs on the limb contralateral from the injury[47]. MuSCs in the G_{alert} state have increased cell size, increased mitochondrial mass and activity and enhanced mTORC1 activity[46,47].

Quiescent MuSCs also display a high level of heterogeneity in terms of their expression levels of specific quiescence markers[43,48]. The differential expression of multiple quiescence and myogenic markers can directly influence the stemness of MuSCs and their fate decisions. Notably, quiescent MuSCs that do not express Myf5 outperform Myf5-positive quiescent MuSCs in re-establishing the stem cell pool following transplantation[43]. Additionally, expression levels of Pax7 also determine the depth of quiescence, whereby Pax7^{high} MuSCs display lower basal metabolic rates, increased time to re-enter the cell cycle and maintenance of stemness following serial transplantations[49,50]. A previous study has also shown that quiescent MuSCs can be categorized into two groups based on CD34 expression, CD34^{high} and CD34^{low}. The population of CD34^{high} quiescent MuSCs reside in a deep quiescent state and have better engraftment and self-renewal potential than CD34^{low} MuSCs[48].

1.2.2 MuSC activation and proliferation

Upon damage to muscle fibers, quiescent MuSCs must rapidly exit their quiescent state and re-enter the cell cycle to begin proliferating. Multiple checkpoints exist during the exit from quiescence. An early checkpoint during the exit from quiescence is mediated through PI3K functions[51]. Activation of the PI3K complex following an activating stimulus leads to downstream activation of the kinase Akt, which through its functions, allows for induction of the AP-1 transcription factor complex, promoting genes involved in cell cycle[51]. Furthermore, the tyrosine phosphatase PTPN11 promotes the exit from quiescence and activation of MuSCs through MAPK signalling[52]. In addition, circulating factors such as HGF serve as an activating stimulus for MuSCs to exit quiescence[47,53,54]. As MuSCs activate, the expression of quiescence markers such as CalcR, Spry1 and CD34 are rapidly downregulated, and expression of the myogenic factor MyoD is increased[25-27,29,32,41,43,55]. This is accompanied by a subsequent downregulation of cell cycle inhibitory genes like p27 and p51, and concomitant increases in cell cycle promoting genes such as cyclins and cyclin-dependent kinases[38,56]. This coordinated effect results in the efficient exit from quiescence and re-entry into the G_1 phase of the cell cycle. Following cell cycle re-entry, MuSCs undergo several rounds of proliferation before undergoing fate decisions. Interestingly, division-independent differentiation of MuSCs has been recently observed[57].

1.2.3 Fate decisions

As previously mentioned, MuSCs possess the ability to either commit and differentiate to a myogenic lineage or self-renew and re-populate the stem cell pool[1,2,58]. The balance in these fate decisions is essential for ensuring efficient repair of damaged muscle tissue and maintaining the stem cell pool for future need. Proliferating MuSCs can undergo symmetric or asymmetric divisions[58-62]. Symmetric divisions give rise to two daughter cells of the same identity, either self-renewing or committed, and asymmetric divisions give rise to one self-renewing and one committed cell[63,64]. Symmetric divisions favouring self-renewal leads to expansion of the stem cell pool, whereas symmetric divisions promoting commitment may lead to exhaustion and depletion of the stem cell pool. An important regulator of symmetric and asymmetric division is cell polarity whereby the fate of daughter cells is determined by the apical-basal polarity of certain factors within the MuSC[60,65,66]. The polarity of these factors within MuSCs and angle of division determines the identity of the resulting daughter cells.

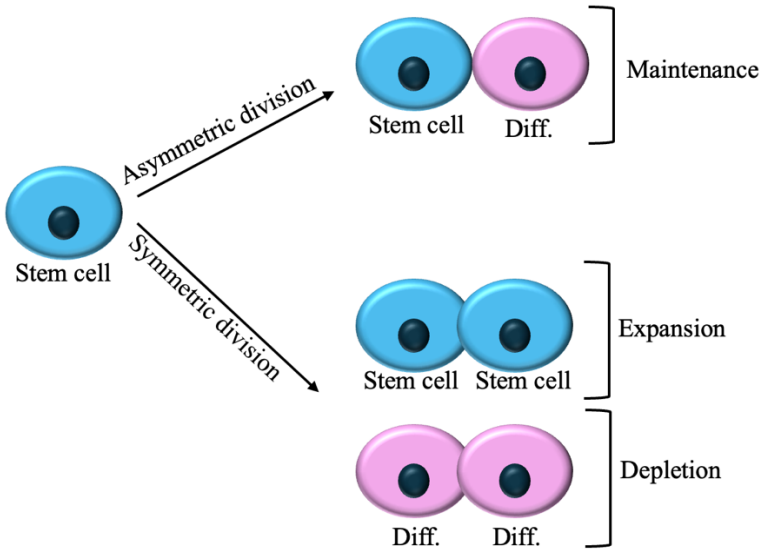

Figure 2. Stem cells undergo symmetric and asymmetric divisions. As MuSCs proliferate, they undergo symmetric divisions to give rise to two daughter cells of the same identity, or asymmetric divisions to give rise to one stem cell and one differentiated cell. Asymmetric divisions promote maintenance of the stem cell pool and efficient regeneration whereas symmetric divisions promoting self-renewal or differentiate lead to expansion or depletion of the stem cell pool, respectively. Figure adapted from Murke et al (2015) *Symmetry*.

Furthermore, the decisions to commit or self-renew are tightly regulated at the transcriptional level. Proliferating MuSCs undergoing commitment rapidly downregulate Pax7 and maintain MyoD expression[58,67-69]. This is accompanied by significant genome remodelling orchestrated by Pax7, which includes the acquisition of histone marks that are associated with enhancer activity and enhanced chromatin accessibility[70]. After loss of Pax7 following commitment and during differentiation, epigenetic memory is maintained at a subset of Pax7 enhancers[71]. In addition to this, following an asymmetric division, the PAR complex is segregated to the apical cell which induces p38/MAPK activity, resulting in MyoD expression and generation of a committed progenitor[72]. During the differentiation stage, other MRFs such as MyoG are upregulated and maintain their trajectory towards terminal differentiation[73,74]. MyoD re-organizes the 3D genome architecture to promote the formation of myogenesis-specific chromatin loops, which are required for myogenic specification[75]. The process of self-renewal is also dominated by major transcriptional changes. Here, Pax7 levels are upregulated and MyoD expression is reduced[49,72,76]. Upregulation of Pax7 and previously mentioned stemness markers such as Spry1 and CalcR induces the exit from cell cycle and re-entry into quiescence[25,27,29].

1.3 MuSC metabolism

As discussed, the progression of MuSCs is a highly coordinated hierarchy of transcriptional, translational, systemic and cell-autonomous events which ensure the efficient repair of damaged muscle tissue and maintenance of the stem cell pool. An emerging characteristic of MuSCs required for the function is their metabolic state. While it had been previously assumed that the metabolic state of stem cells was merely consequential to their developmental stage, much work has been done to demonstrate that metabolism is not a consequence but rather a guiding force in dictating stem cell function and progression. This can also be said in the context of metabolism guiding MuSC progression and fate.

1.3.1 Metabolic regulation of MuSC progression

Quiescent MuSCs display a low level of basal metabolism[15,21]. Transcriptomic profiling of quiescent MuSCs has revealed a predominant reliance on fatty acid oxidation[77]. Fatty acid oxidation in MuSCs maintains high levels of NAD+, which stimulates the NAD+ sensor SIRT1 to be recruited and deacetylate histone 4 lysine 16 (H4K16ac), preserving the repression of cell cycle

genes[77]. Deletion of SIRT1 leads to increased H4K16ac and promotes the transcription of cell cycle genes and MyoD, leading to quiescence exit[77]. Additionally, high levels of NAD+ favours quiescence retention as this leads to decreased levels of acetyl-CoA and decreased global protein and histone acetylation that is associated with the initiation of the myogenic program[77]. Promoting production of ROS via deletion of the mitochondrial uncoupling protein, UCP2, increases glucose utilization and promotes MuSC proliferation[78]. Interestingly, a recent paper identified that mitochondrial fatty acid oxidation may also play a role in the expansion of MuSCs[79]. Deletion of Cpt2, the rate limiting step in fatty acid oxidation, resulted in defects in MuSC expansion and differentiation, highlighting potential dual roles for fatty acid oxidation in the quiescent and proliferative stages of MuSC progression[79]. It is important to note that earlier papers demonstrating decreased FAO following culture were done using bulk RNA-seq, whereas the newer studies which identify increased FAO utilized single cell RNAseq (scRNAseq). It is well established that MuSCs display high levels of heterogeneity at baseline as well as during the myogenic process[49,80,81]. Thus, these studies have differences in the population of cells being analyzed as well as the depth of sequencing which could partially explain the opposing results. Additionally, early studies demonstrating a decrease in FAO during activation were done using MuSCs that had been isolated and placed in cultured. In contrast, newer studies showing increased FAO were done using isolated MuSCs following *in vivo* injury. The environment in which these MuSCs reside in prior to their isolation and sequencing are profoundly different and could affect the interpretation of results. Lastly, it is imperative to note that these studies have not truly measured FAO in quiescent or activated MuSCs but rather inferred based on gene expression. Furthermore, it has been demonstrated that reliance on ketone bodies, either via fasting or through a ketogenic diet, induces a deep quiescent state in MuSCs, which improves their resilience and survival when faced with sources of cellular stress[80].

Once MuSCs exit quiescence and re-enter the cell cycle, a metabolic shift is observed. MuSCs transition from a reliance on fatty acid oxidation towards anaerobic glycolytic metabolism[77]. Gene expression of fatty acid oxidation and OXPHOS genes are dramatically reduced as MuSCs begin proliferating and genes involved in glycolytic metabolism are subsequently increased[77,81,82]. Preventing this metabolic switch with inhibitors of glycolysis prevents MuSC proliferation and self-renewal, while promoting glycolysis enhanced proliferation[83].

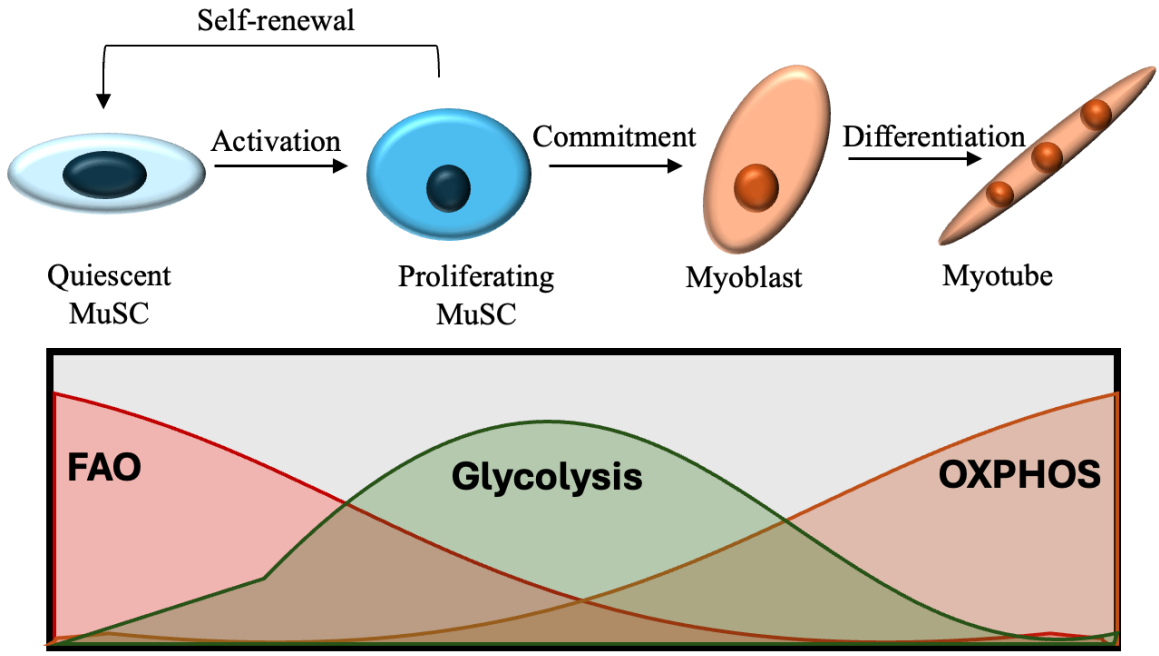

Figure 3. Metabolic plasticity is a key feature of MuSC progression. In quiescence, MuSCs rely predominantly on fatty acid oxidation. During the activation process, a decrease in FAO occurs concomitantly with an increase in glycolytic metabolism. The differentiation process is accompanied by an increase in oxidative metabolism and reliance on oxidative phosphorylation. Figure adapted from Relaix et al. (2021) *Nature Communications*.

MuSC differentiation is associated with a further increase in oxidative metabolism[82]. Gene expression of fatty acid oxidation and mitochondrial biogenesis associated genes are increased concomitantly with increased respiration[82,84]. Increased oxidative metabolism is necessary to support the bioenergetic needs of differentiating myoblasts[85-87]. Interestingly, while proliferating myoblasts also display enhanced glucose utilization, there is a divergence in the fate of glucose in proliferating versus differentiating myoblasts[85]. Proliferating myoblasts' glucose utilization maintains high levels of histone acetylation via generation of acetyl-CoA, whereas differentiating myoblasts predominantly use glucose for respiration, decreasing acetyl-CoA and histone acetylation, promoting the differentiation program[85]. Additionally, specific substrate catabolism directs the fate of MuSCs[88]. Glutamine anaplerosis through the citric acid cycle (TCA) reduces MuSC differentiation[88]. This coincides with decreased abundance of the mitochondrial glutamate deaminase, GLUD1[88]. In this context, GLUD1 serves to prevent mitochondrial glutamate accumulation, thereby sustaining the malate/aspartate shuttle and maintaining appropriate NAD+/NADH ratios[88].

1.3.2 Metabolite signalling in stem cells

While metabolism, through the generation of energy-yielding products, supports MuSC function and progression, it is also the source of secondary molecules with essential roles in regulating stem cell function[89-95]. These metabolites participate in a wide variety of cellular processes with downstream functions affecting gene expression, protein function, folding, stability and localization[96]. It is well established that metabolite signalling is a critical factor in regulating the function of various stem cell populations and their fate[89,96]. One well-known function of metabolites in regulating stem cell function is through covalent modifications to proteins[97,98]. These modifications include methylation, acetylation, lactylation, succinylation, glutathionylation and formylation[98]. A majority of these covalent modifications to proteins occur on lysine residues, however other residues such as arginine and cysteine are also rapidly modified[98]. Metabolite signalling affects gene expression in part through post-translational modifications to histone tails[89,99,100]. Modifications to histone tails, such as acetylation, reduces the charge of lysine residues thereby weakening the interaction between DNA and histones, decreasing the compaction of chromatin[101,102]. Decreased chromatin compaction allows for the transcriptional machinery to gain access to specific DNA regions and thus initiate transcription[102-104]. Other histone modifications such as methylation may serve to recruit the transcriptional machinery thereby affecting transcription without directly altering chromatin compaction[105]. Much research has gone into uncovering the role of metabolites in regulating stem cell function. The TCA cycle metabolite, alpha-ketoglutarate (αKG), has been demonstrated to have extensive roles in multiple stem cell populations in dictating fate[90,106-108]. Embryonic stem cells consume high levels of glutamine and glucose in order to maintain elevated levels of αKG[107]. This high level of αKG results in an elevated ratio of αKG to succinate, another TCA cycle metabolite, and this elevated ratio dictates multiple histone and DNA methylation programs to maintain expression of pluripotency genes[107]. In primed pluripotent stem cells, many TCA cycle metabolites are produced despite their low OXPHOS rate[106]. In particular, hPSCs accumulate high levels of αKG and promotes their early differentiation[106]. In intestinal stem cells, differential regulation of αKG levels is accomplished by a dual, lineage-specific role for the oxoglutarate dehydrogenase (OGDH), which allows for the specification of intestinal stem cell fate[109]. Naïve T cell differentiation is attenuated by αKG, via contribution to remodeling of the lipidome, and suppresses their fate towards T reg cells[90]. Thus, metabolites play extensive roles in regulating stem cell metabolism, signalling and fate.

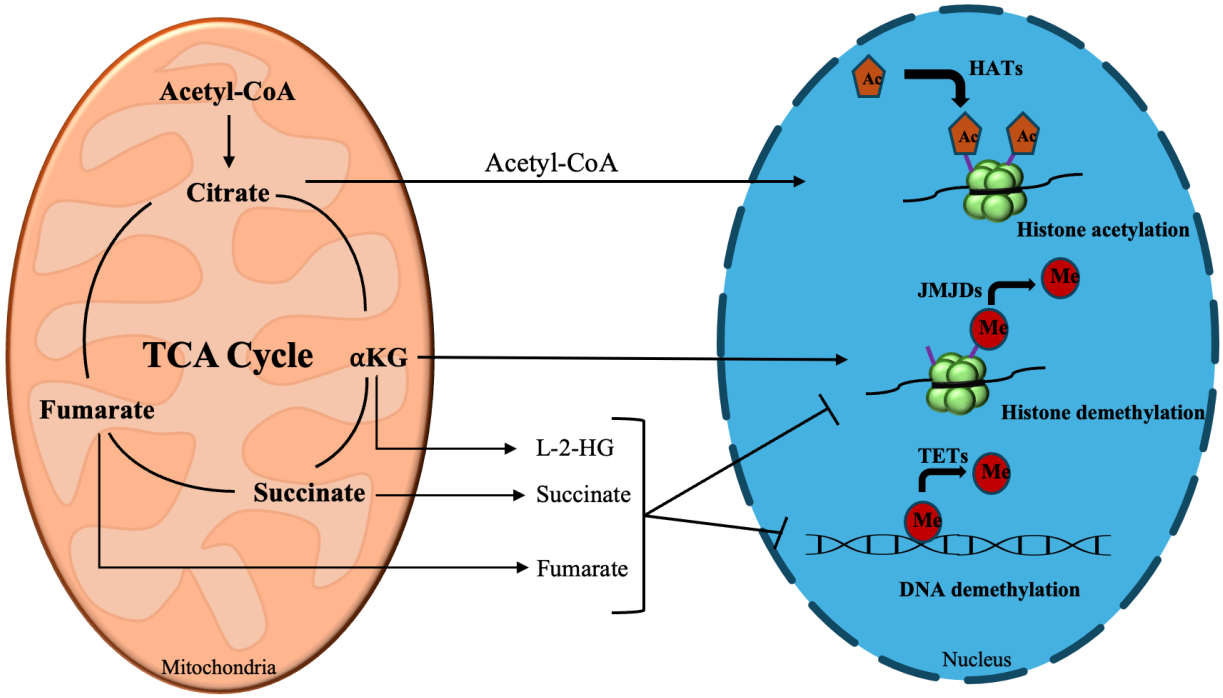

Figure 4. Mitochondrial metabolites alter cell signalling and epigenetics. Mitochondrial metabolites participate in various covalent modifications to proteins, including histones and DNA. These modifications can alter gene expression and subsequently stem cell fate by directly altering chromatin compaction or by marking sites for active transcription. Figure adapted from Martinez-Reyez and Chandel (2021) *Nature Communications*.

The regulation of MuSC fate via metabolite signalling has recently garnered attention. During the differentiation process, MuSCs utilize their glucose metabolism to alter levels of acetyl-CoA, which then in turn alters global histone acetylation levels[85]. Decreased histone acetylation allows for the initiation of the differentiation program[85]. Additionally, the transcription factor Pax7 contains two acetylation sites and acetylation of Pax7 is necessary to positively regulate its transcriptional activity[110]. Acetylation of Pax7 is directly controlled by MYST1, which is stimulated by acetyl-CoA, and the deacetylase SIRT2, stimulated by NAD^+[110]. This signalling of acetyl-CoA by directly affecting Pax7 transcriptional activity is responsible for dictating MuSC fate. Furthermore, it has been recently identified that in proliferating myoblasts, αKG generation by the serine biosynthesis enzyme Psat1, is required for their proliferation and efficient

differentiation[111]. Deletion of Psat1, and subsequent depletion of Psat1-generated αKG impairs muscle regeneration and is rescued by exogenous αKG or glutamine[111]. MuSC progression and fate is also controlled by non-TCA cycle metabolites. In a recent study, it was identified that spermidine, a metabolite in the polyamine biosynthesis pathway, acts as a regulatory metabolite to promote MuSC activation and proliferation[112]. Spermidine generates hypusinated eIF5A, which allows for the translational control of MyoD[112]. Thus, multiple metabolites have been identified as regulators of MuSC function and progression, however the full scope of metabolite signalling in MuSCs remains unknown.

1.4 Mitochondria

1.4.1 Mitochondrial metabolism

Mitochondria are double-membraned organelles that are essential for the metabolic and overall health of cells. These organelles are the site for a wide variety of metabolic reactions and generation of secondary metabolites which, as discussed, have essential roles in cellular function. A major metabolic output of mitochondria is the generation of adenosine triphosphate (ATP) which serves as the energetic currency of many cellular processes[113-115]. Mitochondria are also the site of two metabolic pathways participating in the metabolism of glucose: the TCA cycle and OXPHOS. The TCA cycle is a closed loop metabolic cycle whose primary function in oxidative metabolism is to generate the reducing agent NADH as well ATP through the metabolism of acetyl-CoA[91,94]. However, as mentioned, TCA cycle intermediates have other functions including as precursors for other catabolic and anabolic reactions, and serving as signalling molecules. Mitochondria are also home to the electron transport chain (ETC). The ETC is composed of 5 complexes, namely complexes I-V, which transports electrons from electron carriers to electron acceptors[116,117]. The transfer of electrons is coupled with the transfer of protons (H^+) across the inner mitochondrial membrane into the intermembrane space[117]. Generation of ATP is carried out by Complex V, ATP synthase, which harnesses the energy produced by protons diffusing to the matrix to generate the production of ATP from ADP[115]. The electron transport chain is also the site of reactive oxygen species (ROS) generation[118]. The generation of ROS is particularly seen at Complex I and Complex III, when electrons leaking from the ETC prematurely react with oxygen[119,120]. Prominent reactive oxygen species include superoxide (O_2^-), hydroperoxide (H_2O_2) and hydroxyl radicals (OH^-)[119,120].

In high concentrations, reactive oxygen species can lead to oxidation of lipids, proteins and DNA damage[118,121-126]. However, it should be appreciated that physiological increases in reactive oxygen species serve important functions in signal transduction[89,121,123,125-132]. In addition to the TCA cycle and OXPHOS, mitochondria are also the site of fatty acid oxidation, also known as beta-oxidation. This process involves the metabolism of fatty acids into acetyl-CoA, which can then participate in the TCA cycle.

1.4.2 Mitochondrial dynamics

As mentioned, mitochondria are most well-known for their roles in metabolism and ATP generation. However, the role of mitochondria extends beyond being the site of metabolic reactions. Mitochondria are also highly dynamic organelles, possessing the ability to remodel their morphology and ultrastructure[128,133-135]. The process of mitochondrial remodeling is known as mitochondrial dynamics. Mitochondrial dynamics is essential in maintaining mitochondrial health, mitochondrial DNA (mtDNA) integrity and adapting to the metabolic needs of a cell[128,134]. Mitochondria alter their morphology via opposing events of fission and fusion. Mitochondrial fission sees the segregation of one mitochondrion into two. Opposingly, mitochondrial fusion describes the joining of two separate mitochondria. The processes of mitochondrial fission and fusion are carried out by a family of GTPases, which utilize the energy produced from GTP hydrolysis to power these events[136].

Mitochondrial fusion first occurs by fusion of the outer mitochondrial membrane (OMM). The proteins mitofusin 1 and 2 (MFN1/2) are tethered to the OMM and through GTP hydrolysis, undergo conformational changes to bridge contact between mitochondria and allow for membrane fusion[137,138]. Fusion of the inner mitochondrial membrane (IMM) is mediated by optic atrophy protein 1 (OPA1)[139-141]. OPA1 also regulates cristae ultrastructure by locating itself at cristae junctions whereby it controls cristae widening and constriction[142-146]. Given its localization to cristae, OPA1 also plays a role in regulating cell death by controlling the release of cytochrome c, which normally resides within cristae invaginations[144].

Mitochondrial fission first begins with a pre-constriction step, whereby endoplasmic reticulum (ER) tubules contact and wrap around mitochondria[147,148]. After constriction, cytosolic dynamin-related protein 1 (DRP1) is recruited to the outer mitochondrial membrane and oligomerizes to form a ring[148]. Drp1 recruitment to the mitochondria is accomplished by its

Figure 5. Mitochondria undergo continuous cycles of fission and fusion. In response to various cellular signals, mitochondria may undergo fission or fusion. Fusion is initiated by the OMM proteins MFN1/2. Inner membrane fusion and cristae architecture is achieved by OPA1. Mitochondrial fission occurs with DRP1 recruitment and constriction of mitochondria into separate mitochondrion. Figure adapted from Wade and Khacho (2020) *International Journal of Biochemistry and Cell Biology.*

phosphorylation at Ser616[134]. Drp1 then interacts with the membrane-anchored mitochondrial fission factor Fis1 and adaptor proteins MiD49/51[149-152]. Oligomerization of Drp1 further constricts the mitochondrion until it is segmented into two separate mitochondria.

1.4.3 Mitochondrial dynamics in MuSC progression and fate

Recently, mitochondrial dynamics has been demonstrated to be a key regulator of MuSC quiescence, cell cycle re-entry, and fate decisions. During quiescence, MuSCs maintain an elongated mitochondrial morphology, that coincides with elevated levels of OPA1 mRNA and protein[153]. Strikingly, following an activating stimulus, mitochondria within MuSCs rapidly fragment, as early as 4-hours post-activation[153]. This fragmentation is maintained until 48-hours, when mitochondria undergo re-elongation[153]. Fragmentation of mitochondria within MuSCs is accomplished through systemic HGF/mTOR signalling[153]. In a model of forced mitochondrial fragmentation via a MuSC-specific deletion of the fusion protein OPA1 (OPA1-KO), MuSCs exist in G_{alert} quiescence[46,153]. This is characterized by their increased cell size, nuclear morphology consistent with a more activated state and increased abundance of phosphorylated ribosomal protein S6 (pS6), a marker of mTORC1 pathway activation[46,153]. Additionally, OPA1-KO MuSCs have decreased basal gene expression of quiescence markers Pax7, CD34 and Hes1[150]. Consistent with the G_{alert} state, OPA1-KO MuSCs have enhanced activation and cell cycle entry kinetics[150]. Furthermore, global transcriptomic profiling of OPA1-KO MuSCs via RNAseq reveals an enrichment for terms associated with cell cycle, chromosome segregation, muscle regeneration and kinetochore assembly[150]. Loss of OPA1 also revealed severe regenerative defects *in vivo*

whereby OPA1-KO MuSCs commit at the expense of self-renewing, leading to a significant depletion of the stem cell pool. It should be noted that this loss of self-renewing cells was not due to increased apoptosis, DNA damage or circulating myokines Atrogin1 and MuRF1. Acute OPA1 loss did not affect MuSC respiration or cristae integrity.

It was demonstrated that mitochondrial fragmentation, during the transition from quiescence to activation, was necessary to induce a ROS/glutathione (GSH) mito-nuclear signalling cascade[150]. Mitochondrial fragmentation induced a transient rise in ROS and GSH levels, which act as signalling molecules to enhance the expression of cell cycle and myogenic genes while simultaneously downregulating quiescence-associated genes[150]. Interestingly, given that mitochondria within OPA1-KO MuSCs already exit in a fragmented state, levels of ROS and GSH were already elevated in comparison to their WT counterparts[150]. The phenotype of OPA1-KO MuSCs could be reverted by decreasing ROS and GSH levels with exogenous compounds such as mitoTEMPO and BSO[150].

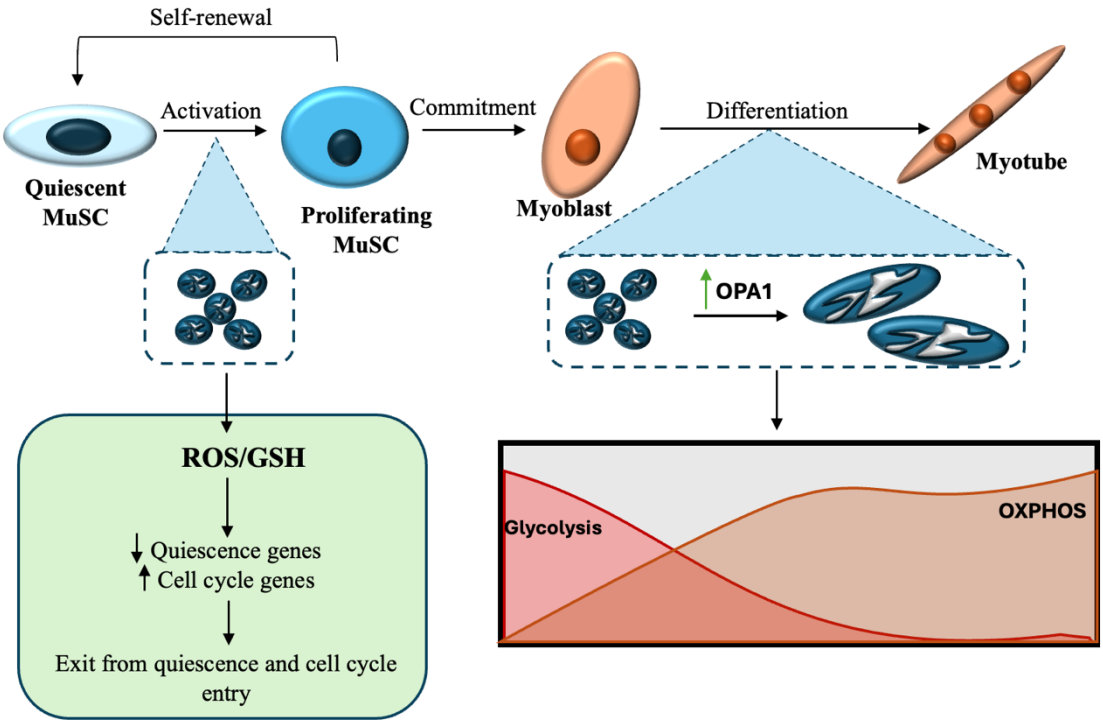

Figure 6. The role of mitochondrial dynamics in MuSCs. During the transition from quiescence to activation, mitochondria within MuSCs undergo fragmentation. Mitochondrial fragmentation induces ROS/GSH mito-nuclear signalling to increase cell cycle and myogenic genes while simultaneously downregulating genes involved with quiescence. This promotes quiescence exit and cell cycle re-entry. During the differentiation process, mitochondria transition from

fragmented to elongated, with a subsequent increase in OPA1 protein. Here, in conjunction with the supercomplex assembly factor SCAF1, OPA1 is required to promote the metabolic switch necessary for muscle differentiation. Figure adapted from Baker et al (2022) *Cell Stem Cell* and Triolo et al (2024) *iScience*.

Furthermore, treatment of WT MuSCs with compounds to enhance ROS and GSH, such as rotenone and exogenous GSH, recapitulated the phenotype of OPA1-KO MuSCs; enhancing activation and cell cycle entry, increasing expression of cell cycle related genes, and biasing fate decisions towards commitment[150]. As MuSCs undergo fate decisions, divergence in mitochondrial length can also be seen. Committing MuSCs maintain their fragmented mitochondrial morphology whereas self-renewing MuSCs see mitochondrial elongation re-instigated[150].

The roles of mitochondrial dynamics in MuSCs was also demonstrated in another study, whereby the authors found increased expression of mitochondrial fission factors as MuSCs exit quiescence[154]. In this study, the authors deleted the fission protein Drp1 from MuSCs and found that MuSCs exhibited defects in their ability to exit quiescence and begin expansion[154]. Loss of mitochondrial fission blunted OXPHOS metabolic reprogramming and mitophagy and prevented the efficient expansion of the stem cell pool[154]. Furthermore, restoration of mitochondrial adynamism by deleting MFN1 in DRP1-KO MuSCs restored their proliferative capacity[154].

The role of mitochondrial dynamics in MuSCs also extends to their differentiation ability[155]. Here, as myoblasts begin to differentiate, there is a significant upregulation of OPA1 protein levels[155]. At 24-hours post-differentiation, mitochondria within myoblast fragment and then re-elongate at 72-hours post-differentiation which is accompanied by an increase in OPA1 protein levels and significant cristae remodelling[155]. In contrast to quiescence exit where mitochondrial shape change serves as a signalling stimulus, mitochondrial remodeling during differentiation serves to support a metabolic switch towards OXPHOS with the supercomplex assembly factor SCAF1[153,155].

In summary, changes in mitochondrial shape are essential regulators of MuSC progression, from quiescence to differentiation. Perturbations to this dynamic process results in severe MuSC dysfunction and impairs muscle regeneration. Mitochondria are also the site of production of many metabolites with signalling roles in other stem cells. However, whether mitochondrial shape changes alter metabolites to regulate MuSC fate is unknown.

Chapter 2: Hypothesis and Aims

2.1 Rationale

Stem cell maintenance is essential for whole-body homeostasis and regenerative capacity. An emerging regulator of stem cell maintenance and progression is their metabolic state. Switches in metabolism are necessary to fuel stem cells as they transition through their lineage specifications and provide necessary building blocks for anabolic reactions. However, changes in metabolism are also accompanied by alterations in metabolic intermediates, metabolites, which have profound downstream effects and regulation of stem cell function and progression. Alterations in metabolite abundance in stem cell populations, including MuSCs, may dictate stem cell fate independently of their roles in metabolism.

We have previously demonstrated that mitochondrial shape and OPA1 are essential regulators of MuSC function and progression. Alterations in mitochondrial shape via deletion of OPA1 results in shallow quiescence depth, enhanced activation and cell cycle entry kinetics, and biased fate decisions towards commitment, resulting in stem cell depletion. We identified ROS and GSH as mito-nuclear signals that dictate cell cycle and myogenic gene expression. However, it is unclear whether ROS and GSH are the only signalling molecules regulated by mitochondrial shape that regulate MuSC progression and fate.

2.2 Hypothesis

We hypothesize that mitochondrial dynamics regulates the quiescence to activation transition and cell cycle re-entry through a metabolite signalling mechanism.

2.3 Aims

To determine the role of mitochondrial dynamics in metabolite signalling in MuSCs, there are two experimental aims:

1. Characterize the role of mitochondrial dynamics in MuSC activation, cell entry and progression of MuSCs.
2. Determine the metabolite signalling mechanism regulated by mitochondrial dynamics.

Chapter 3: Materials and Methods

3.1 Animal models

Animal protocols were approved by the University of Ottawa's Animal Care Ethics Committee and adhered to the guidelines of the Canadian Council on Animal Care. All mice were housed and maintained at the Animal Care and Veterinary Service (ACVS) of the University of Ottawa. OPA1-Pax7CreERT2 mouse line was generated in-house (Baker et al., 2022). Mice that were OPA1-floxed and expressed the CreERT2 recombinase were used as OPA1 MuSC knockout (OPA1-KO) mice, and littermate mice that were OPA1-floxed but did not possess the CreERT2 recombinase were used as wild-type controls (OPA1-WT). At 8-10 weeks of age, all mice received Tamoxifen (200 mg/kg) (Sigma T5648, 50 mg/mL dissolved in corn oil) administration via oral gavage for five consecutive days, followed by three days' rest. Mice were used 3-days post-TAM. For OPA1 over-expression mice, transgenic mice with a targeted whole-body mild (1.5x) OPA1 overexpression (OPA1-OE) were utilized (Varanita et al., 2015). OPA1-OE mice were rederived from mice originally described in Varanita et al. (2015) and provided as a gift from Dr. Ruth Slack.

3.2 Cardiotoxin Injury

Prior to cardiotoxin injury, mice were anesthetized by gas inhalation and injected intraperitoneally with 0.1mg/kg buprenorphine. Following anesthesia, 50µl of 10µM cardiotoxin (Sigma 217503) dissolved in phosphate buffered saline (PBS), was injected into the *tibialis anterior* muscle. Mice were left to recover with a heating pad and were monitored for signs of distress. Injured muscles were harvested 7-days post-injury following cervical dislocation.

3.3 *In vivo* succinate injections

For *in vivo* succinate experiments, 8–10-week-old OPA1-WT and OPA1-KO mice were used. At 8-10 weeks of age, all mice underwent tamoxifen gavage (200mg/kg) for five consecutive days followed by three days rest. Three days following the last tamoxifen gavage, the right tibialis anterior muscle of all mice was injured using cardiotoxin, as described above. OPA1-WT mice were injected intraperitoneally with 100µl of PBS and OPA1-KO mice were injected intraperitoneally with 100µl of PBS or 100µl of 100mg/kg succinate. Intraperitoneal injections started at the onset of TAM injections and persisted every other day until harvest at 7-days post-

injury. TA muscles were harvested for cross-section immunofluorescent and H&E analysis, while EDLs from the contralateral uninjured limb were also harvested for further analysis.

3.4 Harvesting TA muscle

Fixation and freezing

At the time of isolation, TA muscles were harvested following cervical dislocation. TA muscle was immediately transferred to a 15mL tube containing cold 5mL of 2% (w/v) paraformaldehyde (PFA) solution (Sigma P6148). TA muscle was left to fix for 30 minutes on ice while rocking. Following fixation, TA muscle was washed in 5mL cold 1XPBS, followed by two rounds of washes in 5mL of cold 0.25M glycine for 10 minutes. Glycine was removed and replaced with 5% w/v sucrose for 2 hours, shaking on ice. TA muscles were then transferred to a 1.5mL Eppendorf tube containing 20% w/v sucrose for 2-3 days at 4°C while rocking. For freezing, TA muscle was embedded by placing the TA in a layer of Clear Frozen Section Compound (VWR-CA95057-838) in a halved 1000µl pipette tip, and frozen in isopentane cooled in liquid nitrogen for 30 seconds. Embedded tissue was immediately placed in a cryogenic tube and stored at -80°C.

Tissue sectioning

Embedded TA muscles were sectioned using the HM525NX Cryostat at the University of Ottawa Histology core. TA muscles were cut in half and the middle portion of the TA was sectioned. 14µm cross-sections were placed on charged glass slides, with three sections per slide. Slides were stored at -80°C for future analysis.

3.5 Isolation of MuSCs

Isolation of MuSCs was done using Magnetic-Activated Cell Sorting (MACS) and Fluorescence Activated Cell Sorting (FACS). For isolation of MuSCs for qPCR, Figure 3C was done using Magnetic-Activated Cell Sorting (MACS) as previously described[153]. For all other experiments where MuSCs were isolated, Fluorescence-activated cell sorting (FACS) was used.

Mice were euthanized by cervical dislocation and all hindlimb muscle was harvested and placed in a 60mm dish containing 3mL 1xPBS. Tendons and excess fat tissue were removed and trimmed muscle was placed in a gentleMACS C-tube (Miltneyi 130-093-237) containing a warmed digestion solution containing 1% w/v Collagenase B (Roche 11088831001) and 0.4% w/v Dispase II (Roche 4942078001) in HAMs F-10 (Wisent 318-050-CL). Using dissection scissors, the

muscle tissue was further minced in the digestion solution and placed in a 37°C bead bath for 10 minutes. The C-tube was then placed in a Miltenyi GentleMACS Octo-Dissociator and dissociated for 27 minutes using the "SLICE_FACS" program. Following dissociation, 5mL of Newborn Calf Serum (NCS) (Wisent 075-150) was added and the slurry was passed through a 100µm filter (Fisher 22363549) into a 50mL tube. The C-tube was rinsed with 10mL of 1xPBS and passed through the 100µm filter. The slurry was divided equally into two 15mL tubes and subsequently spun at 600g for 10 minutes. Supernatant was removed and the first pellet was resuspended in 400µl of red blood cell (RBC) lysis buffer (Sigma R7757) and then transferred to the second tube to resuspend. RBC lysis buffer was incubated for 30 seconds and 10mL of FACS buffer (3mM EDTA, 10% (v/v) FBS in 1xPBS) was added and then spun at 600g for 5 minutes. Supernatant was aspirated and pellet was resuspended in 1mL FACS buffer. Samples were incubated for 30-45 minutes with 2µl of negative selection antibodies including CD31 (mouse, BD Pharmigen 553373), CD45 (mouse, BD Pharmigen 553081), CD11b (mouse, eBioscience 12-0112-82) and Sca1 (mouse, BD Pharmigen 553108) and 10µl of positive selection including VCAM (mouse, Biolegend 105720) and integrin α7 (mouse, Ablab 67-0010-05). Following incubation, FACS buffer was added to a final volume of 15mL and spun at 600g for 5 minutes. Supernatant was removed and pellet was resuspended in 2mL FACS buffer. Samples were then passed through a 50µm Celltrics cell filter (Sysmex 04-29 004-2327). Cells were brought to the Ottawa Hospital Research Institute's Flow Cytometry and Cell Sorting Facility and sorted using a Beckham Coulter MoFlo XDP. Cells were sorted into a 1.5mL Eppendorf containing 200µl FACS buffer and 200µl FBS. Cells were spun down at 4200rpm for 2 minutes and supernatant was removed. Cell pellets were then used immediately or stored at -20°C for future use.

Isolation of GFP MuSCs

For the isolation of GFP^+ MuSCs, preparation of cell suspension is as described above. In contrast, here, only negative selection antibodies were added. Identification of MuSCs during sorting was done by gating for GFP^+ cells.

3.6 MuSC culture

For 24-hour cultures for gene expression analysis, a 24-well plate was used and FBS was used to coat the desired number of wells. Following this, 500µl of culture media (20% (v/v) FBS, 1% (v/v) Chicken Embryo Extract, 1% (v/v) penicillin-streptomycin and 7.5ng/mL bFGF in DMEM 4.5g/L glucose) was added to each well with desired treatments (see Table 3) and placed in a 37°C incubator at 5% CO_2. Immediately following isolation, MuSCs were gently resuspended in 500µl of culture media and cells were transferred to a 24-well plate. Samples were cultured for 24-hours at 37°C, 5% CO_2.

For culture conditions for immunofluorescent analysis, MuSCs were cultured on Matrigel (Corning 354234) coated 8-chamber cell culture slides (CellTreat 229168). Briefly, Matrigel was prepared by diluting 1mL of 5mg/mL Matrigel with 9mL of DMEM (Wisent 319-005-CL). 8-chamber cell culture slides were coated with 200µl of prepared Matrigel and incubated at 37°C for 40 minutes. After incubation, excess Matrigel was removed and each well washed 3x1 minute with PBS. After washing, 250µl of MuSC culture media (DMEM 4.5 g/L glucose, 20% (v/v) FBS, 1% (v/v) chicken embryo extract (CEE), 1% (v/v) penicillin-streptomycin, 7.5 ng/mL bFGF) was added to each well. Following isolation of MuSCs, cells were pelleted at 4200rpm for 2 minutes and supernatant was removed. Cells were resuspended in culture media at a concentration of 10,000 cells per 100µl. 250µl of cell suspension was added to each well, bringing the final volume to 500µl, achieving an approximate cell number of 25,000 MuSCs per well. MuSCs were cultured for 72-hours with designated treatments. Following culture, media was removed from each well and cells were fixed with 250µl of 4% cold PFA for 10 minutes while rocking. Cells were washed 3x5 minutes with 1xPBS and left at 4°C in PBS until future use.

3.7 Isolation of cultured GFP^{high}/GFP^{low} MuSCs

Isolated GFP^{+} MuSCs were cultured on Matrigel coated 6-well plates for 72-hours. After 72-hours in culture, media was aspirated from the 6-well plate. Cells were detached by adding 1.5mL of TrypLE Express (Gibco 12605-010) and incubating at 37°C for 5 minutes, monitoring detachment. After confirming cells were detached, 1.5mL of MuSC culture media was added and the entire volume was transferred to a 15mL falcon tube and spun at 600g for 5 minutes to achieve a cell

pellet. Supernatant was removed and cells were resuspended in 1mL of FACS buffer. Cells were then passed through a 50µm CellTrics filter (04-004-2327) into a 5mL polypropylene round-bottom tube (Falcon 352063). A 2mg/mL stock of DAPI was diluted 1:100 in PBS, and 10µl of this diluted stock was added to the cells. DAPI was used as a viability dye. Samples were taken to the FACS sorter at the Flow Cytometry facility at the Ottawa Hospital Research Institute (OHRI). Sorting was gated on GFP and from all GFP^{+} MuSCs, cells within the 30% upper-limit of GFP intensity (referred hereafter as GFP^{high}) and the 30% lower-limit of GFP intensity (referred hereafter as GFP^{low}) were collected in separate 1.5mL tubes. After isolation, cells were spun down at 4200rpm for 2 minutes, supernatant was removed, and cell pellets were stored at -80°C until further use.

3.8 Isolation and culture of single EDL myofibers

Single EDL myofibers were isolated as previously described by Baker et al. (2022). The Extensor Digitorum Longus (EDL) muscles from both hindlimbs were dissected immediately following cervical dislocation and placed in 2mL of 0.5% (w/v) Collagenase B (Roche 11088815001) for 35-40 minutes in a 37°C water bath. Following digestion, EDL muscles were placed in an FBS-coated 6-well plate (Ultident, 229105) containing EDL wash media (Dulbecco's Modified Eagle's Medium (DMEM) containing 4.5 g/L glucose and 1% (v/v) penicillin-streptomycin) and were allowed to rest for 5 minutes. EDL muscle was gently triturated using P1000 pipette with an FBS-coated tip. to release single myofibers. Debris was removed by washing single EDL fibers in wash media. EDL fibers were fixed in warm 2% PFA in a 24-well plate for 10 minutes at room temperature, followed by 3x5 minute PBS washes. To culture, single EDL fibers were placed in an FBS-coated 24-well plate containing 1mL of EDL culture media (DMEM 4.5 g/L glucose, 20% (v/v) FBS, 1% (v/v) chicken embryo extract (CEE), 1% (v/v) penicillin-streptomycin, 7.5 ng/mL bFGF) and cultured for 4-72 hours. For metabolite treatments, EDL myofibers were treated with 10mM L-Methionine (Millipore Sigma, M9625), 0.1mM Octyl-(S)-2HG (MedChem Express, HY-103641A), 0.2mM Uridine (Millipore Sigma, U3750), 1mM Dimethyl-alpha-ketoglutarate (Millipore Sigma, 349631) or 0.1mM Diethyl-succinate (MedChem Express, HY-Y0836) for 4-72h depending on experimental design. Metabolites were prepared as described in Table 3.

3.9 Immunofluorescence analysis

Immunofluorescence staining of MuSCs

Following culture, media was removed, and cells were fixed with cold 4% PFA for 10 minutes on a rocker at RT. Cells were then washed 3x5 minutes with PBS. Cells were permeabilized with 200µl of permeabilization solution (0.1% (v/v) Triton-X and 100 mM glycine) for 10 minutes while rocking. Permeabilization was removed and cells were blocked with 200µl of blocking solution (5% (v/v) horse serum, 2% (w/v) BSA and 0.1% (v/v) Triton-X in PBS) for 3-hours at room temperature while rocking. After blocking, 100µl of primary antibodies (see Table 2) diluted in blocking solution was added and left to incubate at 4°C overnight on a rocker. Primary antibodies include mouse Pax7 (1:13, DSHB Pax7-S), rabbit Pax7 (1:250, Thermo Fisher Scientific PA1-117), mouse MyoD (1:100, SantaCruz sc-32758), rabbit Ki67 (1:500, ab15580), rabbit Tom20 (1:500 Proteintech 11802-AP), rabbit Calcitonin Receptor (1:100, BioRad AHP3115), chicken GFP (1:1000, Abcam 13970). Primary antibodies were removed, and cells were washed twice with PBS. Secondary antibodies were diluted 1:500 in blocking solution and incubated at room temperature for 1-hour, protected from light. 10 minutes prior to the end of the 1-hour incubation, DAPI (Sigma D9542), was added, diluted 1:500 in blocking solution. Secondary antibodies include Cy3 (1:1000, Jackson 715-165-150) and AlexaFluoro 488 (1:1000, Thermo Fisher Scientific A11001). Cells were washed 3x5 minutes with PBS and a coverslip was mounted using using Epredia Immumount (ThermoFisher, 9990402).

Immunofluorescence staining of EDL myofibers

Following fixation, single myofibers were permeabilized in 0.1% (v/v) Triton-X and 100 mM glycine for 10 minutes at room temperature. Myofibers were blocked in blocking solution containing 5% (v/v) horse serum, 2% (w/v) BSA and 0.1% (v/v) Triton-X in PBS for 5 hours at room temperature. Primary antibodies were diluted in blocking solution and 100µl was added to each well of a 24-well plate and left to incubate rocking overnight at 4°C. Primary antibodies include mouse Pax7 (1:13, DHSB PAX7-S), rabbit Pax7 (1:250, Thermo Fisher Scientific PA1-117), mouse MyoD (1:100, SantaCruz sc-32758), rabbit Ki67 (1:500, ab15580), rabbit Tom20 (1:500 Proteintech 11802-AP). Following primary antibody incubation, myofibers were washed 3x5 minutes with PBS. 200µl of secondary antibodies diluted in blocking solution was added and

left to incubate rocking, covered from light for 1-hour at room temperature. Secondary antibodies include Cy3 (1:1000, Jackson 715-165-150) and AlexaFluoro 488 (1:1000, Thermo Fisher Scientific A11001). After 1-hour, 200µl of blocking solution containing DAPI (1:750, Sigma D9542) was added for 5 minutes. EDL myofibers were mounted on a charged glass slide (Fisher Scientific, 12-550-15) using Epredia Immumount (ThermoFisher, 9990402).

Immunofluorescence staining of muscle sections

Prior to staining, muscle sections were sent for antigen retrieval with citrate buffer (pH=6.0) at the Louise Pelletier Histology Core Facility at the University of Ottawa. Following antigen retrieval, slides were dried using a Kimwipe and a hydrophobic marker was used to circle around each tissue section. Tissue sections were washed with 1xPBS and PBS was aspirated. TA sections were incubated with 50µl blocking solution (3% (w/v) BSA (Tocris 5217) in 1xPBS) in a humidified chamber, by placing a damp piece of paper towel inside of a slide box, for 1-hour. Blocking solution was removed and 50µl of primary antibodies diluted in 3% BSA were added and left to incubate overnight at 4°C. Following incubation, sections were washed 5x2 minutes in 1xPBS and then incubated with IgG-specific biotin (1:250, Jackson Immuno 115-065-205) for 30 minutes. Sections were washed with 1xPBS and incubated with secondary antibodies and DAPI (see Table 2) diluted in 3% BSA for 15 minutes at room temperature. Sections were washed with 1xPBS and coverslips were mounted using Immumount (Fisher Scientific 9990402). Slides were left to dry, covered from light and then placed at 4°C for future use.

Hematoxylin and eosin staining of muscle sections

Slides were retrieved from storage at -80°C and sent the Louise Pelletier Histology Core Facility for Hematoxylin and Eosin staining. Slides were stored at 4°C for future use.

3.10 Microscopy

MuSC activation and cell cycle entry

For imaging of MuSC activation and cell cycle entry (4-hour and 24-hour culture), EDL myofibers were imaged on the 63X objective of a Zeiss Axio.Observer Epifluorescent microscope in the Khacho lab at the University of Ottawa. For each mouse, approximately 6-10 fibers per condition were imaged.

MuSC fate decisions

To evaluate MuSC fate decisions, clusters residing on 72-hour cultured EDL myofibers were imaged on the Zeiss LSM880 (for figures 1D,H and 2K-O, S and V) and the Leica Thunder Imager microscope on the 63X objective at the University of Ottawa Cell Biology and Image Acquisition (CBIA) core. To obtain full images of 3D clusters, Z-stacks with 1.5µm spacing were used. Z-stacked images were and 3D-projected using Fiji in order to produce a 3D image of all z-stacks. For representative images, images were reconstructed using Imaris Viewer. For each mouse, approximately 6-10 fibers per condition were imaged.

Mitochondrial length

To evaluate mitochondrial length, mitochondria within MuSCs residing on EDL myofibers were imaged using the Zeiss LSM880 confocal microscope with Airyscan. Z-stacks with 0.16µm spacing were used to capture all mitochondria within the cell. Airyscan processing was then applied to all images to enhance resolution and signal-to-noise ratio.. Evaluation of mitochondrial length was done by 3D projecting images in Fiji and manually measuring mitochondrial length as previously described[156]. For mitochondrial length quantifications, approximately 50-100 mitochondria were quantified per cell with 5-10 cells imaged.

3.11 Gene expression analysis

RNA extraction from MuSCs

MuSC pellets were retrieved from storage at -80°C and left to thaw on ice. MuSC RNA was isolated using the PicoPure column-based RNA isolation kit (ThermoFisher KIT0214). Following isolation, RNA was quantified using the NanoDrop 2000 spectrophotometer, located at the University of Ottawa. Following quantification, RNA was aliquoted into 5µl aliquots in separate, RNAse-free Eppendorf tubes and stored at -80°C for later use.

Quantitative real-time PCR (RT-qPCR)

RNA was retrieved from storage at -80°C and left to thaw on ice. RNA was then diluted to 5ng/µl in sterile, DNase-free/RNase-free water. Mastermixes for each gene were prepared using 2 kits:

the Qiagen QuantiNova SYBR Green RT-PCR kit (Qiagen 208154) and the Rotor-Gene SYBR RT-QPCR kit (Qiagen, 204174). Each 10µl of Mastermix contained 6.25µl SYBR Green, 1.25µl forward and reverse primer (1.25µM), 1.152µl RNase-free H_2O and 0.1µl reverse transcriptase. Samples were run in triplicate and GAPDH was used as a housekeeping gene. Samples were then added to the Qiagen RotorGene and run with the following parameters: 50°C for 10 minutes, 95°C for 2 minutes, cycling of 95°C for 5 seconds and 60 C for 10 seconds for 40 repeat cycles, melting from 50-99°C with a 1°C rise each step with 90 seconds of pre-melt conditioning on the first step and 5 seconds for each subsequent step. Analysis was done using the Qiagen RotorGene software, using previously generated standard curves for each gene of interest.

3.12 Metabolomic analysis of MuSCs

MuSCs were isolated by FACS and pelleted at 4200rpm for 2 minutes. Following centrifugation, supernatant was removed, and MuSCs were washed with 1mL PBS followed by centrifugation at 4200rpm for 2 minutes. PBS washes were repeated two more times to ensure removal of FACS buffer components. Following PBS washes, cells were fixed by resuspending the pellet in freshly prepared ice-cold 150mM ammonium formate buffer. Cells were then transferred to a new pre-chilled 2mL Eppendorf bead beater tube (Eppendorf; 022363352) and spun down at 4200rpm for 3 minutes using the benchtop centrifuge in the Khacho lab. Fixation buffer was removed, and the pellet was resuspended in 380µl of 50% MeOH/ 50% water solution pre-equilibrated to -20°C, along with 6 washed 1.4mm ceramic beads. Samples were kept in 50% MeOH / 50% water solution at -80°C until all samples were ready for phase-separation extraction. The remaining steps in extraction were done in a 4°C cold-room when possible while keeping samples on dry ice. To extract water-soluble metabolites, samples were vortexed for 10 seconds and 220µl of ice-cold LC/MS-grade ACN (Acetonitrile) was added to each sample, followed by vortexing for another 10 seconds. Samples were then placed in the Roche MagNA Lyser, in the University of Ottawa Common Equipment room 4258 and beat at 4000rpm in 1-minute intervals to ensure samples do not warm, for a total of 2 minutes of beating. Samples were returned to the cold room following beating, 600µl of ice-cold dichloromethane and 300µl of ice-cold water was added to each sample and vortexed for 1 minute. Samples were then left to partition on ice for 10 minutes. Next, samples were spun down in a cooled 1°C centrifuge for 10 minutes at 4000rpm. The upper aqueous phase was pipetted, careful not to disturb the lower 2 phases, and transferred to a fresh, pre-chilled 1.5mL

Eppendorf tube (Eppendorf 022363204). Samples were then sent to the uOttawa Metabolomics Core Facility for analysis. A minimum of 100,000 MuSCs was used for each biological replicate.

3.13 Statistical analyses

Statistical analyses were done using Excel (paired and un-paired student's t-test) and GraphPad Prism (ANOVAs). For all statistical tests, significance is presented as follows: $p<0.05$*, $p<0.01$**, $p<0.001$***.

Primer	Forward sequence (5' → 3')	Reverse sequence (5' → 3')	Method
OPA1 flox	TTAAGACACCCCAAGAGCTTGC	CCAGCTTAGATCCCATTTGTTGACAG	Genotyping
Control	TTACGTCCATCGTGGACAGC	TGGGCTGGGTGTTAGCCTTA	Genotyping
Cre	GAACCTGATGGACATGTTCAGG	AGTGCGTTCGAACGCTAGAGCCTGT	Genotyping
OPA1tg-WT	CTCCGGAAAGCAGTGAGGTAAG	GAGGGAGAAAAATGCGGAGTG	Genotyping
OPA1tg-OE	GATAGGTCAGGTAAGCAAGCAAC	GCAATGACGTGGTCCTGTTTTG	Genotyping
Pax7	GACGACGAGGAAGGAGACAA	ACATCTGAGCCCTCATCCAG	qPCR
CD34	CGCAGTTGGAGCCCTACAG	CCTCCACCATTCTCCGTGTAAT	qPCR
MyoD	TACAGTGGCGACTCAGATGC	CTGGGTTCCCTGTTCTGTGT	qPCR
MyoG	CAGTGAA TGCAACTCCCACA	ACCCAGCCTGACAGACAATC	qPCR
OPA1	CGACTTTGCCGAGGATAGCTT	CGTTGTGAACACACTGCTCTTG	qPCR
DRP1	TTACGGTTCCCTAAACTTCACG	GTCACGGGCAACCTTTTACGA	qPCR
MFN1	CCTACTGCTCCTTCTAACCCA	AGGGACGCCAATCCTGTGA	qPCR
MFN2	CTGGGGACCGGATCTTCTTC	CTGCCTCTCGAAATTCTGAAACT	qPCR
IDH3	TGGGTGTCCAAGGTCTCTC	CTCCCACTGAATAGGTGCTTTG	qPCR
OGDH	GTTTCTTCAAACGTGGGGTTCT	GCATGATTCCAGGGGTCTCAAA	qPCR
SDHA	GGAACACTCCAAAAACAGACCT	CCACCACTGGGTATTGAGTAGAA	qPCR
GAPDH	TCGGTGTGAACGGATTTG	GGTCTCGCTCCTGGAAGA	qPCR

Table 1. List of primers used for genotyping and qPCR.

Assay	Antibody	Company	Cat. #	Dilution	Type
FACS	PE rat anti-mouse Sca1	BD Pharmingen	553108	2µl/mouse	Negative selection
	PE rat anti-mouse CD45	BD Pharmingen	553081	2µl/mouse	Negative selection
	PE rat anti-mouse CD31	BD Pharmingen	553373	2µl/mouse	Negative selection
	PE rat anti-mouse CD11b	eBiosciences	12-0112-82	2µl/mouse	Negative selection
	647 conjugated alpha integrin 7	Ablab	67-0010-05	10µl/mouse	Positive selection
	PE-Cy7 conjugated CD106	Biolegend	105720	10µl/mouse	Positive selection
Immunofluorescent staining of MuSCs	Pax7 (mouse)	DSHB	PAX7-S	1:13	Primary
	Pax7 (rabbit)	Invitrogen	PA1-117	1:50	Primary
	Tom20 (rabbit)	ProteinTech	11802-1-AP	1:500	Primary
	MyoD (mouse)	SantaCruz	sc-32758	1:100	Primary
	Ki67 (rabbit)	Abcam	ab16667	1:500	Primary
	GFP (chicken)	Abcam	ab13970	1:1000	Primary
	CalcR (rabbit)	BioRad	AHP3115	1:500	Primary
	Alexa-Fluor 488 (mouse)	Invitrogen	A11001	1:1000	Secondary
	Alexa-Fluor 488 (rabbit)	Invitrogen	A11008	1:1000	Secondary
	Cy3 (mouse)	Jackson	765-165-150	1:1000	Secondary
	Cy3 (rabbit)	Jackson	711-165-152	1:1000	Secondary
Immunofluorescent staining of muscle sections	Pax7 (mouse)	DSHB	PAX7-S	1:13	Primary
	Pax7 (rabbit)	Invitrogen	PA1-117	1:50	Primary
	Ki67 (rabbit)	Abcam	ab15580	1:1000	Primary
	MyoG (mouse)	DSHB	FD5	1:100	Primary
	Alexa-Fluor 488 (rabbit)	Invitrogen	A11008	1:500	Secondary
	Biotin	Jackson	115-065-205	1:250	Secondary
	Streptavidin-Cy3	Jackson	016-160-084	1:250	Secondary

Table 2. List of antibodies used.

Metabolite	Concentration	Solvent	Use
Dimethyl-αKG	1mM	DMSO	*In vitro*
Diethyl-succinate	0.1mM	DMSO	*In vitro*
Octyl-(S)-2-hydroxyglutarate	0.1mM	DMSO	*In vitro*
L-Methionine	10mM	H_2O	*In vitro*
Uridine	0.2mM	H_2O	*In vitro*
Succinic acid	100mg/kg	PBS	*In vivo*

Table 3. List of metabolites and their concentrations used in this study.

Chapter 4: Results

4.1 Changes in OPA1 expression alter the metabolome of MuSCs

To understand the role of mitochondrial shape changes as a signalling mechanism governing stem cell function, we utilized two mouse models of altered mitochondrial shape: a MuSC-specific deletion of the mitochondrial fusion protein OPA1 (OPA1-KO) and a whole-body OPA1 overexpression (OPA1-OE). Single EDL myofibers were isolated from OPA1-WT and OPA1-KO and fixed immediately after isolation (t=0h) or cultured for 4, 24 and 72-hours to monitor activation ($Pax7^{+}/MyoD^{+}$), cell cycle entry ($Pax7^{+}/Ki67^{+}$) and fate decisions ($Pax7^{+/-}/MyoD^{+/-}$), respectively. We confirmed our previous findings showing that OPA1-KO MuSCs display highly fragmented mitochondria (Figure 7A), have enhanced activation and cell cycle entry kinetics (Figure 7B and C) and show a bias in fate decisions towards commitment at the expense of self-renewal (Figure 7D). Next, we sought to understand the effect of OPA1 overexpression in MuSCs. Mitochondria within OPA1-OE MuSCs display longer mitochondria compared to their WT counterparts (Figure 7E). To evaluate the kinetics of OPA1-OE MuSCs *in vitro*, we utilized the single EDL myofiber system with the above mentioned timepoints to evaluate their activation, cell cycle entry and fate decisions. In contrast to OPA1-KO MuSCs, we find that OPA1-OE MuSCs display decreased activation and cell cycle entry kinetics (Figure 7F and G) and have biased fate decisions towards self-renewal (Figure 7H). This suggested that overexpression of OPA1 and increased mitochondrial length in MuSCs alters their activation and cell cycle entry kinetics. Taken together, deletion of OPA1 places MuSCs in a primed quiescent state and biases fate towards commitment, whereas overexpression of OPA1 and mitochondrial elongation places MuSCs in a state of deeper quiescence and biases fate decisions towards self-renewal.

Mitochondrial metabolites have distinct signalling capacities and can alter various cellular functions[89,91]. Metabolites, through various downstream events, can also dictate the fate of various stem cell populations[88,90,106,107,111,157]. This led us to question whether changes in mitochondrial shape may alter essential signalling metabolites responsible for the opposing phenotypes observed in OPA1-KO and OPA1-OE MuSCs (Figure 7I and J). To this end, we profiled the metabolome of freshly FACS isolated OPA1-KO and OPA1-OE MuSCs using targeted metabolomic analysis (Figure 7I and J). Heatmaps of metabolomics data were generated using MetaboAnalyst by inputting metabolite concentrations normalized to cell number. The data was further log transformed and scaled using Pareto scaling to reduce the impact of variables with high variability

while retaining their original importance in the dataset[158]. Generation of heatmaps was done using Euclidean distance and Ward clustering. Heatmaps show metabolite fold-change for each biological replicate for each metabolite. This revealed a total of 29 significantly altered metabolites ($p<0.05$, LogFC > 1.5) in OPA1-KO MuSCs and 39 significantly altered metabolites in OPA1-OE MuSCs (Figure 7K). Strikingly, all significantly altered metabolites in OPA1-KO MuSCs were decreased in abundance relative to OPA1-WT, whereas all significantly altered metabolites in OPA1-OE displayed increased abundance compared to WT (Figure 7I-K). In addition, 19 significantly altered metabolites were shared between OPA1-KO and OPA1-OE MuSCs (Figure 7K). Next, we performed pathway enrichment analysis using Metaboanalyst by uploading the names of commonly altered metabolites between OPA1-KO and OPA1-OE MuSCs. Metabolites were matched against the KEGG database to uncover possible altered metabolic pathways. Pathway enrichment analysis of the 19 significantly altered common metabolites revealed an enrichment for metabolic pathways including the malate-aspartate shuttle, glutamate metabolism, urea cycle, purine metabolism and the TCA cycle (Figure 7L). Furthermore, significantly altered metabolites shared between OPA1-KO and OPA1-OE MuSCs included alpha-ketoglutarate, succinate, 2-hydroxyglutarate, uridine, methionine (Figure 7M and N). Taken together, the above results demonstrate that changes in mitochondrial shape are sufficient to alter the global metabolite profile of MuSCs, including metabolites with known downstream signalling roles.

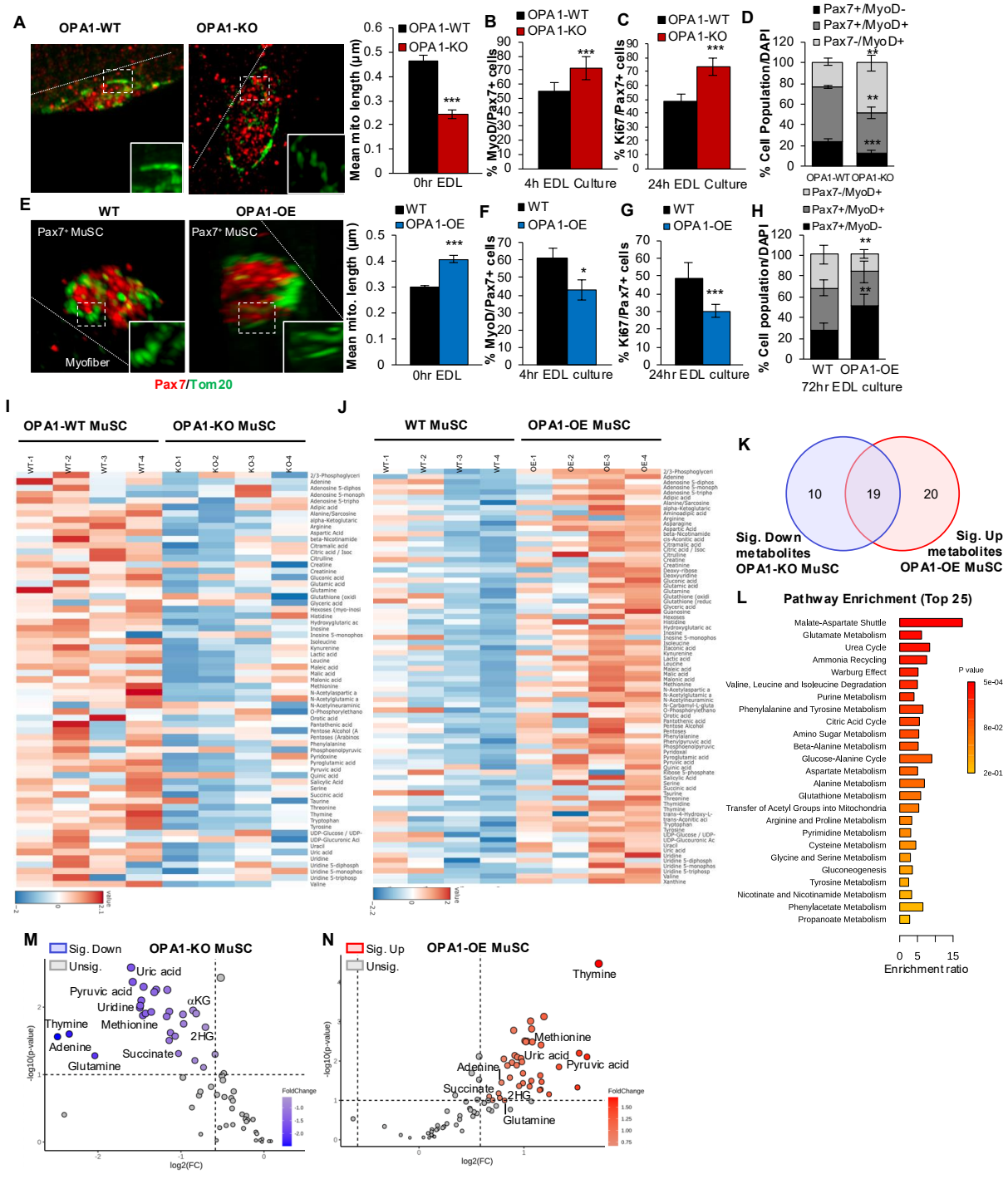

Figure 7. OPA1 regulates the metabolite profile of MuSCs. (A) Confocal 3D reconstruction of mitochondria stained with Tom20 in OPA1-WT and OPA1-KO MuSCs at T=0h. n=5-6 mice, mean ± SD. (B) Quantification of Pax7+ cells expressing MyoD in OPA1-WT and OPA1-KO EDL myofibers at 4h in culture. n=8 mice, mean ± SD. (C) Quantification of Pax7+ cells expressing Ki67 on OPA1-WT and OPA1-KO EDL myofibers at 24h in culture. n=7 mice, mean ± SD. (D) Quantification of Pax7+ and MyoD+ cells at 72h in culture on OPA1-WT and OPA1-KO

myofibers. n=4 biological replicated, mean ± SD. (E) Confocal 3D reconstruction of mitochondrial length in WT and OPA1-OE MuSCs at T=0h. n=4 mice, mean ± SD. (F) Pax7+ cells expressing MyoD on WT and OPA1-OE EDL myofibers at 4h in culture. n=3 mice, mean ± SD. (G) Pax7+ cells expressing Ki67 on WT and OPA1-OE EDL myofibers at 24h in culture. n=7 mice, mean ± SD. (H) Pax7+ and MyoD+ cells at 72h in culture on OPA1-WT and OPA1-KO myofibers. n=5 mice, mean ± SD. (I) Schematic representing the experimental paradigm for metabolomics in OPA1-KO and OPA1-OE MuSCs. (J) Heatmap of all identified metabolites in OPA1-WT and OPA1-KO MuSC metabolomics. n=4 mice. (K) Heatmap of all identified metabolites in WT and OPA1-OE MuSC metabolomics. n=4 mice. (L) Venn diagram showing the significantly altered metabolites in common between OPA1-KO and OPA1-OE MuSCs. (M and N) Fold change of significantly altered metabolites in OPA1-KO (M) and OPA1-OE (N) MuSCs, generated using MetaboAnalyst. (O) Pathway enrichment analysis of the significantly altered metabolites in common between OPA1-KO and OPA1-OE MuSCs, generated using MetaboAnalyst. *Panels I-N were generated by Dr. Mireille Khacho.*

4.2 OPA1-regulated metabolites alter MuSC progression and fate

We next questioned whether commonly altered metabolites in OPA1-KO and OPA1-OE MuSCs are sufficient to alter the progression and fate of WT MuSCs *in vitro*. To investigate this, we selected 5 metabolites that were significantly altered in both OPA1-KO and OPA1-OE MuSCs: alpha-ketoglutarate (αKG), succinate, 2-hydroxyglutarate (2-HG), methionine and uridine. Single EDL myofibers were isolated from WT mice, and cultured for 4, 24 and 72-hours to monitor activation, cell cycle entry and fate decisions. Additionally, given the cell-impermeable nature of some metabolites in their native form (αKG, Succinate and 2-HG), we utilized esterified forms of these metabolites to ensure cell permeability (dimethyl-αKG, diethyl succinate and octyl-(S)-2HG). At 4-hours in culture, we find that exogenous treatment with αKG, succinate, uridine and 2-HG lead to a significantly increased proportion of activated cells (Pax7+/MyoD+) (Figure 8A-C and E). Treatment of WT fibers with methionine had no effect on their activation (Figure 8D). At 24-hours in culture, we find similar results whereby αKG, succinate, 2-HG and uridine enhanced the cell cycle entry of WT MuSCs (Figure 8F-H and J). In contrast to having no effect at 4-hours in culture, here we find that methionine leads to a significant decrease in WT MuSC cell cycle entry (Figure 8I). We next investigated whether 72-hour treatment with exogenous metabolites is sufficient to alter MuSC fate decisions. Here, conversely, we observe metabolite-specific capacities to alter MuSC fate. WT MuSCs treated with αKG led to a significant shift in fate towards commitment at the expense of self-renewal (Figure 8K). Opposingly, succinate treatment was sufficient to significantly enhance self-renewal, while also decreasing the proportion of committed cells (Figure 8L). Treatment with 2HG bore no effect on MuSC fate (Figure 8M) whereas methionine slightly, but significantly, decreased self-renewal (Figure 8N). Lastly, uridine treatment significantly reduced self-renewal and enhanced commitment, albeit not as drastically as is observed with αKG treatment (Figure 8O). Taken together, metabolites altered by mitochondrial shape possess both converging and diverging abilities to alter MuSC progression and fate.

As previously stated, OPA1-KO MuSCs have enhanced activation, cell cycle entry and biased fate decisions towards commitment at the expense of self-renewal, whereas OPA1 overexpression delays activation and cell cycle entry and promotes self-renewal over commitment (Figure 7A-H). Given these drastically opposing phenotypes, we next sought to determine whether

addition of exogenous metabolites in OPA1-KO and OPA1-OE MuSCs could rescue their phenotypes. Since methionine was the only tested metabolite sufficient to decrease cell cycle entry, we treated OPA1-KO myofibers with exogenous methionine for 24-hours and find that methionine is sufficient to rescue the enhanced cell cycle entry of OPA1-KO MuSCs (Figure 8Q). Additionally, succinate was the only tested metabolite that promoted self-renewal and decreased commitment. Thus, we questioned whether addition of succinate to OPA1-KO MuSCs would be sufficient to rescue their fate. We find that succinate can restore the biased fate decisions of OPA1-KO and restores their self-renewal and commitment to WT levels (Figure 8R). Multiple tested metabolites were sufficient to enhance the activation and cell cycle entry of WT MuSCs, thus we supplemented OPA1-OE MuSCs with these metabolites to determine if they would rescue delayed activation and cell cycle entry. We cultured OPA1-OE myofibers with either αKG, 2-HG, succinate or uridine and find that these metabolites restore both the delayed activation and delayed cell cycle entry of OPA1-OE MuSCs (Figure 8S and T). Lastly, we attempted to restore the fate decisions of OPA1-OE MuSCs by addition of αKG, which promoted commitment at the expense of self-renewal in WT MuSCs (Figure 8K). We find OPA1-OE MuSCs treated with αKG restores their fate decisions to WT (Figure 8U). With this data, we have identified multiple metabolites altered by mitochondrial shape which possess distinct abilities to alter MuSC progression and fate and restores the phenotypes of OPA1-KO and OPA1-OE MuSCs in a metabolite-specific manner.

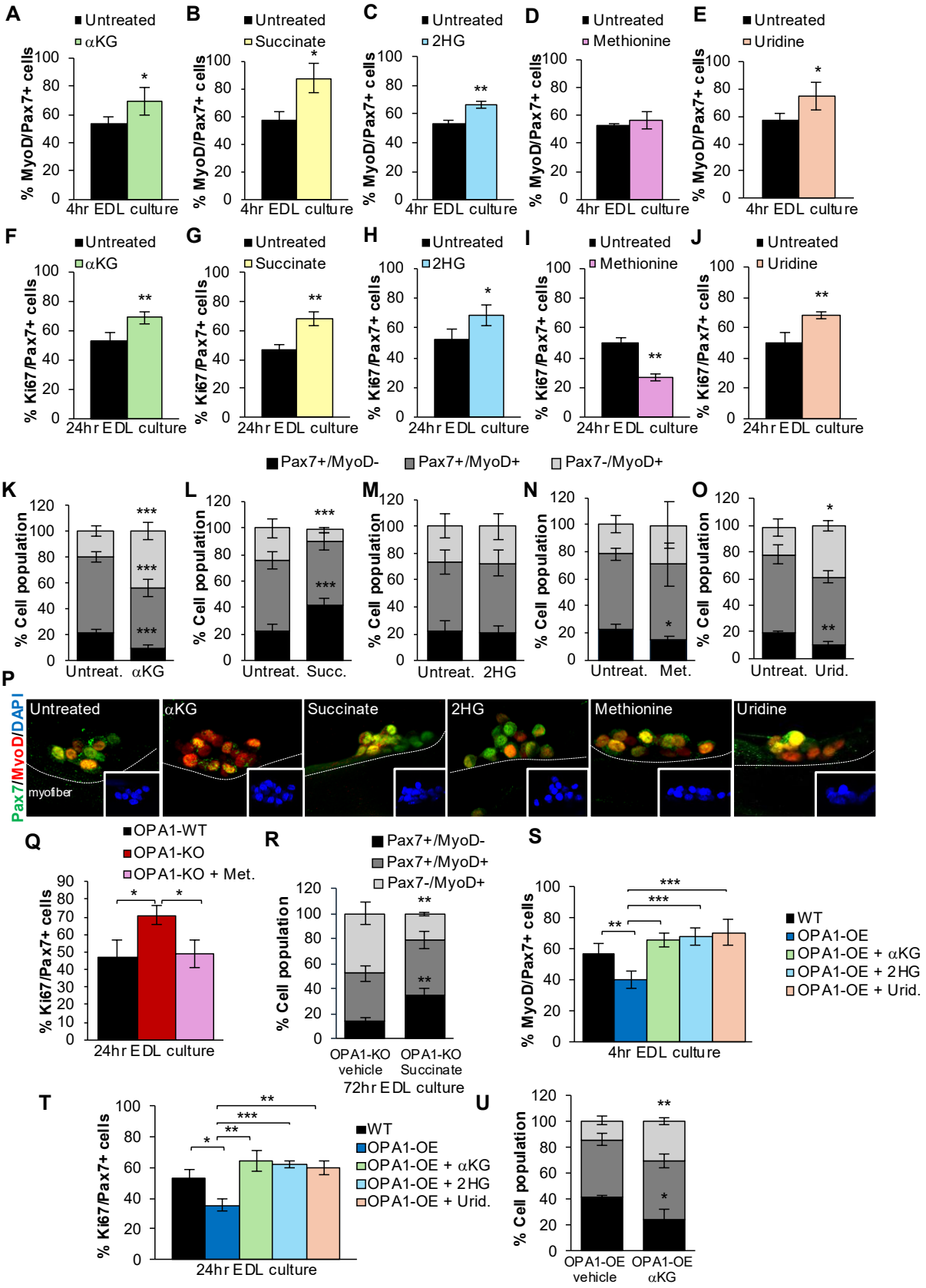
A
Untreated
αKG
% MyoD/Pax7+ cells
4hr EDL culture
B
Untreated
Succinate
% MyoD/Pax7+ cells
4hr EDL culture
C
Untreated
2HG
% MyoD/Pax7+ cells
4hr EDL culture
D
Untreated
Methionine
% MyoD/Pax7+ cells
4hr EDL culture
E
Untreated
Uridine
% MyoD/Pax7+ cells
4hr EDL culture
F
Untreated
αKG
% Ki67/Pax7+ cells
24hr EDL culture
G
Untreated
Succinate
% Ki67/Pax7+ cells
24hr EDL culture
H
Untreated
2HG
% Ki67/Pax7+ cells
24hr EDL culture
I
Untreated
Methionine
% Ki67/Pax7+ cells
24hr EDL culture
J
Untreated
Uridine
% Ki67/Pax7+ cells
24hr EDL culture
Pax7+/MyoD-
Pax7+/MyoD+
Pax7-/MyoD+
K
% Cell population
Untreat.
αKG
L
% Cell population
Untreat.
Succ.
M
% Cell population
Untreat.
2HG
N
% Cell population
Untreat.
Met.
O
% Cell population
Untreat.
Urid.
P
Pax7/MyoD/DAPI
Untreated
αKG
Succinate
2HG
Methionine
Uridine
myofiber
Q
OPA1-WT
OPA1-KO
OPA1-KO + Met.
% Ki67/Pax7+ cells
24hr EDL culture
R
Pax7+/MyoD-
Pax7+/MyoD+
Pax7-/MyoD+
% Cell population
OPA1-KO vehicle
OPA1-KO Succinate
72hr EDL culture
S
% MyoD/Pax7+ cells
4hr EDL culture
WT
OPA1-OE
OPA1-OE + αKG
OPA1-OE + 2HG
OPA1-OE + Urid.
T
% Ki67/Pax7+ cells
24hr EDL culture
WT
OPA1-OE
OPA1-OE + αKG
OPA1-OE + 2HG
OPA1-OE + Urid.
U
% Cell population
OPA1-OE vehicle
OPA1-OE αKG

Figure 8. OPA1-regulated metabolites play distinct roles in directing MuSC activation, cell cycle entry and fate decisions. (A) Pax7+ cells expressing MyoD on WT myofibers treated with alpha-ketoglutarate (αKG) for 4h. n=4 mice, mean ± SD. (B) Pax7+ cells expressing MyoD on WT myofibers treated with succinate for 4h. n=3 mice, mean ± SD. (C) Pax7+ cells expressing MyoD on WT myofibers treated with 2-hydroxyglutarate (2HG) for 4h. n=4 mice, mean ± SD. (D) Pax7+ cells expressing MyoD on WT myofibers treated with methionine for 4h. n=3 mice, mean ± SD. (E) Pax7+ cells expressing MyoD on WT myofibers treated with uridine for 4h. n=4 mice, mean ± SD. (F) Pax7+ cells expressing Ki67 on WT myofibers treated with αKG for 24h. n=6 mice, mean ± SD. (G) Pax7+ cells expressing Ki67 on WT myofibers treated with succinate for 24h. n=3 mice, mean ± SD. (H) Pax7+ cells expressing Ki67 on WT myofibers treated with 2HG for 4h. n=5 mice, mean ± SD. (I) Pax7+ cells expressing Ki67 on WT myofibers treated with methionine for 4h. n=4 mice, mean ± SD. (J) Pax7+ cells expressing Ki67 on WT myofibers treated with uridine for 4h. n=4 mice, mean ± SD. (K) Pax7+ and MyoD+ cells on WT myofibers treated for 72h with αKG. n=8 mice, mean ± SD. (L) Pax7+ and MyoD+ cells on WT myofibers treated for 72h with succinate. n=6 mice, mean ± SD. (M) Pax7+ and MyoD+ cells on WT myofibers treated for 72h with 2HG. n=3 mice, mean ± SD. (N) Pax7+ and MyoD+ cells on WT myofibers treated for 72h with methionine. n=3 mice, mean ± SD. (O) Pax7+ and MyoD+ cells on WT myofibers treated for 72h with uridine. n=3 mice, mean ± SD. (P) Representative 3D reconstructions of cell clusters imaged at 72h following treatment with identified metabolites. (Q) Schematic summarizing the effect of exogenous treatment of OPA1-regulated metabolites on MuSC progression. (R) Pax7+ cells expressing Ki67 on 24h untreated OPA1-WT and OPA1-KO and methionine treated OPA1-KO myofibers. n=3 mice, mean ± SD. (S) Pax7+ and MyoD+ cells in 72h untreated and succinate treated OPA1-KO myofibers. n=3 mice, mean ± SD. (T) Pax7+ cells expressing MyoD on 4h cultured WT and OPA1-OE myofibers treated with identified metabolites. n=7 mice, mean ± SD. (U) Pax7+ cells expressing Ki67 on 24h cultured WT and OPA1-OE myofibers treated with identified metabolites. n=3 mice, mean ± SD. (V) Pax7+ and MyoD+ cells in 72h untreated and αKG treated OPA1-OE myofibers. n=3 mice, mean ± SD.

4.3 αKG and succinate differentially guide MuSCs towards opposing fates

Treatment of WT MuSCs with αKG results in a similar fate decisions phenotype to OPA1-KO MuSCs (Figure 7D and 8K), whereas succinate treatment promoted self-renewal in a manner similar to OPA1-OE MuSCs (Figure 7H and 8L). Given the striking similarities between these treatments and genotypes, we questioned whether there is fine-tuned balance or ratio of these two metabolites in MuSCs that is responsible for directing MuSC fate. Thus, we investigated the [αKG]:[succinate] ratio in OPA1-KO and OPA1-OE MuSCs. Interestingly, while all significantly altered metabolites in OPA1-KO MuSCs are decreased, we identified a significant increase in the [αKG]:[succinate] ratio in OPA1-KO MuSCs compared to their wild-type counterparts (Figure 9A). In contrast to this, we find that the [αKG]:[succinate] ratio in OPA1-OE MuSCs is significantly decreased (Figure 9B). To find a potential explanation for differences in this ratio, we analyzed the expression of key TCA cycle enzymes involved in αKG and succinate synthesis. Specifically, we examined the expression of isocitrate dehydrogenase (IDH) which convert isocitrate to αKG; oxoglutarate dehydrogenase (Ogdh) which converts αKG to succinyl-CoA; and Sdha which is a component of the succinate dehydrogenase complex which converts succinate to fumarate. This revealed that OPA1-KO MuSCs exhibit an increase in *Idh3* expression, which is the rate limiting step in the TCA cycle, and decrease in *Ogdh* (Figure 9C). This would suggest an increase in αKG synthesis and decrease in its downstream utilization (Figure 9C and F). In contrast, OPA1-OE MuSCs exhibit a significant increase in *Ogdh* expression and a significant decrease in *Idh3* and *Sdha* (Figure 9D and E). This would suggest an overall decrease in αKG synthesis and an increase in its utilization and formation towards succinate (Figure 9F). Taken together, differences in the [αKG]:[succinate] ratio may originate from the TCA cycle (Figure 9F).

We hypothesized that increased [αKG]:[succinate] ratio pushes MuSCs towards commitment, as is observed in OPA1-KO MuSCs (Figure 7D), while a decreased ratio may promote self-renewal, as is seen in OPA1-OE MuSCs (Figure 7H). To investigate this, we exogenously altered the ratio of [αKG]:[succinate] in WT myofibers by culturing for 72h with αKG and increasing concentrations of succinate. As previously demonstrated (Figure 8K), treatment with αKG alone promoted commitment, however addition of succinate at increasing concentrations, thereby decreasing the [αKG]:[succinate] ratio, led to a ratio-dependent increase in self-renewal and decrease in commitment (Figure 9G). Of note, co-treatment of WT MuSCs

with αKG and succinate at their established concentrations had no effect of fate decisions. Taken together, this demonstrates that manipulation of the [αKG]:[succinate] ratio is sufficient to direct the fate of MuSCs.

Currently, we have demonstrated that treatment of WT MuSCs for 72h with αKG or succinate is sufficient to alter the fate decisions. However, we questioned whether the full 72h treatment was necessary to direct MuSC fate. To investigate this, we isolated WT myofibers and cultured for 72h with different timings of succinate treatment; from 0 to 24h, 0 to 48h and 0 to 72h (Figure 9H). As seen previously, a full 72h treatment of succinate from 0 to 72h lead to a significant increase in self-renewal and decrease in commitment (Figure 9I). Interestingly, succinate treatment for only the first 24h of culture, significantly decreased commitment (Figure 9I). Self-renewal was also increased however did not reach significance. Additionally, succinate treatment for the first 48h of the total 72h culture time significantly increased self-renewal and decreased commitment to similar levels as the full 72h succinate treatment (Figure 9I). Furthermore, we find that treatment of WT MuSCs with αKG for the first 24 or 48h lead to significant increases in commitment and decreased self-renewal, similar to the full 72h treatment (Figure 9J). Next, we questioned whether delayed treatment with αKG or succinate would yield similar changes to fate decisions. To investigate, we isolated WT myofibers and cultured for 72-hours, however, here, we added treatments from 24h-72h or from 48-72h (Figure 9K). Strikingly, while succinate treatment from 0-24h or 0-48h lead to decreased commitment and increased self-renewal, here we find that delayed treatment from 24-72h had no effect on self-renewal but maintained its inhibitory effet on commitment (Figure 9L). Succinate treatment from 48-72h had a more drastic effect whereby in this case, both self-renewal and commitment are greatly reduced, and the vast majority of cells remain in their activated state (Pax7+/MyoD+) (Figure 9L). Lastly, delayed αKG treatment from 24-72h was sufficient to maintain enhanced commitment at the expense of self-renewal, however, treatment from 48-72h lead to fate decisions similar to untreated (Figure 9M). Altogether, this data demonstrates that αKG and succinate are required at the onset of MuSC progression to alter their fate.

We were particularly interested that succinate, regardless of the time or timing of treatment, maintained its inhibitory effect on commitment (Figure 9I and L). This prompted us to consider whether the decisions to self-renew or commit occur concomitantly or whether one precedes the other. We reasoned that commitment may occur prior to self-renewal given that many of the

cellular processes that promote the exit from quiescence and activation of MuSCs, such as mitochondrial fragmentation, ROS/GSH signalling, increased myogenic gene expression, enhanced metabolism, etc., need to drastically revert in order to self-renew and return to quiescence, whereas these processes are maintained during the commitment stage[1,153,154]. Thus, we performed a time course analysis of MuSC fate decisions in WT myofibers and analyzed the proportion of cells expressing Pax7 and/or MyoD at 0, 24, 36, 48, 60 and 72 hours in culture. MuSCs at 0h are predominantly Pax7+/MyoD-, indicating a majority of quiescent MuSCs (Figure 9N). At 24 hours, a drastic switch in population is observed, whereby the majority of MuSCs are activated and co-express both Pax7 and MyoD. Interestingly, a small proportion of cells are Pax7-/MyoD+ (Figure 9N). As time continued, we observed a gradual increase in the number of committed (Pax7-/MyoD+) cells that precedes the emergence of self-renewing cells (Pax7+/MyoD-). In fact, at 36h in culture, approximately 15% of cells are committed whereas no cells are self-renewed (Figure 9O). From 36h onwards to 72h in culture, there is consistently a significantly higher number of committed cells than there are self-renewed. This time course demonstrates that the emergence of committed MuSCs occurs prior to self-renewal.

Given that succinate and αKG treatment for only the first 24h of culture is sufficient to alter MuSC fate, we questioned whether differences in cell identity are observed prior to the first cell division. Thus, we cultured WT myofibers for 24h with αKG or succinate and analyzed the proportion of cells expressing Pax7 and/or MyoD. Similar to our time course data (Figure 9P), we find that at 24h, untreated MuSCs are predominantly Pax7+/MyoD+, with a very small percentage committed cells (Pax7-/MyoD+). Interestingly, 24h αKG treatment led to a significant increase in the percentage of committed cells (Figure 9P and Q). In contrast, 24h succinate treatment led to a significant increase in self-renewing cells (Pax7+/MyoD-) and fully abolished the population of committed cells (Figure 9P and Q). Thus, αKG and succinate can alter the fate of MuSCs prior to their first division.

This prompted us to question whether αKG and succinate alter the fate of MuSCs by altering their gene expression. Therefore, we isolated WT MuSCs and treated for 24h with αKG or succinate. After 24h treatment, we find that αKG significantly decreases Pax7 expression whereas succinate significantly increased its expression (Figure 9R). Furthermore, gene expression of MyoD is greatly reduced in succinate treated MuSCs, whereas no effect was seen in αKG treated

cells (Figure 9S). With the above data, this demonstrates that αKG and succinate alter the identity of MuSCs by rapidly modifying the expression of key stemness and myogenic genes.

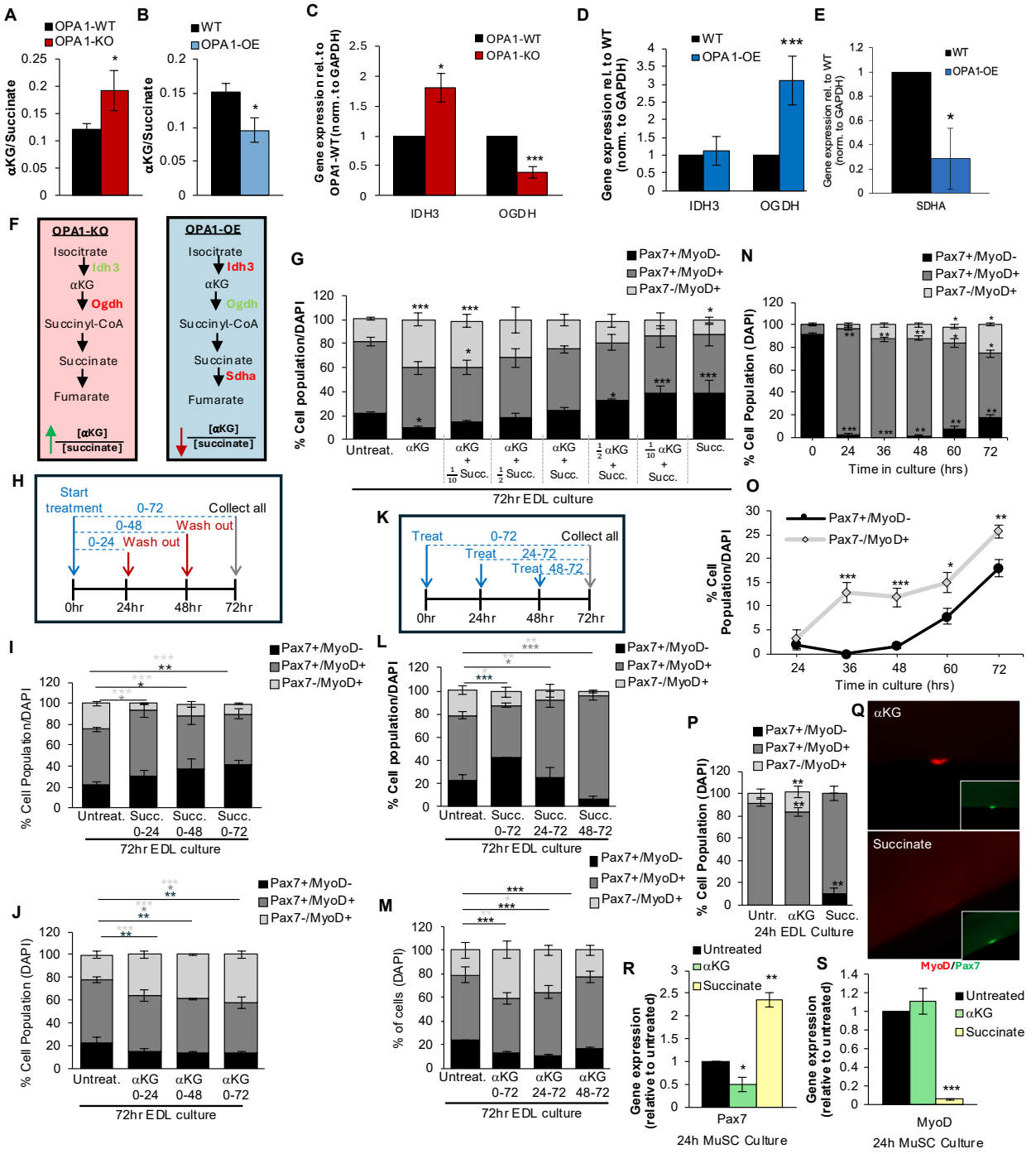

Figure 9. aKG and succinate differentially guide MuSCs towards opposing cell fate decisions
(A) Ratio of αKG to succinate in OPA1-WT and OPA1-KO MuSCs identified in metabolomic analysis. (B) Ratio of αKG to succinate in WT and OPA1-OE MuSCs identified in metabolomic analysis. (C) qPCR of IDH3 and OGDH gene expression in OPA1-KO MuSCs. n=3 mice, mean ± SD. (D) qPCR of IDH3 and OGDH gene expression in OPA1-OE MuSCs. n=3 mice, mean ± SD. (E) qPCR of Sdha gene expression in OPA1-OE MuSCs. n=3 mice, mean ± SD. (F) Schematic

demonstrating how observed differences in TCA cycle enzymes may contribute to altered [αKG]:[succinate] ratio in OPA1-KO and OPA1-OE MuSCs. (G) Pax7+ and MyoD+ expressing MuSCs at 72h in WT myofibers treated with altered ratios of exogenous αKG and succinate. n=4 mice, mean ± SD. (H) Schematic of experimental procedure for assessing the impact of αKG and succinate treatment times on WT MuSC fate decisions. (I) Pax7+ and MyoD+ cells on WT myofibers cultured for 72h following designated succinate treatment times. n=3 mice, mean ± SD. (J) Pax7+ and MyoD+ cells on WT myofibers cultured for 72h following designated αKG treatment times. n=4 mice, mean ± SD. (K) Schematic of experimental procedure for assessing the impact of αKG and succinate treatment timing on WT MuSC fate decisions. (L) Pax7+ and MyoD+ cells on WT myofibers cultured for 72h following designated delayed succinate treatment times. n=3 mice, mean ± SD. (M) Pax7+ and MyoD+ cells on WT myofibers cultured for 72h following designated delayed αKG treatment times. n=3 mice, mean ± SD. (N) Time course of WT MuSCs expressing Pax7 and MyoD on EDL myofibers. n=6 mice, mean ± SD. (O) Percentage of Pax7+/MyoD- and Pax7-/MyoD+ cells from (N). n=6 mice, mean ± SD. (P) Pax7+ and MyoD+ cells on 24h untreated, αKG or succinate treated WT myofibers. n=6 mice, mean ± SD. (Q) Representative microscopy images of the presence of Pax7+/MyoD+ and Pax7+/MyoD- cells on WT myofibers following 24h αKG and succinate treatment. (R) qPCR of Pax7 gene expression in WT MuSCs following 24h αKG or succinate treatment. n=3 mice, mean ± SD. (S) qPCR of MyoD gene expression in WT MuSCs following 24h αKG or succinate treatment. n=3 mice, mean ± SD. *Panels 9H and K were generated by Dr. Mireille Khacho.*

4.4 αKG and succinate alter mitochondrial morphology in MuSCs

Thus far, we have presented data highlighting that the [αKG]:[succinate] ratio alters the fate of MuSCs by rapidly altering the expression of both stemness and myogenic genes. Our previous work and work by others have demonstrated that mitochondrial shape is a key driver of MuSC fate[153,154]. As mentioned previously, forced mitochondrial fragmentation via deletion of OPA1 pushes MuSCs towards commitment at the expense of self-renewal, whereas mitochondrial elongation via overexpression of OPA1 pushes MuSCs towards self-renewal (Figure 7D and H). Since αKG presents a similar phenotype to OPA1-KO MuSCs and succinate presents a similar phenotype to OPA1-OE MuSCs, we questioned whether these treatments alter mitochondrial shape to drive MuSC fate decisions. Therefore, we isolated WT myofibers and cultured for 0, 4, 12 and 24-hours in the presence of αKG or succinate and analyzed their mitochondrial morphology. We find that at 4-hours in culture, both αKG and succinate treated MuSCs display a highly fragmented mitochondrial network, similar to untreated (Figure 10A). This is in line with the fact that mitochondrial fragmentation is required for the exit from quiescence and the activation of MuSCs[153,154], and no defects in activation are seen in MuSCs treated with αKG or succinate (Figure 8A,B,F and G). Interestingly, however, at 12-hours, a divergence in mitochondrial length can be seen in αKG and succinate treated MuSCs. At 12-hours in culture, mitochondria within succinate treated MuSCs begin to re-elongate, and this elongation continues at 24-hours (Figure 10A and C). In contrast, mitochondria within αKG treated MuSCs maintain a highly fragmented morphology until 24-hours in culture (Figure 10A and B). Given that mitochondrial fragmentation promotes commitment, whereas mitochondrial elongation promotes self-renewal, this data suggested that succinate may promote self-renewal by inducing mitochondrial elongation, whereas αKG may promote commitment by maintaining fragmented mitochondria.

We were particularly interested in analyzing mitochondrial morphology after 24h αKG or succinate treatment, given that at this time point, these treatments significantly alter the identity of MuSCs and their gene expression (Figure 9L-O). We cultured WT myofibers with αKG or succinate for 24h and analyzed their mitochondrial morphology. At 24h, succinate-treated MuSCs have an elongated mitochondrial morphology, whereas a shift towards more fragmented

mitochondria is seen in αKG-treated cells (Figure 10D and E). While we were interested to see differences in mitochondrial length following 24h αKG or succinate treatments in Pax7+ MuSCs, which includes self-renewing (Pax7+/MyoD-) and activated cells (Pax7+/MyoD+) but excludes committed MuSCs (Pax7-/MyoD+) we questioned whether this was truly due to the treatments, or whether this was due to differences in cell identity at 24-hours. Thus, we analyzed mitochondrial morphology in MyoD+ cells rather than Pax7+ cells to exclude self-renewing cells and include committed cells. Interestingly, here, we find that mitochondria within MyoD+ cells after 24h αKG treatment continue to display a greater degree of fragmented mitochondria compared to control, however, mitochondria within succinate treated MyoD+ MuSCs show no difference in length compared to control (Figure 10F and G). Furthermore, we investigated the expression of the fission and fusion genes, DRP1 and OPA1, in MuSCs treated with αKG or succinate for 24h. We find that succinate significantly increased gene expression of OPA1, whereas αKG had no effect (Figure 10H). In contrast, αKG significantly increased expression of the fission factor DRP1 (Figure 10I). Next, we questioned whether αKG, which restored the biased fate decisions of OPA1-OE MuSCs, was also manipulating mitochondrial length within these cells. Thus, we isolated OPA1-OE myofibers and cultured for 24h with exogenous αKG and analyzed their mitochondrial length. Strikingly, αKG treatment induced a significant degree of mitochondrial fragmentation (Figure 10J and K). This data highlights that αKG and succinate alter the expression of fission and fusion genes, which in turn promotes mitochondrial fragmentation or elongation, respectively.

Next, we questioned whether mitochondrial fission and fusion are necessary for αKG and succinate to alter MuSC fate. To this end, we isolated WT myofibers and cultured for 72-hours in the presence of low dose (2μM) Mdivi-1 to inhibit DRP1 and mitochondrial fragmentation, or MYLS22, a small molecule inhibitor of OPA1 GTPase activity[159], to prevent mitochondrial elongation. As previously demonstrated[153], 72h treatment with Mdivi-1 enhanced self-renewal and decreased commitment (Figure 10L). Treatment of WT myofibers with the OPA1 inhibitor MYLS22 resulted in a severe inhibition of self-renewal, in accordance with the fate decisions phenotype of OPA1-KO MuSCs (Figure 10M). To determine whether mitochondrial fission and fusion are necessary for the altered fate decisions in αKG and succinate treated MuSCs, we isolated WT myofibers and treated with αKG or succinate alone or co-treated with αKG and Mdivi-1 or succinate and MYLS22. While αKG alone promoted commitment and inhibited self-

renewal, co-treatment of αKG and Mdivi-1 restored fate decisions to WT levels (Figure 10N). Treatment with succinate promoted self-renewal and inhibited commitment, whereas co-treatment of succinate with MYLS22 returned self-renewal to WT levels but was not sufficient to revert commitment (Figure 10M). Altogether, this data highlights the requirements for mitochondrial plasticity in αKG- and succinate-induced alterations in MuSC fate decisions.

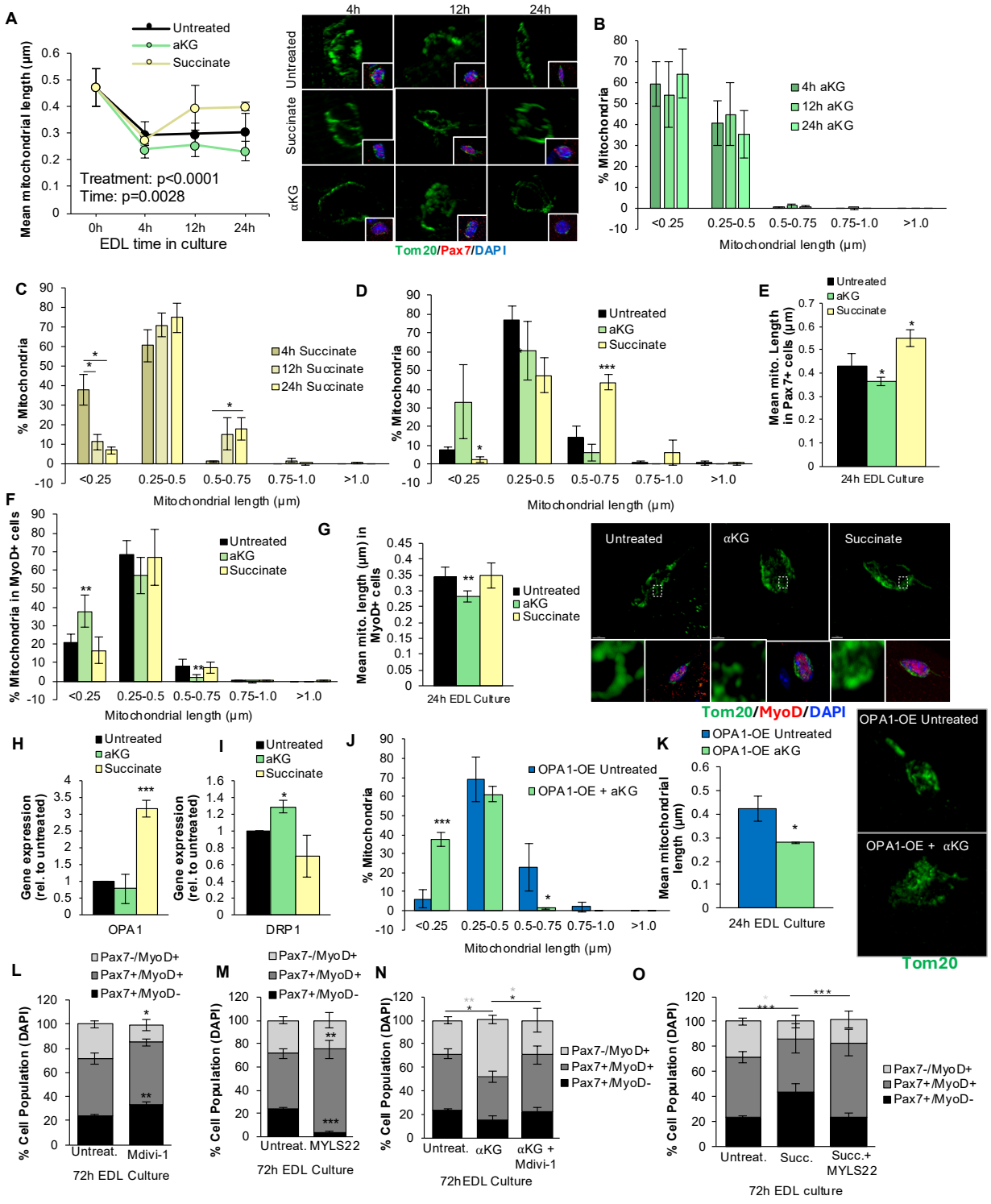

Figure 10. aKG and Succinate alter mitochondrial morphology of MuSCs. (A) Quantification and representative confocal images of mitochondrial length using Tom20 in MuSCs on myofibers cultured for 0, 4, 12 and 24-hours with aKG or succinate. n=3 mice with ≥ 500 total mitochondria quantified, mean ± SD. (B) Distribution of mitochondrial length using Tom20 in Pax7+ MuSCs cultured with αKG for 4, 12 and 24 hours. n=3 mice with ≥ 500 total mitochondria quantified,

mean ± SD. (C) Distribution of mitochondrial length using Tom20 in Pax7+ MuSCs cultured with succinate for 4, 12 and 24 hours. n=3 mice with ≥ 500 total mitochondria quantified, mean ± SD. (D) Distribution of mitochondrial length using Tom20 in Pax7+ MuSCs following 24-hour culture with αKG or succinate. n=3 mice with ≥ 300 total mitochondria quantified, mean ± SD. (E) Average mitochondrial length using Tom20 in Pax7+ MuSCs following 24-hour culture with αKG or succinate. n=3 mice with ≥ 300 total mitochondria quantified, mean ± SD. (F) Distribution of mitochondrial length using Tom20 in MyoD+ MuSCs following 24-hour culture with αKG or succinate. n=3 mice with ≥ 300 total mitochondria quantified, mean ± SD. (G) Average mitochondrial length using Tom20 in MyoD+ MuSCs following 24-hour culture with αKG or succinate. n=3 mice with ≥ 300 total mitochondria quantified, mean ± SD. (H) qPCR of OPA1 expression in WT MuSCs treated for 24h with αKG or succinate. n=3 mice, mean ± SD. (I) qPCR of Drp1 expression in WT MuSCs treated for 24h with αKG or succinate. n=3 mice, mean ± SD. (J) Distribution of mitochondrial length in OPA1-OE MuSCs following 24-hour culture with aKG. n=3 mice with 1300-1500 mitochondria total mitochondria quantified, mean ± SD. (K) Average mitochondrial length from (J) and representative confocal 3D reconstruction images of mitochondria. n=3 mice, mean ± SD. (L) Quantification of Pax7+ and MyoD+ expressing MuSCs at 72h in WT myofibers treated with 2μM Mdivi-1. n=3 mice, mean ± SD. (M) Quantification of Pax7+ and MyoD+ expressing MuSCs at 72h in WT myofibers treated with 2.5μM MYLS22. n=3 mice, mean ± SD. (N) Quantification of Pax7+ and MyoD+ expressing MuSCs at 72h in WT myofibers treated with aKG and 2uM Mdivi-1. n=3 mice, mean ± SD. (N) Quantification of Pax7+ and MyoD+ expressing MuSCs at 72h in WT myofibers treated with 2.5uM MYLS22. n=3 mice, mean ± SD. (O) Quantification of Pax7+ and MyoD+ expressing MuSCs at 72h in WT myofibers treated with succinate and 2.5μM MYLS22. n=3 mice, mean ± SD.

4.5 Differential [αKG]:[succinate] status is observed in self-renewing and committed cells

We have demonstrated that αKG and succinate direct MuSCs towards opposing fate. Furthermore OPA1-KO MuSCs, which have a bias towards commitment, have an increased ratio, whereas OPA1-OE MuSCs, which have a bias towards self-renewal, have a decreased ratio. Thus, we questioned whether self-renewing and committed cells also display differential [αKG]:[succinate] status. In order to investigate this, we utilized the Pax7-GFP mouse line to isolate committed and self-renewing MuSCs based on GFP expression. We isolated Pax7-GFP MuSCs and cultured for 72h on Matrigel coated plates. First, 100% of isolated cells were GFP+, and differences in GFP intensity were seen at the time of isolation whereby approximately 80% of cells were GFP^{high} and 20% were GFP^{low} (Figure 11A). Given the nature of isolating MuSCs, which itself serves as an activating stimulus[81], these differences in GFP intensity may be attributed to a portion of cells becoming activated during the isolation process. After 72 hours in culture, all cells maintained some level of GFP expression, however the majority fell into the GFP^{high} population, which may include self-renewing and activated cells, whereas the remaining GFP^{low} cells could be indicative of committed MuSCs (Figure 11B). In support of this, self-renewing and quiescent MuSCs (GFP^{high}/Ki67-) and committed/differentiating MuSCs (GFP^{low}/Ki67-) could also be seen following 72-hours in culture (Figure 11C). To further characterize these cells, following 72h in culture, MuSCs were then re-sorted based on GFP intensity and cells within the top (GFP^{high}) and bottom (GFP^{low}) 30% GFP intensity were collected. Gene expression analysis revealed that the GFP^{high} population had significantly increased expression of Pax7 and CD34 relative to the GFP^{low} population, indicating a more stem-like population (Figure 11D). In contrast, expression of the myogenic genes MyoD and MyoG were greatly reduced in the GFP^{high} population, relative to GFP^{low} (Figure 6E). This further corroborates that following 72h in culture, GFP^{high} MuSCs represent a more stem-like, self-renewing population, whereas the GFP^{low} population are indicative of committing and differentiating MuSCs. To further support this notion, we characterized the mitochondrial morphology of these two populations of cells. We find that the GFP^{high} cells have an elongated mitochondrial morphology, in comparison to the fragmented mitochondrial network seen in GFP^{low} MuSCs (Figure 11F and G). This is in line with our previous work demonstrating that mitochondrial fragmentation is maintained in committing MuSCs, whereas mitochondrial

elongation is seen in self-renewing cells[153]. Additionally, we find that OPA1 expression is significantly higher in GFP^{high} MuSCs with a trending increase in MFN2 and decrease in DRP1 (Figure 11H). This provides some insight into the divergence of mitochondrial morphology in self-renewing and committing MuSCs.

Lastly, to gain insight into potential differences in the [αKG]:[succinate] ratios in GFP^{high} and GFP^{low} MuSCs, we examined the gene expression of IDH3, OGDH and SDHA given that these enzymes were differentially altered in OPA1-KO and OPA1-OE MuSCs in a manner suggestive of their altered ratios (Figure 9C-E). We find that GFP^{high} MuSCs have decreased IDH3 and SDHA expression, and increased OGDH expression (Figure 11I). This would suggest a decrease in αKG synthesis, increased αKG conversion and decreased succinate conversion, therefore decreasing the [αKG]:[Succinate] ratio in these cells. Furthermore, an opposite expression profile of these genes in GFP^{low} MuSCs would suggest an increased ratio, as is seen in OPA1-KO MuSCs which have a bias towards commitment. Altogether, this data further strengthens that self-renewing MuSCs undergo mitochondrial elongation which in turn leads to decreased [αKG]:[succinate] ratio status, similar to OPA1-OE MuSCs, whereas committing and differentiating MuSCs maintain a fragmented mitochondrial network which promotes an increased ratio status, similar to OPA1-KO MuSCs (Figure 11J).

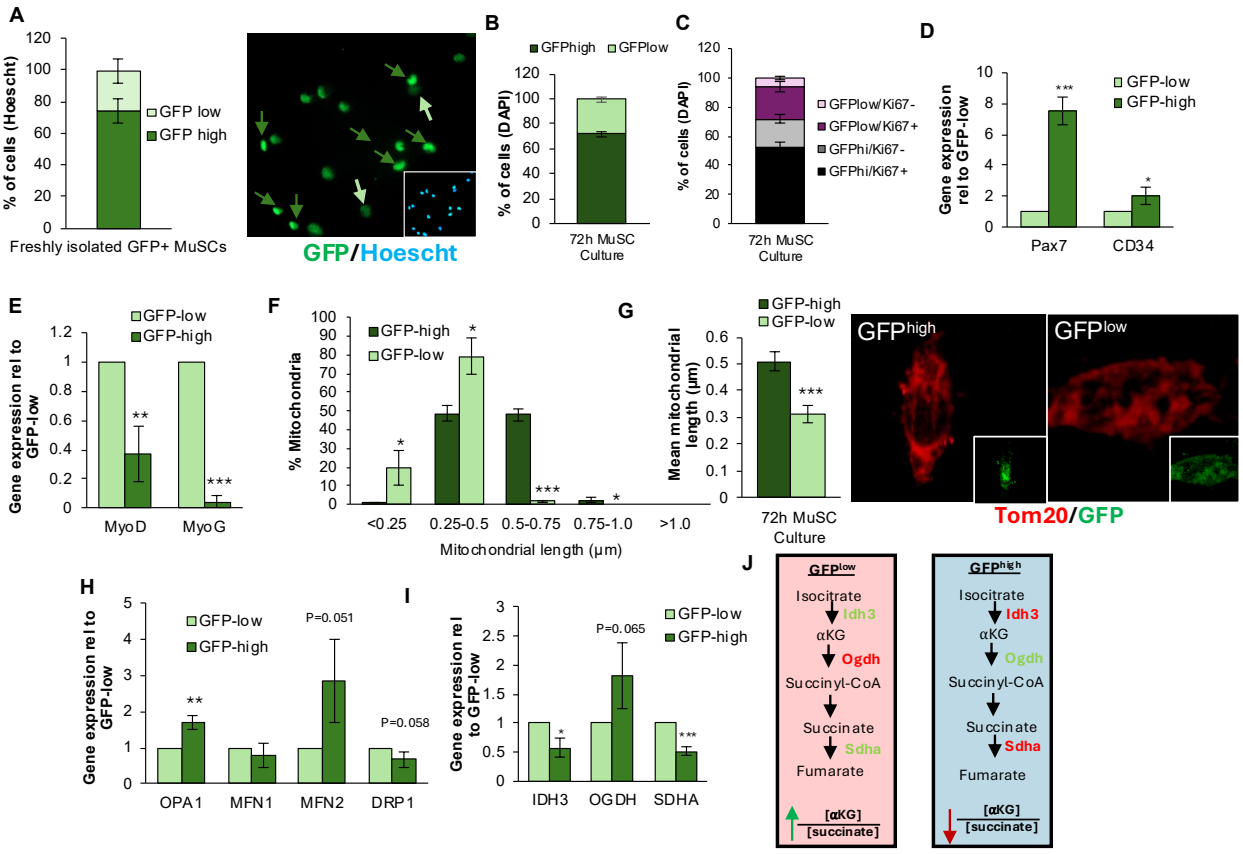

Figure 11. Committed and self-renewing MuSCs have opposing mitochondrial morphology and gene expression profiles. (A) Purity assessment of Pax7-GFP MuSCs immediately following isolation. (B) Proportion of GFP-high and GFP-low MuSCs following 72h culture. n=3 mice, mean ± SD. (C) GFP-high and GFP-low MuSCs expressing Ki67 following 72h culture. n=3 mice, mean ± SD. (D) qPCR of Pax7 and CD34 gene expression in GFP-high and GFP-low MuSCs following 72h in culture. n=3 mice, mean ± SD. (E) qPCR of MyoD and MyoG gene expression in GFP-high and GFP-low MuSCs following 72h in culture. n=3 mice, mean ± SD. (F) Distribution of mitochondrial length in 72-hour cultured GFP-high and GFP-low MuSCs. n=16-20 cells, mean ± SD. (G) Average mitochondrial length in GFP-high and GFP-low MuSCs following 72h in culture. n=≥600 mitochondria, mean ± SD. (H) qPCR of OPA1, MFN1, MFN2 and DRP1 gene expression in GFP-high and GFP-low MuSCs following 72h in culture. n=3 mice, mean ± SD. (I) qPCR of IDH3, OGDH and SDHA gene expression in GFP-high and GFP-low MuSCs following 72h in culture. n=3 mice, mean ± SD. (J) Schematic demonstrating how differences in TCA cycle enzymes in GFP^{high} and GFP^{low} MuSCs may alter the [αKG]:[succinate] ratio.

4.6 Succinate requires OPA1 to promote return to quiescence

Currently, with the aforementioned data, we have demonstrated that mitochondrial shape dictates the ratio of αKG to succinate and this ratio guides MuSC fate in a mitochondrial dynamics-dependent fashion. Our previous work has demonstrated that committed cells maintain a fragmented mitochondrial network, whereas self-renewal requires mitochondrial re-elongation[153]. While we observed a restoration of self-renewal in OPA1-KO MuSCs treated with succinate (Figure 8T), given the inability of their mitochondria to re-elongate, we questioned whether these cells were truly self-renewing and returning to quiescence. Thus, we first investigated whether succinate treatment in WT MuSCs promoted the return to quiescence. WT EDL myofibers were cultured for 72h with succinate and stained for Pax7 and Ki67 to delineate MuSCs that have exited the cell cycle (Ki67-). First, we confirmed that succinate treatment significantly increased the proportion of Pax7+ cells at 72h in culture (Figure 12A). To our surprise, in untreated fibers, we find that all Pax7+ cells on EDL myofibers at 72h were Ki67+, indicating these cells were within the cell cycle at the time of fixation (Figure 12B). Succinate treatment also resulted in all Pax7+ cells being Ki67+ (Figure 12B). Additionally, in untreated and succinate treated fibers, the majority of Pax7- cells were also Ki67+ (Figure 12C). Thus, this demonstrated that the EDL myofiber culture system at 72h may not be an appropriate assay to assess return to quiescence. We questioned whether MuSCs need to be adherent to assume a quiescent morphology and phenotype, which has been demonstrated in previous studies.[160-163] To investigate this, we isolated WT MuSCs and cultured on Matrigel coated glass slides for 72-hours with succinate. We find succinate treatment enhanced the proportion of Pax7+ cells, indicating an increase in self-renewal, consistent with what is observed in the EDL system (Figure 12E). Next, we quantified the proportion of Ki67+/- cells. In contrast to EDLs where all Pax7+ cells are Ki67+ at 72h, here we find that approximately 20% of untreated Pax7+ cells have exited the cell cycle (Figure 12F and H). Furthermore, succinate treatment in WT MuSCs enhanced the proportion of Ki67-/Pax7+ cell at 72h, indicating enhanced return to quiescence (Figure 12F and H). Additionally, succinate bore no effect on the percentage of differentiating MuSCs (Pax7-/Ki67-) (Figure 12G). Taken together, our results reveal that succinate enhances the proportion of self-renewing MuSCs and return to quiescence.

With this assay to investigate self-renewal and return to quiescence, we then shifted our focus to determining whether succinate supplementation in OPA1-KO MuSCs would be sufficient to enhance their return to quiescence. To this end, we isolated OPA1-WT and OPA1-KO MuSCs and cultured for 72h with succinate and assessed their cell cycle exit. First, we find that succinate treatment in OPA1-WT MuSCs increased the proportion of Pax7+ cells and decreased Pax7- cells (Figure 12I). Furthermore, as was previously seen in EDLs (Figure 8T), succinate restored the population of Pax7+ cells in OPA1-KO (Figure 12I). However, we find that the proportion of Pax7+/Ki67- OPA1-KO MuSCs is drastically reduced in comparison to OPA1-WT, indicating a striking defect in their ability to exit the cell cycle and return to quiescence (Figure 12J). While succinate rescued the self-renewing population in OPA1-KO, we observed no change in the population of cells exiting the cell cycle (Figure 12J). In addition to this, using the Calcitonin receptor (CalcR) as an indicator of MuSCs marked for quiescence return, we find that in both 72-hour untreated, and succinate treated OPA1-KO MuSCs, the majority of Pax7+ cells are CalcR-, further confirming these cells lack the ability to return to quiescence (Figure 12K). Furthermore, pharmacological inhibition of OPA1 with MYLS22 in OPA1-WT MuSCs resulted in a phenotype similar to OPA1-KO MuSCs, whereby these cells were predominantly CalcR- (Figure 12M). Additionally, co-treatment of OPA1-WT MuSCs with MYLS22 and succinate did not restore quiescence return (Figure 12M). Taken together, the above data demonstrates that succinate promotes self-renewal and return to quiescence, however this is dependent on OPA1 being present and functional.

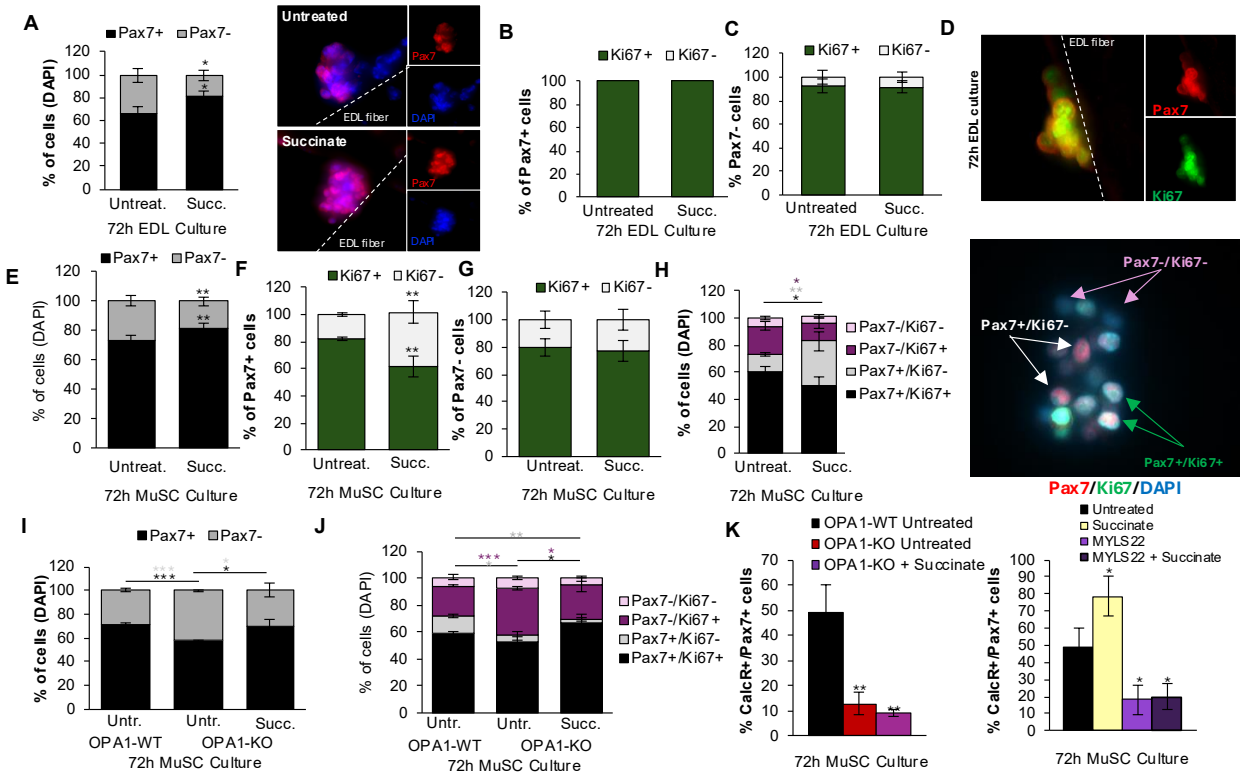

Figure 12. Succinate requires OPA1 to promote return to quiescence. (A) Quantification and representative images of Pax7 expressing MuSCs on WT EDL myofibers cultured for 72h with succinate. n=3 mice, mean ± SD. (B) Quantification of Pax7+ MuSCs expressing Ki67 on WT myofibers cultured for 72h with succinate. n=3 mice, mean ± SD. (C) Quantification of Pax7- MuSCs expressing Ki67 on WT myofibers cultured for 72h with succinate. n=3 mice, mean ± SD. (D) Representative image showing Ki67+ MuSCs on 72h cultured WT myofibers. (E). Quantification of Pax7+ MuSCs expressing Ki67 following 72h culture with succinate. n=4 mice, mean ± SD. (F) Quantification of Pax7 expressing MuSCs cultured for 72h with succinate. n=3 mice, mean ± SD. (G) Quantification of Pax7- MuSCs expressing Ki67 following 72h culture with succinate. n=4 mice, mean ± SD. (H) Quantification of Pax7 and Ki67 expressing MuSCs following 72h culture with succinate. n=2 mice, mean ± SD. (I) Quantification of Pax7 expressing OPA1-WT and OPA1-KO MuSCs following 72h culture with succinate. n=4 mice, mean ± SD. (J) Quantification of Pax7 and Ki67 expressing OPA1-WT and OPA1-KO MuSCs following 72h culture with succinate. n=3 mice, mean ± SD. (K) Quantification of OPA1-WT and OPA1-KO Pax7+ cells expressing CalcR following 72h culture with succinate. n=3 mice, mean ± SD. (L) Quantification of Pax7 expressing OPA1-WT MuSCs following 72h culture with MYLS22 or co-treatment with MYLS22 and succinate. n=3 mice, mean ± SD.

4.7 *In vivo* succinate restores the stem cell pool in OPA1-deficient mice

As previously mentioned, *in vitro* treatment of OPA1-KO MuSCs with succinate restores self-renewal and prevents their bias towards commitment (Figure 8T). However, we were interested in investigating whether *in vivo* administration of succinate would be sufficient to preserve the stem cell pool in OPA1-KO mice. To address this, we utilized the cardiotoxin (CTX) injury model to monitor muscle regeneration and MuSC function in OPA1-KO mice injected with PBS or succinate (Figure 13A). 3-days following the last tamoxifen administration, a CTX injury was performed to the right tibialis anterior (TA) muscle of all mice. At 7 days post-injury, the injured TA was harvested as well as the contralateral EDL muscle. This time point was chosen given that a significant depletion of the stem cell pool can be seen in OPA1-KO mice at 7DPI[153]. Mice were injected intraperitoneally with either 100µl of PBS or 100µl of 100mg/kg succinate at the onset of tamoxifen and injected with PBS or succinate every other day until harvest (7DPI) (Figure 13A). Injured TA muscle sections underwent hematoxylin and eosin (H&E) staining to assess regenerative capacity. As previously described, OPA1-KO mice display significant regenerative failure following CTX, as seen by decreased cross-sectional area (CSA) of centrally nucleated fibers as well as decreased number of centrally nucleated fibers (Figure 13B-D). *In vivo* administration of succinate to OPA1-KO mice was not sufficient to rescue their regenerative capacity (Figure 13B-D). It is worth noting that in addition to their bias towards commitment which depletes the stem cell pool, loss of OPA1 in MuSCs also significantly hinders their differentiation ability[155]. Thus, rescuing muscle regeneration may not be possible in OPA1-KO mice. Upon examining the stem cell pool, PBS-treated OPA1-KO mice display a significant depletion of Pax7+ cells at 7DPI, however, succinate was sufficient to significantly increase the number of Pax7+ cells, although not to WT levels (Figure 13E). Additionally, we find that untreated and succinate treated OPA1-KO mice had a significantly increased proportion of Ki67+/Pax7+ cells at 7DPI (Figure 13F). Although succinate treatment enhanced the population of Pax7+ cells, these cells remain Ki67+ and do not appear to contribute to the proportion of MuSCs returning to quiescence. Furthermore, succinate was sufficient to reduce the proportion of differentiating cells, as shown by MyoG+ cells being returned to OPA1-WT levels (Figure 13G). Taken together, *in vivo* succinate administration is sufficient to restore the self-renewing population in OPA1-KO mice, however these cells are maintained in their proliferative stage and do not return to quiescence.

At the time of harvest, in addition to collecting injured TAs, we also collected the contralateral (uninjured) EDL muscle. EDL myofibers were cultured for 72h with exogenous *in vitro* succinate and their fate decisions were assessed. Interestingly, compared to PBS-treated OPA1-KO mice, in EDLs, *in vivo* succinate was not sufficient to rescue the self-renewal of OPA1-KO MuSCs, however we did observe a significant reduction in commitment (Figure 13H-J). However, in EDL myofibers isolated from PBS-treated OPA1-KO mice and further treated *in vitro* with succinate, we observed a significant increase in self-renewing MuSCs and decreased commitment (Figure 13H-J). Lastly, EDLs from succinate treated OPA1-KO mice that were further supplemented with succinate *in vitro* showed a further increase in self-renewal and decrease in commitment (Figure 13O-Q), suggesting a possible additive effect of both *in vivo* and *in vitro* succinate treatment. In summary, *in vivo* administration of succinate is sufficient to preserve the stem cell pool and rescue the over-commitment phenotype of OPA1-KO MuSCs following an injury.

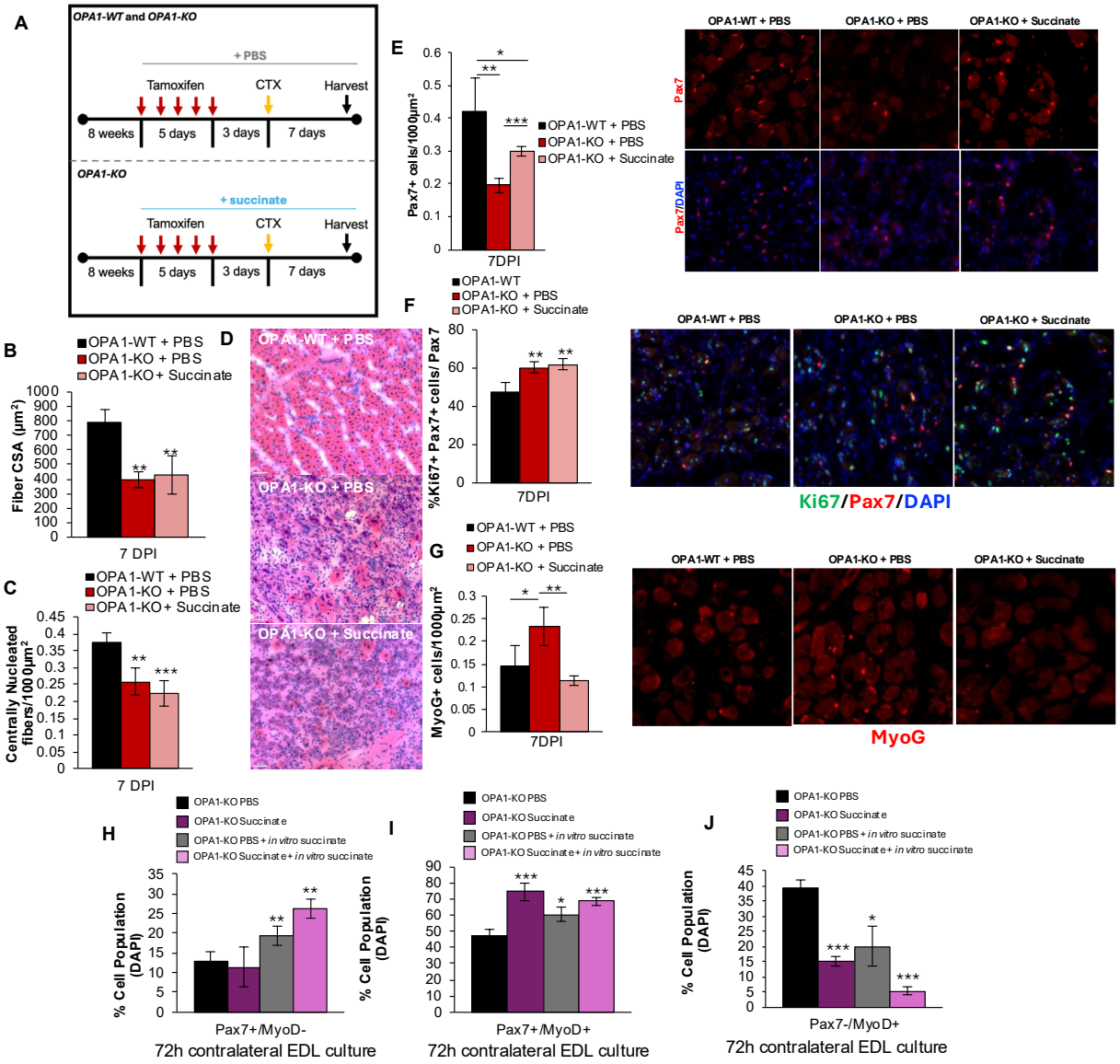

Figure 13. *In vivo* succinate preserves the stem cell pool in OPA1-KO mice. (A) Experimental paradigm for *in vivo* treatment of OPA1-KO mice with 100µl of PBS or succinate (100mg/kg) every other day for 15 days at the onset of tamoxifen administration. On day 8, all mice underwent cardiotoxin injury to the right TA muscle. Tissue was collected 7 days post-injury. (B) Quantification of fiber cross-sectional area of centrally nucleated fibers 7 days post-injury. n=4 mice, mean ± SD. (C) Quantification of the number of centrally nucleated fibers in OPA1-WT and OPA1-KO treated with PBS or succinate. n=4 mice, mean ± SD. (D) Representative images of TA cross-sections stained with H&E to determine regenerative capacity. (E) Quantification and representative images of Pax7+ cells in injured TA muscle from OPA1-WT and OPA1-KO treated with PBS or succinate. n=4 mice, mean ± SD. (F) Quantification and representative images of Pax7+ cells expressing Ki67 in injured TA muscle from OPA1-WT and OPA1-KO treated with PBS or succinate. n=4 mice, mean ± SD. (G) Quantification and representative images of MyoD+ cells in injured TA muscle from OPA1-WT and OPA1-KO treated with PBS or succinate. n=4 mice, mean ± SD. (H) Quantification of Pax7+/MyoD- cells on contralateral EDL fibers cultured

for 72hrs with *in vitro* succinate treatment. n=4 mice, mean ± SD (I) Quantification of Pax7+/MyoD+ cells on contralateral EDL fibers cultured for 72hrs with *in vitro* succinate treatment. n=4 mice, mean ± SD. (J) Quantification of Pax7-/MyoD+ cells on contralateral EDL fibers cultured for 72hrs with *in vitro* succinate treatment. n=4 mice, mean ± SD.

Chapter 5: Discussion

5.0 Discussion

MuSC progression and balanced fate decisions are integral for muscle maintenance. Efficient proliferation and fate decisions simultaneously ensure that the regenerative needs of muscle are met while also preserving the stem cell pool for future insult. Our group's previous work identified mitochondrial shape and OPA1 as a critical regulator of MuSC quiescence, proliferation and fate decisions[153]. In this study, we identify a novel role for mitochondrial shape in guiding MuSC progression and fate. Using two models of altered mitochondrial shape, via deletion or overexpression of the fusion protein OPA1, we identified that mitochondrial shape alters the abundance of key metabolites within MuSCs (Figure 7). These altered metabolites contribute to metabolic pathways such as the TCA cycle, glutamine metabolism, pyrimidine metabolism and methionine metabolism. Interestingly, all significantly altered metabolites in OPA1-KO MuSCs were decreased in abundance while these metabolites were significantly increased in OPA1-OE MuSCs. However, it is difficult to determine whether increases or decreases in metabolite abundance are due to changes in biosynthesis and/or substrate utilization. In addition, we identified multiple commonly altered metabolites in OPA1-KO and OPA1-OE MuSCs including alpha-ketoglutarate, 2-hydroxyglutarate, methionine, succinate and uridine. Some of these metabolites have known signalling roles in other stem cell systems[90,106,107,111,164-170], thus we questioned whether mitochondrial shape may alter MuSC progression and fate via changes in signalling metabolites.

To determine whether metabolites regulated by OPA1 possess the capacity to alter MuSC progression and fate, we treated wild-type MuSCs with exogenous metabolites and monitored their activation, cell cycle entry and fate decisions. Interestingly, we found that these metabolites are sufficient to alter MuSC activation, cell cycle entry and fate decisions in a metabolite-specific manner (Figure 8). We identified that treatment of WT MuSCs with methionine decreased their cell cycle entry. We were particularly surprised at this result given that previous studies have demonstrated that proliferating cells enter a dormant state upon methionine withdrawal[171,172]. It is important to note that these studies were done in cells already in a proliferative state, in comparison to our study where we are monitoring entrance into the cell cycle. However, one study demonstrated that supplementation of methionine decreased cell cycle progression in particular

cancer cells, but not in benign cells[173]. Thus, in our model whereby methionine supplementation decreases cell cycle entry, it is possible that this is due to cell-type differences and different downstream mechanisms, such as disruption to the methionine cycle and the folate cycle or alterations in the methylome, which warrants further investigation.

In particular, we noticed that αKG and succinate had opposing effects on fate whereby αKG promoted commitment at the expense of self-renewal, whereas succinate promoted self-renewal and decreased commitment (Figure 8). Interestingly, in other stem cell populations, αKG and succinate have been demonstrated to be sufficient to alter cell identity[90,106-109,111]. Additionally, their effects on fate appear to be cell-specific and context-specific. Furthermore, we find that succinate is sufficient to rescue the fate decision phenotype of OPA1-KO MuSCs to WT levels. Lastly, exogenous metabolite treatment was sufficient to rescue the delayed activation and cell cycle entry phenotype of OPA1-OE MuSCs, and their fate was restored with the addition of αKG. This highlighted to us that re-introduction of exogenous metabolites altered by OPA1 are sufficient to rescue the fate decision phenotypes of OPA1-deficient and OPA1-overexpressing MuSCs.

We were interested in the opposing fate decision phenotypes of MuSCs treated with αKG or succinate. This striking opposition led us to pursue these two metabolites in-depth. We questioned whether there exists a fine-tuned balance or ratio of these two metabolites that is responsible for dictating MuSC fate. Indeed, we found that exogenous manipulation of this ratio was sufficient to direct MuSC fate (Figure 9). Interestingly, the ratio of αKG to succinate has been described in other stem cell systems as a key regulator of fate and pluripotency, thus strengthening the validity of our results[90,106,107,157]. However, it is important to note that while exogenous αKG or succinate were added to culture, given that the intracellular concentration of these metabolites was not evaluated following treatment, it is difficult to be certain if the observed effects are due to these metabolites, or whether these metabolites are being utilized and converted downstream. We did attempt to answer this by decreasing the time of treatment to only the first 24h of a 72h culture, attempting to capture the immediate and early effects of these metabolites. These experiments reveal that treating MuSCs for only the first 24h of a 72h culture with αKG or succinate yielded a similar fate decision outcome as is observed when treating cells for the full 72h. This may suggest that the fate decisions seen in MuSCs treated with αKG or succinate are specifically due to these metabolites and not a downstream metabolite produced from αKG or succinate. We also show that

24h treatment with αKG and succinate alters the expression of the stemness gene *Pax7* and the myogenic gene *MyoD*. This seemingly direct effect of these metabolites on the expression of key genes provides insight into how they may affect MuSC fate. In other stem cell systems, αKG and succinate, in particular the ratio of these two metabolites, alter gene expression through epigenetic modifications[106,107]. A family of histone and DNA demethylases require αKG as a co-factor and convert it to succinate following the demethylation reaction[91,98,99,174,175]. Interestingly, succinate acts as an inhibitor of these processes. In conditions when the ratio of αKG to succinate is high, demethylation reactions can occur, however as this ratio is decreased, by increasing succinate levels, these reactions are inhibited. In embryonic stem cells, this ratio is responsible for their fate by altering key stemness and differentiation genes through histone and DNA demethylation[107]. In pluripotent stem cells, at later stages of pluripotency, the ratio of αKG and succinate dictates their differentiation by inducing global histone and DNA demethylation programs[106]. In our system, we identified that these metabolites are sufficient to alter gene expression and therefore presents the possibility that these changes in gene expression are accomplished via post-translational modifications of histones and/or DNA.

Our previous work has demonstrated that mitochondrial shape is a key driver of MuSC fate decisions, and impairment in the dynamic nature of mitochondria alters MuSC fate[153]. Furthermore, as previously mentioned, αKG treatment yielded similar fate as is observed in OPA1-KO and succinate treatment led to similar fate seen in OPA1-OE MuSCs. Since mitochondrial fragmentation pushes commitment and elongation promotes self-renewal, we questioned whether these treatments were altering MuSC fate by promoting changes in mitochondrial shape. Time-course analysis of mitochondrial morphology in WT MuSCs treated with αKG or succinate revealed that mitochondria within αKG-treated cells are maintained in a fragmented state, whereas mitochondria within succinate-treated cells undergo rapid re-elongation. It is important to note that in either treatment, mitochondria undergo an initial fragmentation. This is in line with our previous work demonstrating mitochondrial fragmentation is necessary for quiescence exit[153], and no defects in quiescence exit or activation were observed in αKG or succinate treatments. The divergence in mitochondrial length between these two treatments is seen as early as 12-hours in culture. At 24-hours in culture, we observed that in Pax7+ cells, decreased mitochondrial length is seen in αKG-treated cells, whereas an increase in length is seen in succinate-treated cells.

However, since we had identified differences in cell identity as early as 24-hours following αKG or succinate treatment, we questioned whether the differences in mitochondrial length were truly due to treatment or whether these treatments were altering cell identity and the mitochondrial length observed was a consequential effect. Assessment of mitochondrial morphology in MyoD+ cells revealed a fragmented network in αKG-treated cells, similar to what was seen in Pax7+ cells, however the mitochondrial elongation seen in succinate-treated Pax7+ cells was no longer evident. This suggested that differences in length may be due to cell identity and not a direct effect of these treatments. It is important to note that this experiment was done after 24-hours in culture, but the divergence in mitochondrial length was seen as early as 12-hours in culture. Thus, it would be of interest to examine mitochondrial length in MyoD+ cells at 12-hours in culture to further confirm whether changes in length precede differences in identity. We also examined the expression of OPA1 and DRP1 in succinate and αKG treated cells after 24-hours. We identified a significant increase in OPA1 expression in succinate treated cells, and a significant increase in DRP1 following αKG treatment. Here, similarly to our results in EDLs, this gene expression is based on the entire population of cells following treatment. The results of this gene expression analysis would suggest a direct effect of our treatments on the expression of fission and fusion genes, which in turn would affect mitochondrial length. Indeed, in chicken intestinal stem cells, succinate treatment significantly increased OPA1 protein expression and expression of the intestinal stemness marker LGR5[176]. Thus, it appears that in a different stem cell system, succinate is sufficient to directly alter OPA1 protein levels. To distinguish between causative and consequential effects of succinate treatment on OPA1 expression, it would be important to utilize a different cell system, such as C2C12s, to examine OPA1 following succinate treatment. This would eliminate the possibility of cell identity being the causative reason for differences in mitochondrial length, given that C2C12s are already committed to the myogenic lineage.

We also questioned whether mitochondrial fission and fusion were required for succinate and αKG to alter mitochondrial length. To address this, we pharmacologically inhibited fission with low dose of the Drp1-inhibitor, Mdivi-1, and fusion, with MYLS22 which inhibits the GTPase activity of OPA1[153,159]. Treatment of MuSCs with Mdivi-1 resulted in a shift towards self-renewal, as we have previously reported, whereas MYLS22 significantly abolished the population of self-renewing cells. In contrast to fate decisions seen in OPA1-KO MuSCs, whereby self-renewal is inhibited, and commitment is enhanced, treatment of WT cells with MYLS22 had no effect on

their commitment. This could be explained by a few possibilities. First, mitochondria within OPA1-KO MuSCs are already in a fragmented state prior to culture, whereas cells treated with MYLS22 begin with normal mitochondria. Therefore, the mechanisms by which we have previously demonstrated as promoting commitment (i.e. mitochondrial fragmentation leading to elevated ROS/GSH)[153], are already present in OPA1-KO MuSCs, but not in WT cells. Additionally, MYLS22 was only added at the onset of culture. The half-life of this molecule in this context is unknown and inhibition of OPA1 may not be achieved for the entire 72-hour culture. Thus, it is possible that if MYLS22 was repeatedly added to culture, a complete OPA1-KO phenotype may have been observed.

Since fission promotes commitment and fusion promotes self-renewal, we co-treated cells with either αKG and Mdivi-1 or succinate and MYLS22. This revealed that cells co-treated with αKG and Mdivi1 showed no difference in fate decisions compared to WT. Similarly, cells treated with succinate and MYLS22 showed no effect on fate decisions. Interestingly, the results from co-treatment of succinate and MYLS22 had similar results as what we had previously seen when treating OPA1-KO MuSCs with succinate.

While we have demonstrated that MuSCs primed to preferentially commit or self-renew have differences in their [αKG]:[succinate] ratio, we sought to determine whether MuSCs undergoing commitment or self-renewal display alterations in this ratio. Thus, we utilized the Pax7-GFP mouse line to isolate self-renewing and committing cells following 72-hours in culture based on their GFP expression. This strategy was confirmed, showing that GFP^{high} MuSCs were more stem-like, with increased Pax7 and CD34 expression, and an elongated mitochondrial length, consistent with our previous observations[153]. Our GFP^{low} MuSCs were more myogenic, have decreased Pax7 and CD34, increased MyoD and MyoG expression, and maintain a fragmented mitochondrial network. Interestingly, these two populations had differential expression of key TCA cycle enzymes involved in the synthesis of αKG and succinate indicative of a decreased ratio in self-renewing cells and increased in committing cells. However, it is important to note that gene expression profiling does not give a definitive answer as to whether these cells have differences in this ratio. Rather, a targeted metabolomic analysis, as was done in OPA1-KO and OPA1-OE MuSCs, would provide more concrete evidence of whether this ratio is altered in these populations of cells. In other stem cell systems, the establishment of this ratio is accomplished through differential utilization of substrates such as glutamine, as well as differential expression of TCA

enzymes within cell types[106,107]. Recently, it was identified that OGDH is expressed in the intestine in a heterogenous manner, which alters the abundance of αKG in specific cell types, driving their differentiation or maintaining their stemness[109]. In addition, αKG played specific roles in these different cell types, whereby it can be used to fuel the bioenergetic needs of a cell or have more of a signalling role[109].

Our previous work had identified that re-instigation of mitochondrial elongation occurs in MuSCs as they return to quiescence[153]. In our models where elongation is inhibited, such as our OPA1-KO or WT cells treated with MYLS22, succinate was sufficient to restore their self-renewal. However, we questioned whether these self-renewing cells were functional and able to return to quiescence. Our studies revealed that preventing mitochondrial elongation, either genetically through loss of OPA1 or pharmacologically using MYLS22, prevented self-renewing cells from exiting the cell cycle. Furthermore, a dramatic decrease in the number of self-renewing cells expressing the quiescence marker CalcR was also observed. Interestingly, succinate treatment alone in WT cells enhanced cell cycle exit and quiescence return. However, succinate could not restore these defects in OPA1-KO and MYLS22-treated cells, indicating that succinate requires OPA1 to be present and functional to promote quiescence return.

Loss of the stem cell pool and their functionality[177] is a key characteristic of degenerative muscular diseases and aging[178]. Therapeutics to preserve the stem cell pool are thus of great interest to alleviate the burden of disease. Our previous studies have demonstrated that aged MuSCs display fragmentated mitochondria, and depletion of the stem cell pool both *in vivo* following an injury and *in vitro*[153]. Decreased self-renewal in aged MuSCs is also accompanied by preference for these cells to commit, closely resembling the phenotype of OPA1-KO MuSCs[153]. Therefore, since our data highlighted that succinate promotes self-renewal and restores this population of cells in OPA1-KO mice *in vitro*, we questioned whether *in vivo* succinate would be sufficient to restore the self-renewing population in OPA1-KO mice. Thus, we treated OPA1-KO with intraperitoneal injections of succinate and subjected their TA muscle to an injury to stimulate the regenerative process. First, we found that succinate did not prevent the regenerative defects seen in OPA1-KO mice. Our previous work has demonstrated the importance of OPA1 in the differentiation and regeneration of muscle, whereby it plays an important role, in conjunction with SCAF1, in mediating the metabolic switch during differentiation[155]. Here, we find that succinate enhanced the self-renewing population while concomitantly decreasing the proportion of differentiation

cells, in line with what we have seen *in vitro*. While succinate preserves the stem cell pool, these cells are maintained in a proliferative state and thus may not contribute to the self-renewing cells returning to quiescence. It is important to note that these quantifications were done at 7-days post-injury, a time in which massive depletion of the stem cell pool is seen in OPA1-KO mice[153]. While at this time point, MuSCs do begin to return to quiescence, it may not be an appropriate time to assess the full quiescence return potential of self-renewing cells. Future studies could assess the stem cell pool and regeneration of OPA1-KO mice treated with succinate at later time points such as 14 or 21-days post-injury. Additionally, in this experiment, we did not treat WT mice with succinate. It would be of interest to determine whether *in vivo* succinate could expand the self-renewing population in WT mice, to corroborate our *in vitro* data.

Chapter 6: Conclusion

Taken together, this project highlights a novel role by which mitochondrial shape and OPA1 alter MuSC progression and fate. We present evidence that OPA1 alters the global metabolome of MuSCs and specifically alters the ratio of αKG to succinate. This ratio dictates MuSC fate, in part by altering key stemness and myogenic genes and is dependent on the plasticity of mitochondrial shape. We identified potential differences in this ratio in self-renewing and committed cells, consistent with our models of altered OPA1 expression (Figure 13). We present further evidence of the importance of mitochondrial length in the re-establishment of quiescence and find that restoring this ratio *in vivo* is sufficient to restore the stem cell pool but does not rescue regenerative defects.

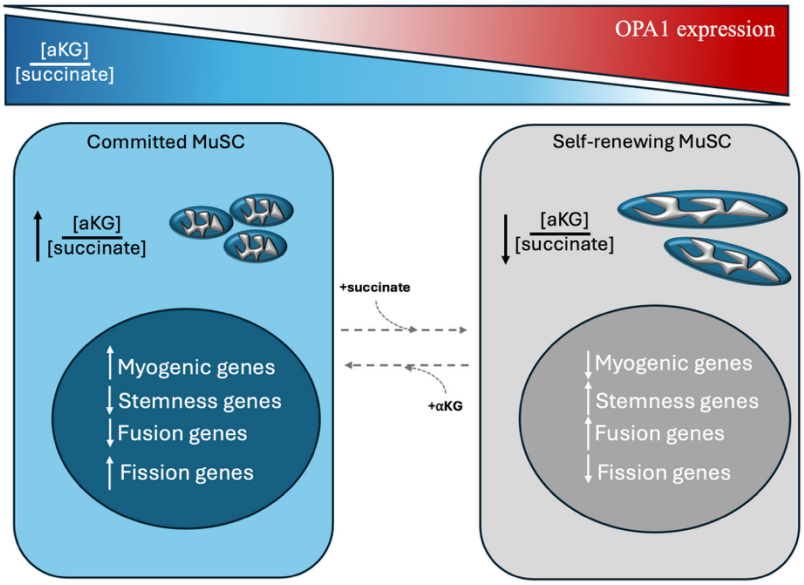

Figure 14. Working Model: OPA1 and mitochondrial shape establish [αKG]:[succinate] ratios to guide MuSC fate. In MuSCs with low OPA1 and fragmented mitochondria, the [αKG]:[succinate] is increased which promotes myogenic gene expression and pushes commitment. Mitochondrial elongation and high OPA1 expression decreases, the [αKG]:[succinate] ratio which increases stemness genes and promotes their self-renewal. MuSC fate can be altered by exogenous αKG and succinate treatments.

Chapter 7: Limitations of the study

While we have presented data highlighting this novel signalling role of mitochondrial shape changes in regulating stem cell fate, there are important limitations to consider. First, while we performed metabolomic analysis of OPA1-KO and OPA1-OE MuSCs and identified significant differences in metabolites, it is important to note that this does not provide information on the metabolic flux of these metabolites. Metabolomic analysis only provides a snapshot of global metabolite abundances at the time of isolation. It is therefore not possible to determine whether differences in metabolite abundance are due to changes in utilization or synthesis. To determine the flux of metabolites, other techniques, such as stable isotope tracing, should be used. However, the use of isotope tracing also presents its own technical considerations such as the decision of what isotope to use, incubation time and cell number. Future studies to assess metabolic flux in MuSCs using isotope tracing would be of great interest and would further build upon this study.

It is also important to note that the process of isolation is itself an activation stimulus. Thus, our metabolomic analysis of MuSCs does not provide insight into the metabolome of quiescent MuSCs, but rather cells that have already begun the activation process. Therefore, it is not clear whether differences in metabolites and the ratio of αKG to succinate are already established in quiescent OPA1-KO and OPA1-OE MuSCs, or whether this is a result of their activation. Current *in situ* fixation procedures to isolate quiescent MuSCs involve the use of fixatives to fix MuSCs in their quiescent state prior to isolating. However, these fixation techniques may not be compatible with further metabolomic analysis.

Our use of exogenous metabolite treatments demonstrated significant effects on MuSC progression and fate. While it is assumed that the resulting phenotype is due to the added metabolite, it is possible that our data may be the result of further downstream metabolites that are altered consequentially by the addition of exogenous metabolites. A limitation of this study is that abundances of intracellular metabolites were not quantified following metabolite treatment. Since this was not done, it is difficult to determine whether addition of our metabolites is increasing its intracellular concentration.

Our gene expression analyses in MuSCs treated with αKG or succinate was done on the entire cell population. However, it is important to note that we identified differences in cell identity following these treatments after 24-hours. A limitation of this study is the lack of gene expression

analysis in distinct cell populations following αKG or succinate treatment. This prevents the determination of whether these effects are consequential to differences in cell identity, or whether there is a direct causative effect.

Lastly, our metabolite treatments were done using supraphysiological concentrations of these metabolites. Concentrations used in this study ranged from 0.1mM to 1mM. Therefore, an important limitation of this study is that the effects seen on progression and fate of MuSCs may not be entirely physiologically relevant given the high concentration of metabolites used.

Chapter 8: Future directions

While this research presents a novel role by which mitochondrial shape alters MuSC fate via changes in metabolites, a direct mechanism has not been identified. As previously mentioned, metabolites altered by mitochondrial shape, alter the expression of key genes in MuSCs. However, the link between these metabolites and changes in gene expression remains unknown. An important and direct avenue of future study would be to determine whether these metabolites alter gene expression via epigenetic changes. The use of techniques such as CUT+Tag following treatment of MuSCs with metabolites would identify alterations in histone modifications and their genomic locations. This technique could be used in combination with other techniques such as ATACseq, to assess chromatin accessibility, and RNAseq, to identify transcriptional changes, to build a global picture as to how metabolite treatments may affect chromatin modifications, accessibility and subsequently gene expression. Additionally, it has been previously reported that post-translational modifications to key transcription factors, such as Pax7, play important roles in the myogenic lineage. It would therefore be of interest to determine whether these metabolites might also be signalling via post-translational modifications to transcription factors, which could also explain differences in gene expression.

As previously described, the identification of differentially altered metabolites was done using metabolomic analysis. Future studies would benefit from the use of isotope tracing to determine the metabolic flux of altered metabolites. Furthermore, to capture the metabolic flux of MuSCs as close to quiescence as possible, the use of *in vivo* labeling would be highly beneficial. This would eliminate the culture time of MuSCs with the labeled isotope following their isolation.

This work focused on altered mitochondrial shape via deletion or overexpression of OPA1. It is therefore not entirely possible to determine whether our observed effects are due to altered mitochondrial shape or due to OPA1 expression. Future studies would benefit from utilizing other models of altered mitochondrial shape, such as DRP1-deficient and MFN1/2-deficient MuSCs. These animal models would provide further clarity on the global scope of mitochondrial shape as a mechanism guiding MuSC progression and fate.

Chapter 9: References

1. Relaix, F., Bencze, M., Borok, M.J., Der Vartanian, A., Gattazzo, F., Mademtzoglou, D., Perez-Diaz, S., Prola, A., Reyes-Fernandez, P.C., Rotini, A., and Taglietti (2021). Perspectives on skeletal muscle stem cells. Nat Commun *12*, 692. 10.1038/s41467-020-20760-6.
2. Dumont, N.A., Bentzinger, C.F., Sincennes, M.C., and Rudnicki, M.A. (2015). Satellite Cells and Skeletal Muscle Regeneration. Compr Physiol *5*, 1027-1059. 10.1002/cphy.c140068.
3. Wang, Y.X., Dumont, N.A., and Rudnicki, M.A. (2014). Muscle stem cells at a glance. J Cell Sci *127*, 4543-4548. 10.1242/jcs.151209.
4. Kang, J.S., and Krauss, R.S. (2010). Muscle stem cells in developmental and regenerative myogenesis. Curr Opin Clin Nutr Metab Care *13*, 243-248. 10.1097/MCO.0b013e328336ea98.
5. Yin, H., Price, F., and Rudnicki, M.A. (2013). Satellite cells and the muscle stem cell niche. Physiol Rev *93*, 23-67. 10.1152/physrev.00043.2011.
6. Hung, M., Lo, H.F., Jones, G.E.L., and Krauss, R.S. (2023). The muscle stem cell niche at a glance. J Cell Sci *136*. 10.1242/jcs.261200.
7. Kann, A.P., Hung, M., and Krauss, R.S. (2021). Cell-cell contact and signaling in the muscle stem cell niche. Curr Opin Cell Biol *73*, 78-83. 10.1016/j.ceb.2021.06.003.
8. Eliazer, S., Muncie, J.M., Christensen, J., Sun, X., D'Urso, R.S., Weaver, V.M., and Brack, A.S. (2019). Wnt4 from the Niche Controls the Mechano-Properties and Quiescent State of Muscle Stem Cells. Cell Stem Cell *25*, 654-665.e654. 10.1016/j.stem.2019.08.007.
9. Goel, A.J., Rieder, M.K., Arnold, H.H., Radice, G.L., and Krauss, R.S. (2017). Niche Cadherins Control the Quiescence-to-Activation Transition in Muscle Stem Cells. Cell Rep *21*, 2236-2250. 10.1016/j.celrep.2017.10.102.
10. Sampath, S.C., Ho, A.T.V., Corbel, S.Y., Millstone, J.D., Lamb, J., Walker, J., Kinzel, B., Schmedt, C., and Blau, H.M. (2018). Induction of muscle stem cell quiescence by the secreted niche factor Oncostatin M. Nat Commun *9*, 1531. 10.1038/s41467-018-03876-8.
11. Dumont, N.A., Wang, Y.X., and Rudnicki, M.A. (2015). Intrinsic and extrinsic mechanisms regulating satellite cell function. Development *142*, 1572-1581. 10.1242/dev.114223.
12. Kuang, S., Gillespie, M.A., and Rudnicki, M.A. (2008). Niche regulation of muscle satellite cell self-renewal and differentiation. Cell Stem Cell *2*, 22-31. 10.1016/j.stem.2007.12.012.
13. Murphy, M.M., Lawson, J.A., Mathew, S.J., Hutcheson, D.A., and Kardon, G. (2011). Satellite cells, connective tissue fibroblasts and their interactions are crucial for muscle regeneration. Development *138*, 3625-3637. 10.1242/dev.064162.
14. Mademtzoglou, D., and Relaix, F. (2022). From cyclins to CDKIs: Cell cycle regulation of skeletal muscle stem cell quiescence and activation. Exp Cell Res *420*, 113275. 10.1016/j.yexcr.2022.113275.
15. Zhou, S., Han, L., and Wu, Z. (2022). A Long Journey before Cycling: Regulation of Quiescence Exit in Adult Muscle Satellite Cells. Int J Mol Sci *23*. 10.3390/ijms23031748.
16. Marescal, O., and Cheeseman, I.M. (2020). Cellular Mechanisms and Regulation of Quiescence. Dev Cell *55*, 259-271. 10.1016/j.devcel.2020.09.029.
17. van Velthoven, C.T.J., and Rando, T.A. (2019). Stem Cell Quiescence: Dynamism, Restraint, and Cellular Idling. Cell Stem Cell *24*, 213-225. 10.1016/j.stem.2019.01.001.

18. Feng, L.T., Chen, Z.N., and Bian, H. (2024). Skeletal muscle: molecular structure, myogenesis, biological functions, and diseases. MedComm (2020) *5*, e649. 10.1002/mco2.649.
19. Abmayr, S.M., and Pavlath, G.K. (2012). Myoblast fusion: lessons from flies and mice. Development *139*, 641-656. 10.1242/dev.068353.
20. de Morree, A., and Rando, T.A. (2023). Regulation of adult stem cell quiescence and its functions in the maintenance of tissue integrity. Nat Rev Mol Cell Biol *24*, 334-354. 10.1038/s41580-022-00568-6.
21. Ancel, S., Stuelsatz, P., and Feige, J.N. (2021). Muscle Stem Cell Quiescence: Controlling Stemness by Staying Asleep. Trends Cell Biol *31*, 556-568. 10.1016/j.tcb.2021.02.006.
22. Seale, P., Sabourin, L.A., Girgis-Gabardo, A., Mansouri, A., Gruss, P., and Rudnicki, M.A. (2000). Pax7 is required for the specification of myogenic satellite cells. Cell *102*, 777-786. 10.1016/s0092-8674(00)00066-0.
23. von Maltzahn, J., Jones, A.E., Parks, R.J., and Rudnicki, M.A. (2013). Pax7 is critical for the normal function of satellite cells in adult skeletal muscle. Proc Natl Acad Sci U S A *110*, 16474-16479. 10.1073/pnas.1307680110.
24. An, Y., Wang, G., Diao, Y., Long, Y., Fu, X., Weng, M., Zhou, L., Sun, K., Cheung, T.H., Ip, N.Y., et al. (2017). A Molecular Switch Regulating Cell Fate Choice between Muscle Progenitor Cells and Brown Adipocytes. Dev Cell *41*, 382-391.e385. 10.1016/j.devcel.2017.04.012.
25. Shea, K.L., Xiang, W., LaPorta, V.S., Licht, J.D., Keller, C., Basson, M.A., and Brack, A.S. (2010). Sprouty1 regulates reversible quiescence of a self-renewing adult muscle stem cell pool during regeneration. Cell Stem Cell *6*, 117-129. 10.1016/j.stem.2009.12.015.
26. Fukada, S., Uezumi, A., Ikemoto, M., Masuda, S., Segawa, M., Tanimura, N., Yamamoto, H., Miyagoe-Suzuki, Y., and Takeda, S. (2007). Molecular signature of quiescent satellite cells in adult skeletal muscle. Stem Cells *25*, 2448-2459. 10.1634/stemcells.2007-0019.
27. Yamaguchi, M., Watanabe, Y., Ohtani, T., Uezumi, A., Mikami, N., Nakamura, M., Sato, T., Ikawa, M., Hoshino, M., Tsuchida, K., et al. (2015). Calcitonin Receptor Signaling Inhibits Muscle Stem Cells from Escaping the Quiescent State and the Niche. Cell Rep *13*, 302-314. 10.1016/j.celrep.2015.08.083.
28. Baghdadi, M.B., Castel, D., Machado, L., Fukada, S.I., Birk, D.E., Relaix, F., Tajbakhsh, S., and Mourikis, P. (2018). Reciprocal signalling by Notch-Collagen V-CALCR retains muscle stem cells in their niche. Nature *557*, 714-718. 10.1038/s41586-018-0144-9.
29. Zhang, L., Noguchi, Y.T., Nakayama, H., Kaji, T., Tsujikawa, K., Ikemoto-Uezumi, M., Uezumi, A., Okada, Y., Doi, T., Watanabe, S., et al. (2019). The CalcR-PKA-Yap1 Axis Is Critical for Maintaining Quiescence in Muscle Stem Cells. Cell Rep *29*, 2154-2163.e2155. 10.1016/j.celrep.2019.10.057.
30. Zhang, L., Kubota, M., Nakamura, A., Kaji, T., Seno, S., Uezumi, A., Andersen, D.C., Jensen, C.H., and Fukada, S.I. (2021). Dlk1 regulates quiescence in calcitonin receptor-mutant muscle stem cells. Stem Cells *39*, 306-317. 10.1002/stem.3312.
31. Blanco-Bose, W.E., Yao, C.C., Kramer, R.H., and Blau, H.M. (2001). Purification of mouse primary myoblasts based on alpha 7 integrin expression. Exp Cell Res *265*, 212-220. 10.1006/excr.2001.5191.
32. Gnocchi, V.F., White, R.B., Ono, Y., Ellis, J.A., and Zammit, P.S. (2009). Further characterisation of the molecular signature of quiescent and activated mouse muscle satellite cells. PLoS One *4*, e5205. 10.1371/journal.pone.0005205.

33. Ozeki, N., Lim, M., Yao, C.C., Tolar, M., and Kramer, R.H. (2006). alpha7 integrin expressing human fetal myogenic progenitors have stem cell-like properties and are capable of osteogenic differentiation. Exp Cell Res *312*, 4162-4180. 10.1016/j.yexcr.2006.09.017.
34. Bjornson, C.R., Cheung, T.H., Liu, L., Tripathi, P.V., Steeper, K.M., and Rando, T.A. (2012). Notch signaling is necessary to maintain quiescence in adult muscle stem cells. Stem Cells *30*, 232-242. 10.1002/stem.773.
35. Mourikis, P., and Tajbakhsh, S. (2014). Distinct contextual roles for Notch signalling in skeletal muscle stem cells. BMC Dev Biol *14*, 2. 10.1186/1471-213X-14-2.
36. Zhang, Y., Lahmann, I., Baum, K., Shimojo, H., Mourikis, P., Wolf, J., Kageyama, R., and Birchmeier, C. (2021). Oscillations of Delta-like1 regulate the balance between differentiation and maintenance of muscle stem cells. Nat Commun *12*, 1318. 10.1038/s41467-021-21631-4.
37. Liu, L., Charville, G.W., Cheung, T.H., Yoo, B., Santos, P.J., Schroeder, M., and Rando, T.A. (2018). Impaired Notch Signaling Leads to a Decrease in p53 Activity and Mitotic Catastrophe in Aged Muscle Stem Cells. Cell Stem Cell *23*, 544-556.e544. 10.1016/j.stem.2018.08.019.
38. Chakkalakal, J.V., Christensen, J., Xiang, W., Tierney, M.T., Boscolo, F.S., Sacco, A., and Brack, A.S. (2014). Early forming label-retaining muscle stem cells require p27kip1 for maintenance of the primitive state. Development *141*, 1649-1659. 10.1242/dev.100842.
39. Naito, M., Mori, M., Inagawa, M., Miyata, K., Hashimoto, N., Tanaka, S., and Asahara, H. (2016). Dnmt3a Regulates Proliferation of Muscle Satellite Cells via p57Kip2. PLoS Genet *12*, e1006167. 10.1371/journal.pgen.1006167.
40. Hosoyama, T., Nishijo, K., Prajapati, S.I., Li, G., and Keller, C. (2011). Rb1 gene inactivation expands satellite cell and postnatal myoblast pools. J Biol Chem *286*, 19556-19564. 10.1074/jbc.M111.229542.
41. de Morrée, A., van Velthoven, C.T.J., Gan, Q., Salvi, J.S., Klein, J.D.D., Akimenko, I., Quarta, M., Biressi, S., and Rando, T.A. (2017). Staufen1 inhibits MyoD translation to actively maintain muscle stem cell quiescence. Proc Natl Acad Sci U S A *114*, E8996-E9005. 10.1073/pnas.1708725114.
42. Hausburg, M.A., Doles, J.D., Clement, S.L., Cadwallader, A.B., Hall, M.N., Blackshear, P.J., Lykke-Andersen, J., and Olwin, B.B. (2015). Post-transcriptional regulation of satellite cell quiescence by TTP-mediated mRNA decay. Elife *4*, e03390. 10.7554/eLife.03390.
43. Beauchamp, J.R., Heslop, L., Yu, D.S., Tajbakhsh, S., Kelly, R.G., Wernig, A., Buckingham, M.E., Partridge, T.A., and Zammit, P.S. (2000). Expression of CD34 and Myf5 defines the majority of quiescent adult skeletal muscle satellite cells. J Cell Biol *151*, 1221-1234. 10.1083/jcb.151.6.1221.
44. Yue, L., Wan, R., Luan, S., Zeng, W., and Cheung, T.H. (2020). Dek Modulates Global Intron Retention during Muscle Stem Cells Quiescence Exit. Dev Cell *53*, 661-676.e666. 10.1016/j.devcel.2020.05.006.
45. Zismanov, V., Chichkov, V., Colangelo, V., Jamet, S., Wang, S., Syme, A., Koromilas, A.E., and Crist, C. (2016). Phosphorylation of eIF2α Is a Translational Control Mechanism Regulating Muscle Stem Cell Quiescence and Self-Renewal. Cell Stem Cell *18*, 79-90. 10.1016/j.stem.2015.09.020.

46. Rodgers, J.T., King, K.Y., Brett, J.O., Cromie, M.J., Charville, G.W., Maguire, K.K., Brunson, C., Mastey, N., Liu, L., Tsai, C.R., et al. (2014). mTORC1 controls the adaptive transition of quiescent stem cells from G0 to G(Alert). Nature *510*, 393-396. 10.1038/nature13255.
47. Rodgers, J.T., Schroeder, M.D., Ma, C., and Rando, T.A. (2017). HGFA Is an Injury-Regulated Systemic Factor that Induces the Transition of Stem Cells into G. Cell Rep *19*, 479-486. 10.1016/j.celrep.2017.03.066.
48. García-Prat, L., Perdiguero, E., Alonso-Martín, S., Dell'Orso, S., Ravichandran, S., Brooks, S.R., Juan, A.H., Campanario, S., Jiang, K., Hong, X., et al. (2020). FoxO maintains a genuine muscle stem-cell quiescent state until geriatric age. Nat Cell Biol *22*, 1307-1318. 10.1038/s41556-020-00593-7.
49. Ancel, S., Michaud, J., Sizzano, F., Tauzin, L., Oliveira, M., Migliavacca, E., Schüler, S.C., Raja, S., Dammone, G., Karaz, S., et al. (2024). A dual-color PAX7 and MYF5 in vivo reporter to investigate muscle stem cell heterogeneity in regeneration and aging. Stem Cell Reports *19*, 1024-1040. 10.1016/j.stemcr.2024.05.005.
50. Rocheteau, P., Gayraud-Morel, B., Siegl-Cachedenier, I., Blasco, M.A., and Tajbakhsh, S. (2012). A subpopulation of adult skeletal muscle stem cells retains all template DNA strands after cell division. Cell *148*, 112-125. 10.1016/j.cell.2011.11.049.
51. Wang, G., Zhu, H., Situ, C., Han, L., Yu, Y., Cheung, T.H., Liu, K., and Wu, Z. (2018). p110α of PI3K is necessary and sufficient for quiescence exit in adult muscle satellite cells. EMBO J *37*. 10.15252/embj.201798239.
52. Griger, J., Schneider, R., Lahmann, I., Schöwel, V., Keller, C., Spuler, S., Nazare, M., and Birchmeier, C. (2017). Loss of Ptpn11 (Shp2) drives satellite cells into quiescence. Elife *6*. 10.7554/eLife.21552.
53. Van Mater, D., Añó, L., Blum, J.M., Webster, M.T., Huang, W., Williams, N., Ma, Y., Cardona, D.M., Fan, C.M., and Kirsch, D.G. (2015). Acute tissue injury activates satellite cells and promotes sarcoma formation via the HGF/c-MET signaling pathway. Cancer Res *75*, 605-614. 10.1158/0008-5472.CAN-14-2527.
54. Sheehan, S.M., and Allen, R.E. (1999). Skeletal muscle satellite cell proliferation in response to members of the fibroblast growth factor family and hepatocyte growth factor. J Cell Physiol *181*, 499-506. 10.1002/(SICI)1097-4652(199912)181:3<499::AID-JCP14>3.0.CO;2-1.
55. Lahmann, I., Bröhl, D., Zyrianova, T., Isomura, A., Czajkowski, M.T., Kapoor, V., Griger, J., Ruffault, P.L., Mademtzoglou, D., Zammit, P.S., et al. (2019). Oscillations of MyoD and Hes1 proteins regulate the maintenance of activated muscle stem cells. Genes Dev *33*, 524-535. 10.1101/gad.322818.118.
56. Zhang, J.M., Wei, Q., Zhao, X., and Paterson, B.M. (1999). Coupling of the cell cycle and myogenesis through the cyclin D1-dependent interaction of MyoD with cdk4. EMBO J *18*, 926-933. 10.1093/emboj/18.4.926.
57. Ismaeel, A., Goh, J., Mobley, C.B., Murach, K.A., Brett, J.O., de Morrée, A., Rando, T.A., Peterson, C.A., Wen, Y., and McCarthy, J.J. (2024). Division-Independent Differentiation of Muscle Stem Cells During a Growth Stimulus. Stem Cells *42*, 266-277. 10.1093/stmcls/sxad091.
58. Kuang, S., Kuroda, K., Le Grand, F., and Rudnicki, M.A. (2007). Asymmetric self-renewal and commitment of satellite stem cells in muscle. Cell *129*, 999-1010. 10.1016/j.cell.2007.03.044.

59. Evano, B., Khalilian, S., Le Carrou, G., Almouzni, G., and Tajbakhsh, S. (2020). Dynamics of Asymmetric and Symmetric Divisions of Muscle Stem Cells In Vivo and on Artificial Niches. Cell Rep *30*, 3195-3206.e3197. 10.1016/j.celrep.2020.01.097.
60. Dumont, N.A., Wang, Y.X., von Maltzahn, J., Pasut, A., Bentzinger, C.F., Brun, C.E., and Rudnicki, M.A. (2015). Dystrophin expression in muscle stem cells regulates their polarity and asymmetric division. Nat Med *21*, 1455-1463. 10.1038/nm.3990.
61. Shinin, V., Gayraud-Morel, B., Gomès, D., and Tajbakhsh, S. (2006). Asymmetric division and cosegregation of template DNA strands in adult muscle satellite cells. Nat Cell Biol *8*, 677-687. 10.1038/ncb1425.
62. Shinin, V., Gayraud-Morel, B., and Tajbakhsh, S. (2009). Template DNA-strand co-segregation and asymmetric cell division in skeletal muscle stem cells. Methods Mol Biol *482*, 295-317. 10.1007/978-1-59745-060-7_19.
63. Berika, M., Elgayyar, M.E., and El-Hashash, A.H. (2014). Asymmetric cell division of stem cells in the lung and other systems. Front Cell Dev Biol *2*, 33. 10.3389/fcell.2014.00033.
64. Ito, K. (2016). Metabolism and the Control of Cell Fate Decisions and Stem Cell Renewal. Annu Rev Cell Dev Biol *32*, 399-409. 10.1146/annurev-cellbio-111315-125134.
65. Wang, Y.X., Feige, P., Brun, C.E., Hekmatnejad, B., Dumont, N.A., Renaud, J.M., Faulkes, S., Guindon, D.E., and Rudnicki, M.A. (2019). EGFR-Aurka Signaling Rescues Polarity and Regeneration Defects in Dystrophin-Deficient Muscle Stem Cells by Increasing Asymmetric Divisions. Cell Stem Cell *24*, 419-432.e416. 10.1016/j.stem.2019.01.002.
66. Ono, Y., Urata, Y., Goto, S., Nakagawa, S., Humbert, P.O., Li, T.S., and Zammit, P.S. (2015). Muscle stem cell fate is controlled by the cell-polarity protein Scrib. Cell Rep *10*, 1135-1148. 10.1016/j.celrep.2015.01.045.
67. Zammit, P.S., Relaix, F., Nagata, Y., Ruiz, A.P., Collins, C.A., Partridge, T.A., and Beauchamp, J.R. (2006). Pax7 and myogenic progression in skeletal muscle satellite cells. J Cell Sci *119*, 1824-1832. 10.1242/jcs.02908.
68. Olguín, H.C., and Pisconti, A. (2012). Marking the tempo for myogenesis: Pax7 and the regulation of muscle stem cell fate decisions. J Cell Mol Med *16*, 1013-1025. 10.1111/j.1582-4934.2011.01348.x.
69. Halevy, O., Piestun, Y., Allouh, M.Z., Rosser, B.W., Rinkevich, Y., Reshef, R., Rozenboim, I., Wleklinski-Lee, M., and Yablonka-Reuveni, Z. (2004). Pattern of Pax7 expression during myogenesis in the posthatch chicken establishes a model for satellite cell differentiation and renewal. Dev Dyn *231*, 489-502. 10.1002/dvdy.20151.
70. Lilja, K.C., Zhang, N., Magli, A., Gunduz, V., Bowman, C.J., Arpke, R.W., Darabi, R., Kyba, M., Perlingeiro, R., and Dynlacht, B.D. (2017). Pax7 remodels the chromatin landscape in skeletal muscle stem cells. PLoS One *12*, e0176190. 10.1371/journal.pone.0176190.
71. Zhang, N., Mendieta-Esteban, J., Magli, A., Lilja, K.C., Perlingeiro, R.C.R., Marti-Renom, M.A., Tsirigos, A., and Dynlacht, B.D. (2020). Muscle progenitor specification and myogenic differentiation are associated with changes in chromatin topology. Nat Commun *11*, 6222. 10.1038/s41467-020-19999-w.
72. Troy, A., Cadwallader, A.B., Fedorov, Y., Tyner, K., Tanaka, K.K., and Olwin, B.B. (2012). Coordination of satellite cell activation and self-renewal by Par-complex-dependent asymmetric activation of p38α/β MAPK. Cell Stem Cell *11*, 541-553. 10.1016/j.stem.2012.05.025.

73. Yablonka-Reuveni, Z., and Rivera, A.J. (1994). Temporal expression of regulatory and structural muscle proteins during myogenesis of satellite cells on isolated adult rat fibers. Dev Biol *164*, 588-603. 10.1006/dbio.1994.1226.
74. Zammit, P.S. (2017). Function of the myogenic regulatory factors Myf5, MyoD, Myogenin and MRF4 in skeletal muscle, satellite cells and regenerative myogenesis. Semin Cell Dev Biol *72*, 19-32. 10.1016/j.semcdb.2017.11.011.
75. Wang, R., Chen, F., Chen, Q., Wan, X., Shi, M., Chen, A.K., Ma, Z., Li, G., Wang, M., Ying, Y., et al. (2022). MyoD is a 3D genome structure organizer for muscle cell identity. Nat Commun *13*, 205. 10.1038/s41467-021-27865-6.
76. Lepper, C., Partridge, T.A., and Fan, C.M. (2011). An absolute requirement for Pax7-positive satellite cells in acute injury-induced skeletal muscle regeneration. Development *138*, 3639-3646. 10.1242/dev.067595.
77. Ryall, J.G., Dell'Orso, S., Derfoul, A., Juan, A., Zare, H., Feng, X., Clermont, D., Koulnis, M., Gutierrez-Cruz, G., Fulco, M., and Sartorelli, V. (2015). The NAD(+)-dependent SIRT1 deacetylase translates a metabolic switch into regulatory epigenetics in skeletal muscle stem cells. Cell Stem Cell *16*, 171-183. 10.1016/j.stem.2014.12.004.
78. Pecqueur, C., Bui, T., Gelly, C., Hauchard, J., Barbot, C., Bouillaud, F., Ricquier, D., Miroux, B., and Thompson, C.B. (2008). Uncoupling protein-2 controls proliferation by promoting fatty acid oxidation and limiting glycolysis-derived pyruvate utilization. FASEB J *22*, 9-18. 10.1096/fj.07-8945com.
79. Yue, F., Gu, L., Qiu, J., Oprescu, S.N., Beckett, L.M., Ellis, J.M., Donkin, S.S., and Kuang, S. (2025). Mitochondrial fatty acid oxidation regulates adult muscle stem cell function through modulating metabolic flux and protein acetylation. EMBO J *44*, 2566-2595. 10.1038/s44318-025-00397-1.
80. Benjamin, D.I., Both, P., Benjamin, J.S., Nutter, C.W., Tan, J.H., Kang, J., Machado, L.A., Klein, J.D.D., de Morree, A., Kim, S., et al. (2022). Fasting induces a highly resilient deep quiescent state in muscle stem cells via ketone body signaling. Cell Metab *34*, 902-918.e906. 10.1016/j.cmet.2022.04.012.
81. Machado, L., Esteves de Lima, J., Fabre, O., Proux, C., Legendre, R., Szegedi, A., Varet, H., Ingerslev, L.R., Barrès, R., Relaix, F., and Mourikis, P. (2017). In Situ Fixation Redefines Quiescence and Early Activation of Skeletal Muscle Stem Cells. Cell Rep *21*, 1982-1993. 10.1016/j.celrep.2017.10.080.
82. L'honoré, A., Commère, P.H., Negroni, E., Pallafacchina, G., Friguet, B., Drouin, J., Buckingham, M., and Montarras, D. (2018). The role of Pitx2 and Pitx3 in muscle stem cells gives new insights into P38α MAP kinase and redox regulation of muscle regeneration. Elife *7*. 10.7554/eLife.32991.
83. Theret, M., Gsaier, L., Schaffer, B., Juban, G., Ben Larbi, S., Weiss-Gayet, M., Bultot, L., Collodet, C., Foretz, M., Desplanches, D., et al. (2017). AMPKα1-LDH pathway regulates muscle stem cell self-renewal by controlling metabolic homeostasis. EMBO J *36*, 1946-1962. 10.15252/embj.201695273.
84. Shintaku, J., Peterson, J.M., Talbert, E.E., Gu, J.M., Ladner, K.J., Williams, D.R., Mousavi, K., Wang, R., Sartorelli, V., and Guttridge, D.C. (2016). MyoD Regulates Skeletal Muscle Oxidative Metabolism Cooperatively with Alternative NF-κB. Cell Rep *17*, 514-526. 10.1016/j.celrep.2016.09.010.
85. Yucel, N., Wang, Y.X., Mai, T., Porpiglia, E., Lund, P.J., Markov, G., Garcia, B.A., Bendall, S.C., Angelo, M., and Blau, H.M. (2019). Glucose Metabolism Drives Histone Acetylation

Landscape Transitions that Dictate Muscle Stem Cell Function. Cell Rep *27*, 3939-3955.e3936. 10.1016/j.celrep.2019.05.092.
86. Hoffmann, C., Höckele, S., Kappler, L., Hrabě de Angelis, M., Häring, H.U., and Weigert, C. (2018). The effect of differentiation and TGFβ on mitochondrial respiration and mitochondrial enzyme abundance in cultured primary human skeletal muscle cells. Sci Rep *8*, 737. 10.1038/s41598-017-18658-3.
87. Lyons, C.N., Leary, S.C., and Moyes, C.D. (2004). Bioenergetic remodeling during cellular differentiation: changes in cytochrome c oxidase regulation do not affect the metabolic phenotype. Biochem Cell Biol *82*, 391-399. 10.1139/o04-040.
88. Soro-Arnáiz, I., Fitzgerald, G., Cherkaoui, S., Zhang, J., Gilardoni, P., Ghosh, A., Bar-Nur, O., Masschelein, E., Maechler, P., Zamboni, N., et al. (2024). GLUD1 determines murine muscle stem cell fate by controlling mitochondrial glutamate levels. Dev Cell *59*, 2850-2865.e2858. 10.1016/j.devcel.2024.07.015.
89. Chakrabarty, R.P., and Chandel, N.S. (2021). Mitochondria as Signaling Organelles Control Mammalian Stem Cell Fate. Cell Stem Cell *28*, 394-408. 10.1016/j.stem.2021.02.011.
90. Matias, M.I., Yong, C.S., Foroushani, A., Goldsmith, C., Mongellaz, C., Sezgin, E., Levental, K.R., Talebi, A., Perrault, J., Rivière, A., et al. (2021). Regulatory T cell differentiation is controlled by αKG-induced alterations in mitochondrial metabolism and lipid homeostasis. Cell Rep *37*, 109911. 10.1016/j.celrep.2021.109911.
91. Martínez-Reyes, I., and Chandel, N.S. (2020). Mitochondrial TCA cycle metabolites control physiology and disease. Nat Commun *11*, 102. 10.1038/s41467-019-13668-3.
92. Harvey, A., Caretti, G., Moresi, V., Renzini, A., and Adamo, S. (2019). Interplay between Metabolites and the Epigenome in Regulating Embryonic and Adult Stem Cell Potency and Maintenance. Stem Cell Reports *13*, 573-589. 10.1016/j.stemcr.2019.09.003.
93. Seim, G.L., Britt, E.C., John, S.V., Yeo, F.J., Johnson, A.R., Eisenstein, R.S., Pagliarini, D.J., and Fan, J. (2019). Two-stage metabolic remodelling in macrophages in response to lipopolysaccharide and interferon-γ stimulation. Nat Metab *1*, 731-742. 10.1038/s42255-019-0083-2.
94. Martínez-Reyes, I., Diebold, L.P., Kong, H., Schieber, M., Huang, H., Hensley, C.T., Mehta, M.M., Wang, T., Santos, J.H., Woychik, R., et al. (2016). TCA Cycle and Mitochondrial Membrane Potential Are Necessary for Diverse Biological Functions. Mol Cell *61*, 199-209. 10.1016/j.molcel.2015.12.002.
95. Chandel, N.S. (2014). Mitochondria as signaling organelles. BMC Biol *12*, 34. 10.1186/1741-7007-12-34.
96. Baker, S.A., and Rutter, J. (2023). Metabolites as signalling molecules. Nat Rev Mol Cell Biol *24*, 355-374. 10.1038/s41580-022-00572-w.
97. Wang, Y.P., and Lei, Q.Y. (2018). Metabolite sensing and signaling in cell metabolism. Signal Transduct Target Ther *3*, 30. 10.1038/s41392-018-0024-7.
98. Figlia, G., Willnow, P., and Teleman, A.A. (2020). Metabolites Regulate Cell Signaling and Growth via Covalent Modification of Proteins. Dev Cell *54*, 156-170. 10.1016/j.devcel.2020.06.036.
99. Wiese, M., and Bannister, A.J. (2020). Two genomes, one cell: Mitochondrial-nuclear coordination via epigenetic pathways. Mol Metab *38*, 100942. 10.1016/j.molmet.2020.01.006.

100. Salminen, A., Kaarniranta, K., Hiltunen, M., and Kauppinen, A. (2014). Krebs cycle dysfunction shapes epigenetic landscape of chromatin: novel insights into mitochondrial regulation of aging process. Cell Signal *26*, 1598-1603. 10.1016/j.cellsig.2014.03.030.
101. Shvedunova, M., and Akhtar, A. (2022). Modulation of cellular processes by histone and non-histone protein acetylation. Nat Rev Mol Cell Biol *23*, 329-349. 10.1038/s41580-021-00441-y.
102. Eberharter, A., and Becker, P.B. (2002). Histone acetylation: a switch between repressive and permissive chromatin. Second in review series on chromatin dynamics. EMBO Rep *3*, 224-229. 10.1093/embo-reports/kvf053.
103. Clayton, A.L., Hazzalin, C.A., and Mahadevan, L.C. (2006). Enhanced histone acetylation and transcription: a dynamic perspective. Mol Cell *23*, 289-296. 10.1016/j.molcel.2006.06.017.
104. Gujral, P., Mahajan, V., Lissaman, A.C., and Ponnampalam, A.P. (2020). Histone acetylation and the role of histone deacetylases in normal cyclic endometrium. Reprod Biol Endocrinol *18*, 84. 10.1186/s12958-020-00637-5.
105. Greer, E.L., and Shi, Y. (2012). Histone methylation: a dynamic mark in health, disease and inheritance. Nat Rev Genet *13*, 343-357. 10.1038/nrg3173.
106. TeSlaa, T., Chaikovsky, A.C., Lipchina, I., Escobar, S.L., Hochedlinger, K., Huang, J., Graeber, T.G., Braas, D., and Teitell, M.A. (2016). α-Ketoglutarate Accelerates the Initial Differentiation of Primed Human Pluripotent Stem Cells. Cell Metab *24*, 485-493. 10.1016/j.cmet.2016.07.002.
107. Carey, B.W., Finley, L.W., Cross, J.R., Allis, C.D., and Thompson, C.B. (2015). Intracellular α-ketoglutarate maintains the pluripotency of embryonic stem cells. Nature *518*, 413-416. 10.1038/nature13981.
108. Baksh, S.C., and Finley, L.W.S. (2021). Metabolic Coordination of Cell Fate by α-Ketoglutarate-Dependent Dioxygenases. Trends Cell Biol *31*, 24-36. 10.1016/j.tcb.2020.09.010.
109. Chaves-Perez, A., Millman, S.E., Janaki-Raman, S., Ho, Y.J., Hinterleitner, C., Barthet, V.J.A., Morris, J.P., Barriga, F.M., Reyes, J., Kyaw, A., et al. (2025). Metabolic adaptations direct cell fate during tissue regeneration. Nature. 10.1038/s41586-025-09097-6.
110. Sincennes, M.C., Brun, C.E., Lin, A.Y.T., Rosembert, T., Datzkiw, D., Saber, J., Ming, H., Kawabe, Y.I., and Rudnicki, M.A. (2021). Acetylation of PAX7 controls muscle stem cell self-renewal and differentiation potential in mice. Nat Commun *12*, 3253. 10.1038/s41467-021-23577-z.
111. Ciuffoli, V., Feng, X., Jiang, K., Acevedo-Luna, N., Ko, K.D., Wang, A.H.J., Riparini, G., Khateb, M., Glancy, B., Dell'Orso, S., and Sartorelli, V. (2024). Psat1-generated α-ketoglutarate and glutamine promote muscle stem cell activation and regeneration. Genes Dev *38*, 151-167. 10.1101/gad.351428.123.
112. Zhang, Q., Han, W., Wu, R., Deng, S., Meng, J., Yang, Y., Li, L., Sun, M., Ai, H., Chen, Y., et al. (2024). Spermidine-eIF5A axis is essential for muscle stem cell activation via translational control. Cell Discov *10*, 94. 10.1038/s41421-024-00712-w.
113. Suomalainen, A., and Nunnari, J. (2024). Mitochondria at the crossroads of health and disease. Cell *187*, 2601-2627. 10.1016/j.cell.2024.04.037.
114. Senior, A.E., Nadanaciva, S., and Weber, J. (2002). The molecular mechanism of ATP synthesis by F1F0-ATP synthase. Biochim Biophys Acta *1553*, 188-211. 10.1016/s0005-2728(02)00185-8.

115. Senior, A.E. (1988). ATP synthesis by oxidative phosphorylation. Physiol Rev *68*, 177-231. 10.1152/physrev.1988.68.1.177.
116. Wikström, M., Pecorilla, C., and Sharma, V. (2023). The mitochondrial respiratory chain. Enzymes *54*, 15-36. 10.1016/bs.enz.2023.05.001.
117. Nolfi-Donegan, D., Braganza, A., and Shiva, S. (2020). Mitochondrial electron transport chain: Oxidative phosphorylation, oxidant production, and methods of measurement. Redox Biol *37*, 101674. 10.1016/j.redox.2020.101674.
118. Zhao, R.Z., Jiang, S., Zhang, L., and Yu, Z.B. (2019). Mitochondrial electron transport chain, ROS generation and uncoupling (Review). Int J Mol Med *44*, 3-15. 10.3892/ijmm.2019.4188.
119. Turrens, J.F. (2003). Mitochondrial formation of reactive oxygen species. J Physiol *552*, 335-344. 10.1113/jphysiol.2003.049478.
120. Turrens, J.F. (1997). Superoxide production by the mitochondrial respiratory chain. Biosci Rep *17*, 3-8. 10.1023/a:1027374931887.
121. Averill-Bates, D. (2024). Reactive oxygen species and cell signaling. Review. Biochim Biophys Acta Mol Cell Res *1871*, 119573. 10.1016/j.bbamcr.2023.119573.
122. Redza-Dutordoir, M., and Averill-Bates, D.A. (2021). Interactions between reactive oxygen species and autophagy: Special issue: Death mechanisms in cellular homeostasis. Biochim Biophys Acta Mol Cell Res *1868*, 119041. 10.1016/j.bbamcr.2021.119041.
123. Sies, H., and Jones, D.P. (2020). Reactive oxygen species (ROS) as pleiotropic physiological signalling agents. Nat Rev Mol Cell Biol *21*, 363-383. 10.1038/s41580-020-0230-3.
124. Chan, C.M., Huang, D.Y., Sekar, P., Hsu, S.H., and Lin, W.W. (2019). Reactive oxygen species-dependent mitochondrial dynamics and autophagy confer protective effects in retinal pigment epithelial cells against sodium iodate-induced cell death. J Biomed Sci *26*, 40. 10.1186/s12929-019-0531-z.
125. Redza-Dutordoir, M., and Averill-Bates, D.A. (2016). Activation of apoptosis signalling pathways by reactive oxygen species. Biochim Biophys Acta *1863*, 2977-2992. 10.1016/j.bbamcr.2016.09.012.
126. Kobayashi, C.I., and Suda, T. (2012). Regulation of reactive oxygen species in stem cells and cancer stem cells. J Cell Physiol *227*, 421-430. 10.1002/jcp.22764.
127. Lindsay, R.T., and Rhodes, C.J. (2025). Reactive Oxygen Species (ROS) in Metabolic Disease-Don't Shoot the Metabolic Messenger. Int J Mol Sci *26*. 10.3390/ijms26062622.
128. Brillo, V., Chieregato, L., Leanza, L., Muccioli, S., and Costa, R. (2021). Mitochondrial Dynamics, ROS, and Cell Signaling: A Blended Overview. Life (Basel) *11*. 10.3390/life11040332.
129. Abuarab, N., Munsey, T.S., Jiang, L.H., Li, J., and Sivaprasadarao, A. (2017). High glucose-induced ROS activates TRPM2 to trigger lysosomal membrane permeabilization and Zn. Sci Signal *10*. 10.1126/scisignal.aal4161.
130. Khacho, M., Clark, A., Svoboda, D.S., Azzi, J., MacLaurin, J.G., Meghaizel, C., Sesaki, H., Lagace, D.C., Germain, M., Harper, M.E., et al. (2016). Mitochondrial Dynamics Impacts Stem Cell Identity and Fate Decisions by Regulating a Nuclear Transcriptional Program. Cell Stem Cell *19*, 232-247. 10.1016/j.stem.2016.04.015.
131. Ogasawara, M.A., and Zhang, H. (2009). Redox regulation and its emerging roles in stem cells and stem-like cancer cells. Antioxid Redox Signal *11*, 1107-1122. 10.1089/ars.2008.2308.

132. D'Autréaux, B., and Toledano, M.B. (2007). ROS as signalling molecules: mechanisms that generate specificity in ROS homeostasis. Nat Rev Mol Cell Biol *8*, 813-824. 10.1038/nrm2256.
133. Wade, S., and Khacho, M. (2022). MITOCHONDRIA: Mitochondrial dynamics in the regulation of stem cells. Int J Biochem Cell Biol *144*, 106158. 10.1016/j.biocel.2022.106158.
134. Tilokani, L., Nagashima, S., Paupe, V., and Prudent, J. (2018). Mitochondrial dynamics: overview of molecular mechanisms. Essays Biochem *62*, 341-360. 10.1042/EBC20170104.
135. Wai, T., and Langer, T. (2016). Mitochondrial Dynamics and Metabolic Regulation. Trends Endocrinol Metab *27*, 105-117. 10.1016/j.tem.2015.12.001.
136. Tábara, L.C., Segawa, M., and Prudent, J. (2025). Molecular mechanisms of mitochondrial dynamics. Nat Rev Mol Cell Biol *26*, 123-146. 10.1038/s41580-024-00785-1.
137. Ishihara, N., Eura, Y., and Mihara, K. (2004). Mitofusin 1 and 2 play distinct roles in mitochondrial fusion reactions via GTPase activity. J Cell Sci *117*, 6535-6546. 10.1242/jcs.01565.
138. Eura, Y., Ishihara, N., Yokota, S., and Mihara, K. (2003). Two mitofusin proteins, mammalian homologues of FZO, with distinct functions are both required for mitochondrial fusion. J Biochem *134*, 333-344. 10.1093/jb/mvg150.
139. Cipolat, S., Martins de Brito, O., Dal Zilio, B., and Scorrano, L. (2004). OPA1 requires mitofusin 1 to promote mitochondrial fusion. Proc Natl Acad Sci U S A *101*, 15927-15932. 10.1073/pnas.0407043101.
140. Meeusen, S., DeVay, R., Block, J., Cassidy-Stone, A., Wayson, S., McCaffery, J.M., and Nunnari, J. (2006). Mitochondrial inner-membrane fusion and crista maintenance requires the dynamin-related GTPase Mgm1. Cell *127*, 383-395. 10.1016/j.cell.2006.09.021.
141. Song, Z., Ghochani, M., McCaffery, J.M., Frey, T.G., and Chan, D.C. (2009). Mitofusins and OPA1 mediate sequential steps in mitochondrial membrane fusion. Mol Biol Cell *20*, 3525-3532. 10.1091/mbc.e09-03-0252.
142. Lee, H., Smith, S.B., and Yoon, Y. (2017). The short variant of the mitochondrial dynamin OPA1 maintains mitochondrial energetics and cristae structure. J Biol Chem *292*, 7115-7130. 10.1074/jbc.M116.762567.
143. Varanita, T., Soriano, M.E., Romanello, V., Zaglia, T., Quintana-Cabrera, R., Semenzato, M., Menabò, R., Costa, V., Civiletto, G., Pesce, P., et al. (2015). The OPA1-dependent mitochondrial cristae remodeling pathway controls atrophic, apoptotic, and ischemic tissue damage. Cell Metab *21*, 834-844. 10.1016/j.cmet.2015.05.007.
144. Frezza, C., Cipolat, S., Martins de Brito, O., Micaroni, M., Beznoussenko, G.V., Rudka, T., Bartoli, D., Polishuck, R.S., Danial, N.N., De Strooper, B., and Scorrano, L. (2006). OPA1 controls apoptotic cristae remodeling independently from mitochondrial fusion. Cell *126*, 177-189. 10.1016/j.cell.2006.06.025.
145. Satoh, M., Hamamoto, T., Seo, N., Kagawa, Y., and Endo, H. (2003). Differential sublocalization of the dynamin-related protein OPA1 isoforms in mitochondria. Biochem Biophys Res Commun *300*, 482-493. 10.1016/s0006-291x(02)02874-7.
146. Olichon, A., Baricault, L., Gas, N., Guillou, E., Valette, A., Belenguer, P., and Lenaers, G. (2003). Loss of OPA1 perturbates the mitochondrial inner membrane structure and integrity, leading to cytochrome c release and apoptosis. J Biol Chem *278*, 7743-7746. 10.1074/jbc.C200677200.

147. Abrisch, R.G., Gumbin, S.C., Wisniewski, B.T., Lackner, L.L., and Voeltz, G.K. (2020). Fission and fusion machineries converge at ER contact sites to regulate mitochondrial morphology. J Cell Biol *219*. 10.1083/jcb.201911122.
148. Friedman, J.R., Lackner, L.L., West, M., DiBenedetto, J.R., Nunnari, J., and Voeltz, G.K. (2011). ER tubules mark sites of mitochondrial division. Science *334*, 358-362. 10.1126/science.1207385.
149. Gandre-Babbe, S., and van der Bliek, A.M. (2008). The novel tail-anchored membrane protein Mff controls mitochondrial and peroxisomal fission in mammalian cells. Mol Biol Cell *19*, 2402-2412. 10.1091/mbc.e07-12-1287.
150. James, D.I., Parone, P.A., Mattenberger, Y., and Martinou, J.C. (2003). hFis1, a novel component of the mammalian mitochondrial fission machinery. J Biol Chem *278*, 36373-36379. 10.1074/jbc.M303758200.
151. Osellame, L.D., Singh, A.P., Stroud, D.A., Palmer, C.S., Stojanovski, D., Ramachandran, R., and Ryan, M.T. (2016). Cooperative and independent roles of the Drp1 adaptors Mff, MiD49 and MiD51 in mitochondrial fission. J Cell Sci *129*, 2170-2181. 10.1242/jcs.185165.
152. Palmer, C.S., Osellame, L.D., Laine, D., Koutsopoulos, O.S., Frazier, A.E., and Ryan, M.T. (2011). MiD49 and MiD51, new components of the mitochondrial fission machinery. EMBO Rep *12*, 565-573. 10.1038/embor.2011.54.
153. N, B., S, W., M, T., J, G., D, C., S, L., P, F., R, F., C, C., MA, R., et al. (2022). The mitochondrial protein OPA1 regulates the quiescent state of adult muscle stem cells. Cell stem cell *29*. 10.1016/j.stem.2022.07.010.
154. Hong, X., Isern, J., Campanario, S., Perdiguero, E., Ramírez-Pardo, I., Segalés, J., Hernansanz-Agustín, P., Curtabbi, A., Deryagin, O., Pollán, A., et al. (2022). Mitochondrial dynamics maintain muscle stem cell regenerative competence throughout adult life by regulating metabolism and mitophagy. Cell Stem Cell *29*, 1506-1508. 10.1016/j.stem.2022.09.002.
155. Triolo, M., Baker, N., Agarwal, S., Larionov, N., Podinić, T., and Khacho, M. (2024). Optic atrophy 1 mediates muscle differentiation by promoting a metabolic switch via the supercomplex assembly factor SCAF1. iScience *27*, 109164. 10.1016/j.isci.2024.109164.
156. Triolo, M., Wade, S., Baker, N., and Khacho, M. (2023). Evaluating mitochondrial length, volume, and cristae ultrastructure in rare mouse adult stem cell populations. STAR Protoc *4*, 102107. 10.1016/j.xpro.2023.102107.
157. Tournaire, G., Loopmans, S., Stegen, S., Rinaldi, G., Eelen, G., Torrekens, S., Moermans, K., Carmeliet, P., Ghesquière, B., Thienpont, B., et al. (2022). Skeletal progenitors preserve proliferation and self-renewal upon inhibition of mitochondrial respiration by rerouting the TCA cycle. Cell Rep *40*, 111105. 10.1016/j.celrep.2022.111105.
158. van den Berg, R.A., Hoefsloot, H.C., Westerhuis, J.A., Smilde, A.K., and van der Werf, M.J. (2006). Centering, scaling, and transformations: improving the biological information content of metabolomics data. BMC Genomics *7*, 142. 10.1186/1471-2164-7-142.
159. Herkenne, S., Ek, O., Zamberlan, M., Pellattiero, A., Chergova, M., Chivite, I., Novotná, E., Rigoni, G., Fonseca, T.B., Samardzic, D., et al. (2020). Developmental and Tumor Angiogenesis Requires the Mitochondria-Shaping Protein Opa1. Cell Metab *31*, 987-1003.e1008. 10.1016/j.cmet.2020.04.007.
160. Monge, C., DiStasio, N., Rossi, T., Sébastien, M., Sakai, H., Kalman, B., Boudou, T., Tajbakhsh, S., Marty, I., Bigot, A., et al. (2017). Quiescence of human muscle stem cells is

favored by culture on natural biopolymeric films. Stem Cell Res Ther *8*, 104. 10.1186/s13287-017-0556-8.
161. Quarta, M., Brett, J.O., DiMarco, R., De Morree, A., Boutet, S.C., Chacon, R., Gibbons, M.C., Garcia, V.A., Su, J., Shrager, J.B., et al. (2016). An artificial niche preserves the quiescence of muscle stem cells and enhances their therapeutic efficacy. Nat Biotechnol *34*, 752-759. 10.1038/nbt.3576.
162. Tao, J., Choudhury, M.I., Maity, D., Kim, T., Sun, S.X., and Fan, C.M. (2023). Mechanical compression creates a quiescent muscle stem cell niche. Commun Biol *6*, 43. 10.1038/s42003-023-04411-2.
163. Jacques, E., Kuang, Y., Kann, A.P., Le Grand, F., Krauss, R.S., and Gilbert, P.M. (2022). The mini-IDLE 3D biomimetic culture assay enables interrogation of mechanisms governing muscle stem cell quiescence and niche repopulation. Elife *11*. 10.7554/eLife.81738.
164. Liu, Y., Wang, M., Guo, Y., Wang, L., and Guo, W. (2023). D-2-hydroxyglutarate dehydrogenase governs adult neural stem cell activation and promotes histone acetylation via ATP-citrate lyase. Cell Rep *42*, 112067. 10.1016/j.celrep.2023.112067.
165. Liu, L., Hu, K., Feng, J., Wang, H., Fu, S., Wang, B., Wang, L., Xu, Y., Yu, X., and Huang, H. (2021). The oncometabolite R-2-hydroxyglutarate dysregulates the differentiation of human mesenchymal stromal cells via inducing DNA hypermethylation. BMC Cancer *21*, 36. 10.1186/s12885-020-07744-x.
166. Schvartzman, J.M., Reuter, V.P., Koche, R.P., and Thompson, C.B. (2019). 2-hydroxyglutarate inhibits MyoD-mediated differentiation by preventing H3K9 demethylation. Proc Natl Acad Sci U S A *116*, 12851-12856. 10.1073/pnas.1817662116.
167. Altundag, Ö., Canpinar, H., and Çelebi-Saltik, B. (2022). Methionine affects the expression of pluripotency genes and protein levels associated with methionine metabolism in adult, fetal, and cancer stem cells. J Cell Biochem *123*, 406-416. 10.1002/jcb.30180.
168. Sim, E.Z., Enomoto, T., Shiraki, N., Furuta, N., Kashio, S., Kambe, T., Tsuyama, T., Arakawa, A., Ozawa, H., Yokoyama, M., et al. (2022). Methionine metabolism regulates pluripotent stem cell pluripotency and differentiation through zinc mobilization. Cell Rep *40*, 111120. 10.1016/j.celrep.2022.111120.
169. Zhu, Q., Cheng, X., Cheng, Y., Chen, J., Xu, H., Gao, Y., Duan, X., Ji, J., Li, X., and Yi, W. (2020). O-GlcNAcylation regulates the methionine cycle to promote pluripotency of stem cells. Proc Natl Acad Sci U S A *117*, 7755-7763. 10.1073/pnas.1915582117.
170. Shiraki, N., Shiraki, Y., Tsuyama, T., Obata, F., Miura, M., Nagae, G., Aburatani, H., Kume, K., Endo, F., and Kume, S. (2014). Methionine metabolism regulates maintenance and differentiation of human pluripotent stem cells. Cell Metab *19*, 780-794. 10.1016/j.cmet.2014.03.017.
171. Rong, Y., Darnell, A.M., Sapp, K.M., Vander Heiden, M.G., and Spencer, S.L. (2023). Cells use multiple mechanisms for cell-cycle arrest upon withdrawal of individual amino acids. Cell Rep *42*, 113539. 10.1016/j.celrep.2023.113539.
172. Homma, T., Kobayashi, S., and Fujii, J. (2022). Methionine Deprivation Reveals the Pivotal Roles of Cell Cycle Progression in Ferroptosis That Is Induced by Cysteine Starvation. Cells *11*. 10.3390/cells11101603.
173. Benavides, M.A., Hagen, K.L., Fang, W., Du, P., Lin, S., Moyer, M.P., Yang, W., Bland, K.I., Grizzle, W.E., and Bosland, M.C. (2010). Suppression by L-methionine of cell cycle

progression in LNCaP and MCF-7 cells but not benign cells. Anticancer Res *30*, 1881-1885.
174. F C Lopes, A. (2020). Mitochondrial metabolism and DNA methylation: a review of the interaction between two genomes. Clin Epigenetics *12*, 182. 10.1186/s13148-020-00976-5.
175. Rasmussen, K.D., and Helin, K. (2016). Role of TET enzymes in DNA methylation, development, and cancer. Genes Dev *30*, 733-750. 10.1101/gad.276568.115.
176. Luo, D., Zou, M., Rao, X., Wei, M., Zhang, L., Hua, Y., Yu, L., Cao, J., Ye, J., Qi, S., et al. (2025). Lactobacillus salivarius metabolite succinate enhances chicken intestinal stem cell activities via the SUCNR1-mitochondria axis. Poult Sci *104*, 104754. 10.1016/j.psj.2024.104754.
177. Sahinyan, K., Lazure, F., Blackburn, D.M., and Soleimani, V.D. (2023). Decline of regenerative potential of old muscle stem cells: contribution to muscle aging. FEBS J *290*, 1267-1289. 10.1111/febs.16352.
178. Brack, A.S., and Muñoz-Cánoves, P. (2016). The ins and outs of muscle stem cell aging. Skelet Muscle *6*, 1. 10.1186/s13395-016-0072-z.